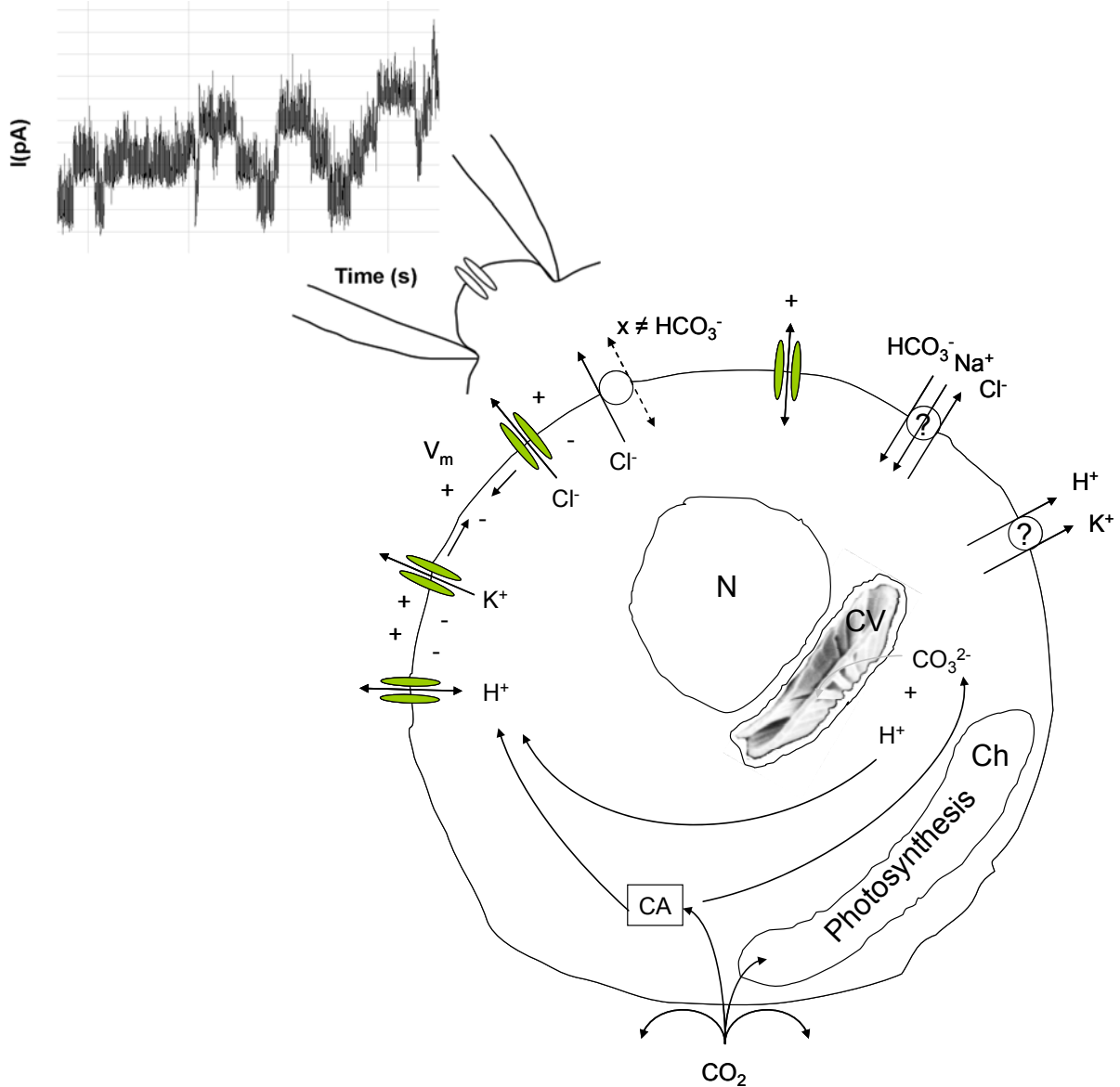


Ion transport and pH homeostasis in coccolithophores



Dissertation

zur Erlangung des Doktorgrades

der Mathematisch-Naturwissenschaftlichen Fakultät

der Christian-Albrechts-Universität zu Kiel

vorgelegt von

Kerstin Suffrian

Kiel, 2010

There is no such thing as a problem.
There are only challenges.

Referent: Prof. Dr. Ulf Riebesell

Koreferent: Prof. Dr. Markus Bleich

Tag der mündlichen Prüfung: 28.10.2010

Zum Druck genehmigt: Kiel, den . . .2010

gez. Prof. Dr.

List of Abbreviations

[A]	Unprotonated form of (HEPES) buffer
[AH]	Protonated form of (HEPES) buffer
ASW	Artificial seawater
ASW _c	Artificial seawater, control conditions
ASW _{culture}	Artificial seawater, culture conditions
ASW _{strip}	Artificial seawater solution for protoplast production
BCECF	2',7'-bis-(2-carboxyethyl)-5-(and-6)-carboxyfluorescein
BCECF-AM	2',7'-bis-(2-carboxyethyl)-5-(and-6)-carboxyfluorescein, acetoxymethyl ester
CC	Current clamp
CCM	Carbon concentrating mechanism
CO ₂ (aq)	Gaseous dissolved CO ₂
CO ₂ *	Combination of CO ₂ (aq) and carbonic acid
<i>C. pelagicus</i>	<i>Coccolithus pelagicus</i>
CV	Coccolith Vesicle
DIC	Dissolved Inorganic Carbon
DIDS	4,4'-Diisothiocyanatostilbene-2,2'-disulfonic acid
DMSO	Dimethyl sulfoxide
DOC	Dissolved Organic Carbon
EGTA	Ethylene glycol-bis(2-aminoethylether)-N,N,N',N'-tetraacetic acid
<i>E. huxleyi</i>	<i>Emiliania huxleyi</i>
HEPES	N-2-Hydroxyethylpiperazine-N'-2-ethanesulfonic acid
IS	Internal Solution
m	Number of experiments
n	Number of cells
NBS	National Bureau of Standards, USA
NMDG	N-Methyl-D-glucamine
NSW	Natural seawater
OOE	Out-of-equilibrium
PAR	Photosynthetically active radiation
pH _{CV}	Intra-coccolith vesicle pH
pH _e	Extracellular pH
pH _i	Intracellular pH
PIC	Particulate Inorganic Carbon
POC	Particulate Organic Carbon
RubisCO	Ribulose-1,5-bisphosphate carboxylase/oxygenase
S	Salinity
SITS	4-Acetamido-4'-isothiocyanato-stilbene-2,2'-disulfonic acid
VC	Voltage clamp
V _m	Membrane potential or voltage

List of Figures

Fig. 1 Bjerrum diagram.....	15
Fig. 2 Long term and recent development of CO ₂ concentration in the atmosphere.....	17
Fig. 3 Compilation of a) ion pumps and b) transporters used in cellular pH homeostasis.....	24
Fig. 4 Cell model of an acid secreting type A intercalated cell.....	24
Fig. 5 Schematic drawings of a coccosphere (left) and a section through an <i>E. huxleyi</i> cell (right).....	26
Fig. 6 Scheme of simulated diurnal cycle in the growth chamber.....	39
Fig. 7 Schematic protoplast production for microfluorimetry.....	40
Fig. 8 Schematic BCECF uptake and retention.....	41
Fig. 9 pH-dependent fluorescence excitation spectra of BCECF.....	42
Fig. 10 Scheme of the microfluorimetric detection system.....	43
Fig. 11 Chemical structure of nigericin.....	45
Fig. 12 Picture of a) the OOE mixing unit and b) the experimental bath chamber.....	46
Fig. 13 Scheme of the patch clamp measuring system.....	49
Fig. 14 Scheme of <i>E. huxleyi</i> protoplast production for electrophysiology.....	50
Fig. 15 Development of abundance (a) and nutrient concentration (b) during cell culture.....	53
Fig. 16 Characteristics of highly calcified <i>E. huxleyi</i> cells before and after protoplast preparation.....	54
Fig. 17 Confocal false colour image of <i>E. huxleyi</i> cells loaded with BCECF-AM.....	55
Fig. 18 Absence of detectable auto fluorescence in <i>E. huxleyi</i> in the experimental setup.....	55
Fig. 19 Frequency distribution of measured emission ratios.....	55
Fig. 20 Typical trace of a pH _i calibration experiment with nigericin.....	56
Fig. 21 Calibration curve for BCECF emission ratio.....	57
Fig. 22 Effect of [H ⁺] _e on fluorescence emission ratio as a measure of pH _i	58
Fig. 23 Reaction kinetics upon mixing of OOE solutions (K. G. Schulz).....	59
Fig. 24 Effect of high [CO ₂] or high [HCO ₃ ⁻] out of equilibrium in comparison to a change in [H ⁺].....	61
Fig. 25 Effect of DIDS on fluorescence ratio as a measure of pH _i	62
Fig. 26 Effect of low [Cl ⁻] on pH _i	63
Fig. 27 Effect of low [HCO ₃ ⁻] on the 2 nd Cl ⁻ induced transient acidification.....	65
Fig. 28 Effect of [HCO ₃ ⁻] and [Na ⁺] on the 2 nd Cl ⁻ induced transient acidification.....	66
Fig. 29 Effect of low [Na ⁺] and low [HCO ₃ ⁻] on the 2 nd K ⁺ induced transient acidification.....	67
Fig. 30 Effect of Ba ²⁺ on the acidification upon return to ASW _c with normal [K ⁺] concentrations.....	68
Fig. 31 Representative images of cellulose staining in <i>E. huxleyi</i>	70
Fig. 32 <i>C. pelagicus</i> cell during protoplast production and experiment.....	71
Fig. 33 Exemplary picture of a patch pipette sealed to a protoplast of <i>C. pelagicus</i>	71
Fig. 34 Current traces of an ion channel in <i>C. pelagicus</i> at different clamp voltages.....	72
Fig. 35 I/V curves of two <i>C. pelagicus</i> experiments.....	72
Fig. 36 Schematic <i>E. huxleyi</i> cell model I.....	82
Fig. 37 Schematic <i>E. huxleyi</i> cell model II.....	90

List of Tables

Table 1 Classification of <i>E. huxleyi</i> and <i>C. pelagicus</i> according to Guiry & Guiry (2010).....	26
Table 2 Ion concentrations of <i>E. huxleyi</i> compared to typical algal ion concentrations.....	28
Table 3 Artificial seawater solutions (1-3)	35
Table 4 Modified ASW solutions (4-8).....	36
Table 5 Out-of-equilibrium (OOE) solutions (9-10).....	37
Table 6 Intracellular solutions (11-13) and enzymatic solution (14).....	38
Table 7 Effects of changes in external $[H^+]$ on pH_i	58
Table 8 Effects of changes in $[CO_2]$, and $[HCO_3^-]$ on pH_i	61
Table 9 Effects of changes in H^+ on pH_i under control conditions and in the presence of DIDS.....	63
Table 10 Effect of decreased $[Cl^-]_e$ on pH_i	64
Table 11 Effect of $[HCO_3^-]$ and $[Na^+]$ on the 2 nd Cl^- induced transient acidification.....	65
Table 12 Effect of increased $[K^+]_e$ on pH_i and effects of HCO_3^- , Na^+ , and Ba^{2+} on the reacidification upon return to control.....	69
Table 13 overview on characteristics of different physiological states of <i>E. huxleyi</i>	73
Table 14 Overview of cellular transport systems involved in pH homeostasis	85

Table of Contents

LIST OF ABBREVIATIONS	4
LIST OF FIGURES	5
LIST OF TABLES	6
TABLE OF CONTENTS	7
1 SUMMARY	10
2 ZUSAMMENFASSUNG	12
3 INTRODUCTION	14
3.1 The marine carbonate system and natural variability	14
3.1.1 <i>The marine carbonate system</i>	14
3.1.2 <i>The change in carbonate system due to anthropogenic CO₂ emissions</i>	16
3.2 Transport across membranes	18
3.2.1 Diffusion	18
3.2.2 Facilitated transport via proteins	19
3.3 Electrophysiological properties of plasma membranes	20
3.4 Acid Base homeostasis on a cellular level	22
3.5 Coccolithophores <i>Emiliana huxleyi</i> and <i>Coccolithus pelagicus</i>	25
3.5.1 Coccolithophores	25
3.5.2 <i>Emiliana huxleyi</i> & <i>Coccolithus pelagicus</i>	27
3.5.3 Current knowledge on physiology	27
3.6 Thesis outline	33
4 MATERIALS AND METHODS	35
4.1 Solutions	35
4.1.1 Artificial seawater solutions (1-3)	35
4.1.2 Modified ASW solutions (4-8)	36
4.1.3 Out of equilibrium solutions (9-10)	37
4.1.4 Intracellular solutions (11-13)	38
4.1.5 Enzymatic stripping solution (14)	38
4.2 Cell culture	39
4.3 Viability tests	40
4.4 Adhesiveness of the bath bottoms	40
4.5 Microfluorimetry	40
4.5.1 Decalcification and Protoplast Isolation for Microfluorimetry	40

4.5.2	General principles in microfluorimetry at the example BCECF	41
4.5.3	Dye loading (BCECF) in <i>E. huxleyi</i>	42
4.5.4	Experimental procedure and devices	42
4.5.5	Experimental procedure: General.....	44
4.5.6	Calibration of pH_i with nigericin	44
4.5.7	Application of OOE solutions.....	45
4.5.8	pH measurements in experimental solutions	46
4.6	Electrophysiological measurements	46
4.6.1	<i>Patch Clamp Method</i>	46
4.6.2	<i>Experimental procedure and devices</i>	48
4.6.3	Decalcification and Protoplast Isolation for Electrophysiology	50
4.6.4	Sealing procedure with <i>E. huxleyi</i> protoplasts	51
4.7	Confocal laser scanning microscopy	51
4.8	Cellulose staining	52
4.9	Statistics	52
5	RESULTS.....	53
5.1	Fluorimetric measurements of intracellular pH	53
5.1.1	General remarks.....	53
5.1.2	Viability tests	54
5.1.3	Dye loading and basal BCECF fluorescence properties	54
5.1.4	Calibration of pH_i with nigericin	56
5.1.5	Effect of $[H^+]$ on pH_i	57
5.1.6	Out of equilibrium solutions	59
5.1.7	Effect of high $[CO_2]$ on pH_i	60
5.1.8	Effect of high $[HCO_3^-]$ on pH_i	61
5.1.9	Effect of DIDS on pH_i	62
5.1.10	Effect of decreased $[Cl^-]_e$ on pH_i	63
5.1.11	Effect of increased $[K^+]$ on pH_i	67
5.2	Electrophysiological measurements	70
5.2.1	General remarks.....	70
5.2.2	<i>C. pelagicus</i>	71
5.2.3	<i>Electric properties of C. pelagicus</i>	71
6	DISCUSSION	73
6.1	General	73
6.2	Methodological.....	73
6.2.1	Culture conditions for microscopy.....	73
6.2.2	Microfluorimetry	74
6.2.3	Calibration of pH_i with nigericin	76
6.2.4	OOEs.....	77
6.3	Membrane properties and pH homeostasis of Coccolithophores	78
6.3.1	Membrane H^+ permeability and effect on pH_i	78
6.3.2	Membrane CO_2 permeability and effect on pH_i	79
6.3.3	Membrane HCO_3^- permeability and effect on pH_i	80
6.3.4	Cell model for membrane permeabilities	82
6.3.5	DIDS effect on membrane H^+ permeability and pH_i	83
6.3.6	Effect of decreased $[Cl^-]$, increased $[K^+]$, the role of V_m and co- or antiporters.....	86
6.4	Electrophysiology.....	87

6.4.1	General (methodological) remarks	87
6.4.2	<i>Electric measurements in C. pelagicus</i>	87
6.5	Synthesis & Outlook	89
	IN PRESS.....	92
	ACKNOWLEDGEMENTS	93
	CURRICULUM VITAE.....	94
	ERKLÄRUNG.....	98

1 SUMMARY

Most metabolic processes are pH dependent. If we want to understand the influence of ocean pH and carbonate chemistry on coccolithophores, it is necessary to gain a better understanding of their physiological properties and metabolic processes. Here *Emiliania huxleyi* and *Coccolithus pelagicus* were chosen to characterise some mechanisms involved in pH homeostasis and ion transport.

Effects of changes in seawater carbon chemistry on intracellular pH (pH_i) were measured by 2',7'-bis-(2-carboxyethyl)-5-(and-6)-carboxyfluorescein (BCECF) fluorescence. Out of equilibrium (OOE) solutions were used to differentiate between membrane permeation pathways for H^+ , CO_2 and HCO_3^- . The ionophore nigericin was used to calibrate the dimension of changes in pH_i measured by BCECF.

pH_i acutely followed the pH of seawater (pH_e) in a linear fashion between pH_e 6.5 and 9.

No pH_i change could be detected when seawater $[\text{CO}_2]$, $[\text{CO}_2]_e$, was increased at constant pH_e and extracellular $[\text{HCO}_3^-]$, $[\text{HCO}_3^-]_e$. An increase in $[\text{HCO}_3^-]_e$ resulted in a slight intracellular acidification.

In the presence of 4,4'-Diisothiocyantostilbene-2,2'-disulfonic acid (DIDS) pH_i in *E. huxleyi* acidified and the effect was not reversible. In addition, DIDS reduced the effect of pH_e on pH_i slightly.

The data for the first time show the occurrence of a direct proton permeation pathway in *E. huxleyi* plasma membrane, a direct acidifying impact of increased $[\text{HCO}_3^-]_e$ on pH_i and no detectable influence of increased $[\text{CO}_2]_e$ on pH_i . pH homeostasis involves a DIDS sensitive mechanism. The data suggest the involvement of ion transport mechanisms which link ocean seawater pH and metabolic processes in *E. huxleyi*.

To further characterise these mechanisms the impact of manipulated extracellular ion concentrations on pH_i was investigated. The data on increased external $[\text{K}^+]$, $[\text{K}^+]_e$, and decreased external $[\text{Cl}^-]$, $[\text{Cl}^-]_e$, i. e. the effect of decreased gradients on pH_i , showed more complex relationships. Both led to a first rapid but transient acidification of pH_i and a second slower, also transient acidification upon return to control conditions. The two pH reactions showed different kinetics. The results indicate coupling of H^+ transport to ion gradients.

Different methods to isolate pure protoplasts and perform electrophysiological measurements on *E. huxleyi* were applied. *E. huxleyi* protoplasts showed a clean cell

membrane by different methods; however the cells did not form gigaseals. In *C. pelagicus* protoplast isolation and sealing were achieved, however, only in limited numbers of cells.

A revision of *E. huxleyi* membrane anatomy by confocal microscopy in collaboration with M. Gutowska and N. Fischer gave first evidence for a dual protoplast outer membrane, which might explain the difficulties in dye loading and patch sealing.

In summary the collected data are a first step in characterising physiological properties of coccolithophores with respect to carbon transport pathways, and pH homeostasis on a cellular level.

2 ZUSAMMENFASSUNG

Metabolische Prozesse sind in der Regel pH abhängig. Um zu verstehen, wie sich Ozeanversauerung und veränderte Carbonatchemie auf Coccolithophoriden auswirken, müssen wir daher zuerst ihre physiologischen Eigenschaften und metabolischen Prozesse verstehen,

Für die vorliegende Arbeit wurden *Emiliana huxleyi* und *Coccolithus pelagicus* ausgewählt, um grundlegende Mechanismen bzgl. pH Homöostase und Ionentransport in Coccolithophoriden zu charakterisieren.

Die Auswirkungen von modifiziertem Seewasser auf den intrazellulären pH (pH_i) wurden mithilfe von 2',7'-bis-(2-carboxyethyl)-5-(and-6)-carboxyfluorescein (BCECF) Fluoreszenz gemessen.

Out of equilibrium (OOE) Lösungen, d.h. Lösungen deren Karbonatchemie temporär nicht äquilibriert war, wurden verwendet, um zwischen Membranpermeabilitäten von H^+ , CO_2 und HCO_3^- unterscheiden zu können. Der Porenbildner Nigericin wurde eingesetzt, um das Verhältnis zwischen intrazellulären pH Änderungen und den tatsächlich gemessenen Änderungen in der BCECF Fluoreszenz zu kalibrieren. In dem Bereich zwischen pH_e 6.5 and 9 folgte der pH_i dem pH des Seewassers direkt und linear.

Wenn wir die $[CO_2]$ bei gleichbleibendem pH_e und konstanter $[HCO_3^-]$ erhöhten, änderte sich der pH_i nicht signifikant. Eine Erhöhung der extrazellulären $[HCO_3^-]$ hingegen führte zu einer leichten intrazellulären Ansäuerung.

In Gegenwart von 4,4'-Diisothiocyanatostilbene-2,2'-disulfonic acid (DIDS) sank der pH_i von *E. huxleyi* irreversibel. Darüber hinaus reduzierte DIDS die Ansäuerung des pH_i durch einen saureren externen pH leicht.

Wir konnten zum ersten Mal eine direkte Protonenpermeabilität in der *E. huxleyi* Plasmamembran, einen direkten, ansäuernden Effekt durch eine erhöhte extrazelluläre $[HCO_3^-]$ und das Fehlen eines messbaren Effektes einer erhöhten extrazellulären $[CO_2]$ auf den pH_i nachweisen.

Die Daten deuten darauf hin, dass Ionentransportmechanismen in *E. huxleyi* eine Verbindung zwischen metabolischen Prozessen und der Veränderung des Ozean pHs, der sogenannten Ozeanversauerung, darstellen.

Um diese Mechanismen weitergehend zu charakterisieren, untersuchten wir den Einfluss veränderter Ionenkonzentrationen in den Seewasser Experimentallösungen

auf den pH_i . Die Daten mit erhöhter $[\text{K}^+]$ bzw. verringerter $[\text{Cl}^-]$ im Seewasser, d.h. der Einfluss verringerter Gradienten über die Membran auf den pH_i , zeigten komplexere Zusammenhänge. Beide Manipulationen führten zuerst zu einer schnellen aber vorübergehenden Ansäuerung der Zellen, und nach Rückkehr zu den Kontrollbedingungen, zu einer zweiten, ebenfalls transienten Ansäuerung, wobei die erste und zweite Ansäuerung jeweils unterschiedliche Kinetiken besaßen. Die Ergebnisse weisen auf eine Kopplung des H^+ Transportes an Ionengradienten hin.

Wir verwendeten verschiedene Methoden, um *E. huxleyi* Protoplasten für elektrophysiologische Experimente zu isolieren. Verschiedene Ansätze führten zu Protoplasten mit optisch sauberer Zellmembran, jedoch formten die Zellen kein Gigaseal. Im Gegensatz dazu waren Protoplastenisolierung und Gigasealformierung in *C. pelagicus* möglich, wenn auch nur in einer begrenzten Anzahl von Zellen.

Unter Zuhilfenahme eines konfokalen Laserrastermikroskops wurde eine erneute Begutachtung der Membrananatomie bei *E. huxleyi* durchgeführt. Diese Kollaboration mit M. Gutowska und N. Fischer ergab erste Hinweise auf eine doppelte äußere Protoplastenplasmamembran, und damit eine mögliche Erklärung für die beobachteten Schwierigkeiten, sowohl bei der Beladung mit Farbstoffen, als auch bei der Gigasealbildung.

Zusammengefasst lässt sich sagen, dass die gesammelten Daten ein erster Schritt sind, um den physiologischen Eigenschaften der Coccolithophoriden in Hinsicht auf Kohlenstoff Transportwege über die Membran und in Hinsicht auf pH Homöostase auf der zellulären Ebene auf die Spur zu kommen.

3 Introduction

3.1 *The marine carbonate system and natural variability*

Organisms depend on the uptake of many different elements for maintenance and propagation. Among these elements carbon (C) is of major importance. On the one hand it can form a lot of different (inorganic and organic) chemical compounds. On the other hand it is the main structural component due to its ability to form a huge variety of complex molecules, which are at the fundament of life. Thus, in biology carbon is, together with oxygen and hydrogen, the most abundant and important element.

Carbon, on a global scale, is present in different compounds, in different reservoirs and exchanged between them in variable rates on a wide spectrum of timescales (e.g. rectifying channels like TRP family, Siegenthaler & Sarmiento). The largest of these reservoirs is the lithosphere, containing about 60 million Pg of C (1 Peta gram equals 1 giga ton, Gt, or 10^{15} g). The second largest reservoir is the ocean, containing about 39,000 Pg C in the form of dissolved inorganic carbon (DIC), some 700 Pg of dissolved organic carbon (DOC) and approximately 3 Pg of particulate organic carbon (POC). In comparison, today's atmosphere only contains around 750 Pg C, mainly in the form of CO_2 , the well known greenhouse gas, which corresponds to a partial pressure ($p\text{CO}_2$) of approximately 380 μatm (μatm are essentially equivalent to ppm).

3.1.1 *The marine carbonate system*

For this study I will focus on the aspects of biological interaction with the carbonate system in the surface ocean, the habitat of the model organisms used.

Autotrophic marine organisms like coccolithophores can take up C in the form of either inorganic ions (HCO_3^- , CO_3^{2-}) or in gaseous form (CO_2), summarised as dissolved inorganic carbon (DIC), or as organic compounds, e.g. in the form of dissolved organic carbon (DOC) such as carbohydrates.

The carbonate system in seawater depends on physicochemical (temperature, depth) and biological (e.g. photosynthesis, respiration, and calcification) parameters (Fig. 1).

The equilibrium relationships between CO_2 , HCO_3^- , and CO_3^{2-} in the marine carbonate system are illustrated in the so called Bjerrum diagram (Fig. 1). It shows examples for the carbon speciation at different temperatures, salinities, and pressure, plotted against pH. Our conditions are best described by the solid line ($T = 25^\circ\text{C}$,

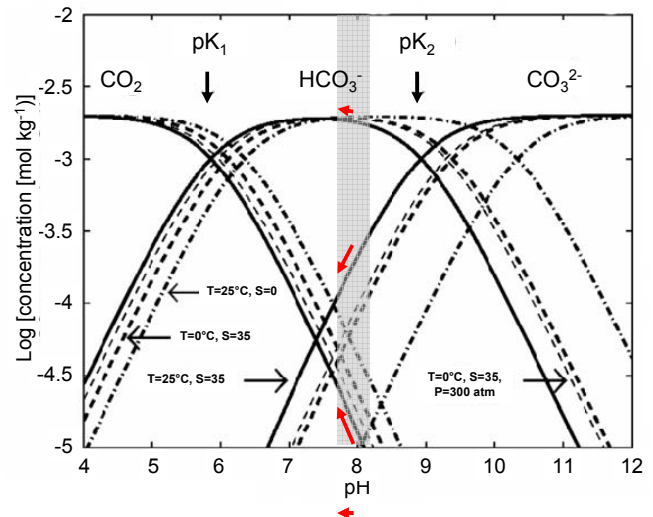


Fig. 1 Bjerrum diagram.

The grey area depicts the typical range of pH in the surface ocean, between 7.9 and 8.25, mean 8.1; $pK_1 = 5.84$; $pK_2 = 8.93$ at $S = 35$, $T = 25^\circ\text{C}$, (adapted from Zeebe & Wolf-Gladrow, 2001)

$S = 35$) in the grey area. The other lines depict the influence of T , S and P on carbonate speciation and pH.

Typical carbon concentrations in the

surface ocean at a pH of ~ 8.1 are $\sim 15 \mu\text{mol kg}^{-1} \text{CO}_2^*$, $\sim 2000 \mu\text{mol kg}^{-1} \text{HCO}_3^-$, and $\sim 200 \mu\text{mol kg}^{-1} \text{CO}_3^{2-}$. CO_2^* denotes the combination of gaseous dissolved CO_2 , $\text{CO}_2(\text{aq})$, and carbonic acid (H_2CO_3), ~ 600 times less abundant in seawater than $\text{CO}_2(\text{aq})$. The chemical and physical context of carbonate chemistry will be explained in more detail in the next passages with a short view on changing climatic conditions as the wider background of this study.

Gases aim to equilibrate between atmosphere and surface ocean.

i) An increase of $[\text{CO}_2]$ in the atmosphere leads to dissolution of more CO_2 in the water, and drives the equilibrium between $[\text{CO}_2]$, $[\text{HCO}_3^-]$, and $[\text{CO}_3^{2-}]$ towards more HCO_3^- and CO_2 and less CO_3^{2-} according to Eq. 1. This results in an increased $[\text{H}^+]$ in the water (see also 3.1.2). In this situation water of the surface ocean is a sink for atmospheric CO_2 .

ii) On the other hand an increase of $[\text{CO}_2]$ in the surface waters due to respiration leads principally to the same shifts in the equilibrium. Due to an out gassing of CO_2 to the atmosphere the system in this case can re equilibrate, turning the ocean into a source of CO_2 for the atmosphere.



In both cases, an increase of $[\text{CO}_2]$ will affect the CaCO_3 solubility product (K_{sp}^* , Eq. 2) and its saturation state in seawater (Ω , Eq. 3), as they are a function of $[\text{CO}_3^{2-}]$ and, consequently, of $[\text{CO}_2]$.

$$K_{sp}^* = [\text{Ca}^{2+}]_{sat} \cdot [\text{CO}_3^{2-}]_{sat} \quad \text{Eq. 2}$$

$$\Omega = \frac{[\text{Ca}^{2+}]_{sw} \cdot [\text{CO}_3^{2-}]_{sw}}{K_{sp}^*} \quad \text{Eq. 3}$$

If Ω is larger than 1, seawater is supersaturated with respect to CaCO_3 , and CaCO_3 formation and conservation is possible. If $[\text{CO}_3^{2-}]$ in the surface ocean decreases due to CO_2 uptake, the saturation state will shift towards undersaturation ($\Omega < 1$). This leads to dissolution of CaCO_3 . Ω is generally taken as a proxy for the calcification ability of organisms, even though it is rather the concentration of certain ions that the organisms detect. However, if CO_3^{2-} among them is unclear.

It is widely accepted nowadays that the ocean has been a relatively stable system on long timescales (~ 7.5 Myr), with respect to pH and the carbonate system (e.g. Spivack *et al.*, 1993). This is of importance, as there might have been no need for marine organisms to evolve - and keep - an adaptive potential.

On the other hand surface ocean carbonate chemistry is regularly changing, e.g. under bloom conditions (high population densities). $[\text{CO}_2]$ in seawater then becomes a function of biological activity (respiration, photosynthesis, and calcification), on a spatially and temporally limited scale.

Hence, it is important to answer the question, to what extent organisms are directly dependent on the ambient carbonate chemistry. Long term as well as short term adaptive potentials have to be taken into consideration. In fact, acid-base-metabolism of calcifying organisms might be challenged in a changing ocean; on the other hand they might be preadapted due to undulating $[\text{CO}_2]$ and $[\text{H}^+]$ conditions.

3.1.2 The change in carbonate system due to anthropogenic CO_2 emissions

Since the beginning of the industrial revolution the amount of CO_2 in the atmosphere, $[\text{CO}_2]_{atm}$, has been continuously increasing due to anthropogenic fossil fuel burning (Fig. 2). As already laid out in 3.1.1 if for example $[\text{CO}_2]$ in the tropic ocean (Fig. 1, solid line, $T = 25^\circ\text{C}$, $S = 35$) increases by invasion from the atmosphere (red arrow) pH will decrease accordingly and the carbonate speciation will react by an increase in

$[\text{HCO}_3^-]$ and a decrease in $[\text{CO}_3^{2-}]$, according to Eq. 1. In relation to their absolute concentrations the increase in $[\text{HCO}_3^-]$ is minor and the decrease in $[\text{CO}_3^{2-}]$ larger. On the long run this brings forth a decrease in the buffering capacity of the marine carbonate system, and also a change in environmental conditions of marine organisms, concerning e.g. pH and Ω .

This might affect especially unicellular calcifying organisms like coccolithophores, as they are directly facing the “extracellular fluid” seawater, without the protection of an ‘own’ extracellular fluid, which is buffered and regulated by specialised tissues. If seawater becomes more acidic and Ω decreases, this might hamper calcification, even if it takes place intracellularly like in coccolithophores (3.5).

Future experiments thus have to show in how far these organisms can cope with an ocean, in which conditions, e.g. carbonate chemistry and temperature are changing at an increasing speed (Solomon *et al.*, 2007).

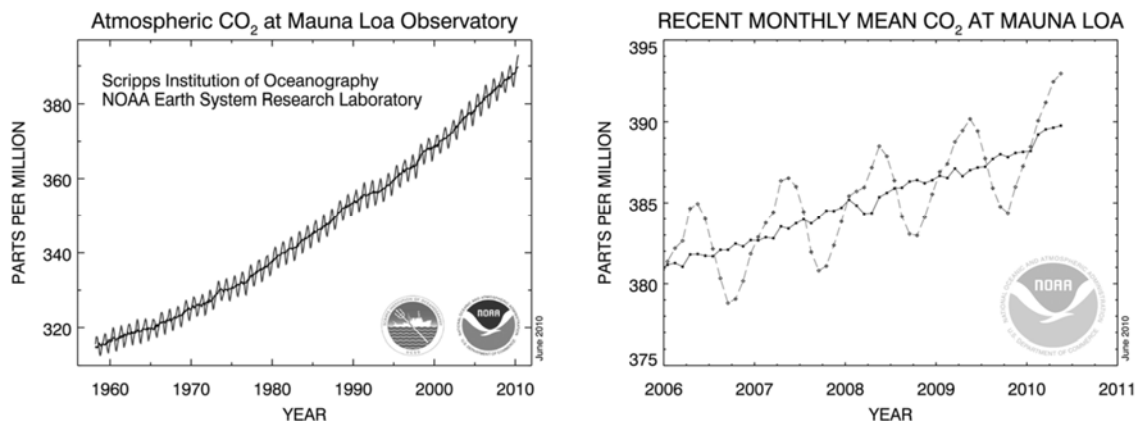


Fig. 2 Long term and recent development of CO₂ concentration in the atmosphere. Long term (left) of atmospheric monthly mean [CO₂] from the 1960s until today. Recent monthly mean is shown at a higher resolution (right). Shown are the annual mean and the seasonal fluctuations, respectively. Source: Dr. Pieter Tans, NOAA/ESRL (www.esrl.noaa.gov/gmd/ccgg/trends)

3.2 Transport across membranes

Carbon is of major importance for organisms. It can be a growth rate limiting factor for some algae, e.g. diatoms (Riebesell *et al.*, 1993). An increase in C thus can fertilise algal growth under certain conditions. On the other hand an increase in C in the form of CO₂* in the marine environment can also be threatening, as it leads to a decrease in pH and thus might impede calcification (see 3.1).

To gain a better understanding of the predominant effect of an increasing [CO₂] in the oceans on single celled calcifying algae it is therefore necessary to understand the essential processes of C handling on a cellular level.

All cells are surrounded by a plasma membrane consistent of a lipid bilayer in which different structural and functional proteins are embedded. This membrane acts as a boundary against the environment, and all elements essential for the formation and maintenance of cells have to overcome this protecting layer.

Membrane permeability for substrates depends on size and charge of the species to be transported, the lipid composition, and, in addition, on the expression of functional membrane proteins like ion channels, transporters, and pumps.

3.2.1 Diffusion

Lipophilic substances, e.g. gases like CO₂ or lipids, can freely diffuse across a membrane. The diffusion flux is dependent on the concentration gradient and on membrane permeability:

$$J = -D \frac{\Delta\Phi}{\Delta X} \quad \text{Eq. 4}$$

- J** diffusion flux in [(amount of substance) length⁻³]
- D** diffusion coefficient in [length⁻² time⁻¹]
- Φ** concentration in [(amount of substance) length⁻² time⁻¹]
- X** length

Diffusion is considered the principal transport process for gases in small organisms, and it is also the principle for gas exchange, e.g. CO₂ vs. O₂.

Membrane permeation of charged substances or larger molecules requires facilitation by membrane proteins.

3.2.2 Facilitated transport via proteins

3.2.2.1 Facilitated diffusion (ion channels)

Diffusion can be facilitated by integration of a functional protein, such as a channel, into the membrane. Channel proteins are forming selective pores and allow the flux of highly hydrophilic, charged substrates, e.g. ions. Transport can only take place following a given gradient, however the transport capacity is high compared to transporters or pumps and can reach up to several million ions per second (Aidley & Stanfield, 1996). Also CO₂ diffusion can be facilitated, e.g. by aquaporins (Endeward *et al.*, 2006; Nakhoul *et al.*, 1998).

3.2.2.2 Primary active transport

If gradients are to be build up or substances have to be transported against their (electrochemical) gradient, energy consuming but very effective primary active transport can be used. For this 'uphill' transport ATPases, 'ion pumps', are used, e.g. the ubiquitously distributed Na⁺K⁺-ATPase. This protein, by transporting 3 Na⁺ ions outside and 2 K⁺ ions inside during one cycle, generates an electrical as well as a chemical gradient (in more detail see 3.3), which can then be further used for secondary active transport.

3.2.2.3 Secondary active transport

Transport of substances against a given gradient needs energy. Alternatively to primary pump activity an existing gradient of another substrate can be used as the driver. This concept of secondary active transport is found in many cotransporters and exchangers.

3.2.2.3.1 Transporters

In contrast to pumps, transporters use the gradient built up for a certain ion to transport other ions or substrates against their gradient. This can be either in the same (cotransporter) or in the opposing direction (antiporter), and for one ion different principles can be used.

Especially the steep gradients for the ions Na⁺, K⁺, and Cl⁻ are thereby most efficiently used to shuttle other substances across the plasma membrane (see also 3.4 for more detail).

Unfortunately, composition of membrane lipids, membrane proteins, and electrical properties are hardly characterised in *E. huxleyi*, and only slightly better in *C. pelagicus* (Taylor & Brownlee, 2003).

3.3 Electrophysiological properties of plasma membranes

The plasma membrane as a lipid bilayer is nearly impermeable for ions, and acts as a capacitor with high electrical resistance. In electrophysiology ions are the charge carriers, and if a chemical gradient is built up and combined with a selective ion conductance (e.g. an ion channel) an electric voltage across the plasma membrane is generated. For a single ion species X this voltage is the Nernst equilibrium voltage (E_x) which can be calculated if internal and external concentrations for an ion are known.

$$E_x = -\frac{RT}{zF} \ln \frac{[X]_i}{[X]_e} \quad \text{Eq. 5}$$

R	universal (ideal) gas constant (8.314472 J K ⁻¹ mol ⁻¹)
T	absolute temperature in K (0K = -273 °C)
z	valence
F	Faraday constant (9.64853399 · 10 ⁴ C mol ⁻¹)
P	permeability coefficient for the respective ion
X _e	extracellular concentration of ion x
X _i	intracellular concentration of ion x

For example we can calculate E_{K^+} and E_{Cl^-} for a marine single celled organism with assumed intracellular concentrations for $[K^+]_i$ of 100 mmol l⁻¹ and $[Cl^-]_i$ of 10 mmol l⁻¹, living in seawater at $[K^+]_e$ of 10 mmol l⁻¹ and $[Cl^-]_e$ of 546 mmol l⁻¹. At a temperature of 17°C (290.16 K) E_{K^+} is -58 mV and E_{Cl^-} is -100 mV.

If several ion channel types are present in the membrane the potential is dependent on the type and permeability of all channels, as defined in the Goldman-Hodgkin-Katz voltage equation (here for N monovalent cationic (C) and M monovalent anionic (A) species):

$$E_m = -\frac{R \cdot T}{z \cdot F} \ln \left(\frac{\sum_i^N P_{C_i^+} [C_i^+]_e + \sum_j^M P_{A_j^-} [A_j^-]_i}{\sum_i^N P_{C_i^+} [C_i^+]_i + \sum_j^M P_{A_j^-} [A_j^-]_e} \right) \quad (\text{mV}) \quad \text{Eq. 6}$$

This formula can be simplified for the most important monovalent ions:

$$E_m = -\frac{R \cdot T}{z \cdot F} \ln \left(\frac{P_K [K^+]_i + P_{Na} [Na^+]_i + P_{Cl} [Cl^-]_e}{P_K [K^+]_e + P_{Na} [Na^+]_e + P_{Cl} [Cl^-]_i} \right) \quad (\text{mV}) \quad \text{Eq. 7}$$

R	universal (ideal) gas constant (8.314472 J K ⁻¹ mol ⁻¹)
T	absolute temperature in K (0 K = -273 °C)
z	valence
F	Faraday constant (9.64853399 · 10 ⁴ C mol ⁻¹)
P	permeability coefficient for the respective ion
e	extracellular
i	intracellular

If permeabilities are translated into conductances and expressed as a fraction of the whole cell conductance, membrane voltage can be calculated by a further simplified and more intuitive version of the Goldman-Hodgkin-Katz equation. It also includes divalent ion species and is based on:

$$E_m = f_{K^+} \cdot E_{K^+} + f_{Na^+} \cdot E_{Na^+} + f_{Cl^-} \cdot E_{Cl^-} + \dots + f_n \cdot E_n \quad (\text{mV}) \quad \text{Eq. 8}$$

f is defined as

$$f_n = \frac{G_n}{G_m} \quad \text{with} \quad \sum f_n = 1 \quad (\text{nS}) \quad \text{Eq. 9}$$

G _n	conductance of the respective ion channel population
G _m	conductance of the entire membrane

Generally the resting V_m is between -60 to -100 mV inside cells, and mostly defined by E_{K+} and / or E_{Cl-}, based on the Nernst potential for the respective ions (E_x) and the ion's fractional conductivity (f). Additional opening of e.g. Na⁺ or Ca²⁺ channels, as they possess positive Nernst equilibrium potentials, will therefore depolarise the plasma membrane, additional opening of K⁺ and Cl⁻ channels will stabilise or even hyperpolarise the plasma membrane. Virtually all cells possess Na⁺K⁺-ATPases and build up a strong gradient for both Na⁺ and K⁺ ions (see 3.2.2.2). In mammalian cells the activity of the Na⁺K⁺-ATPase is an electrogenic process (3 positive charges out, 2 in) and therefore contributes to V_m by around -5 mV. The main effect of Na⁺K⁺-ATPases, however, is the establishment and maintenance of (more or less steep) ion gradients.

Membrane voltage and fractional ion conductances are experimentally accessible by the patch clamp technique. It allows electric measurements of a cell after formation of a tight connection (gigaseal) of a glass electrode with the plasma membrane (for details see 4.6.1). For this, clean protoplasts, cells without remnants of a cell wall, are needed. In the case of unicellular algae with a tight surrounding of unknown composition, and presumably two cell membranes, this becomes a considerable challenge. Nevertheless, since electrogenic processes are most likely involved in H^+ handling we aimed to establish electric measurements in *E. huxleyi*.

3.4 Acid Base homeostasis on a cellular level

A constant pH_i is important for organisms, as metabolic processes to a great extent are pH dependent. Function of enzymes, folding of proteins, and function of channels, which again influence the V_m , are some of the main processes directly dependent on the pH, to name only a few. The challenge is, that cells are exposed to pH fluctuations, as they continuously produce H^+ and also the pH in their environment can be subject to change. To maintain a constant pH_i , or better, to minimise pH fluctuations, cells have to overcome these challenges.

i) Cells need a sufficient buffer capacity, a combined buffer system. This has the advantage that different buffer pairs contribute by their pK at different pH values. As buffering powers are additive, the pH range and the order of magnitude that can be buffered are extended. For example an open buffer system as the carbonate buffer (buffering between 6.2 - 8.6) is often combined with the buffering capacity of proteins. Proteins as huge amphoteric molecules buffer by their amino acids with several $-COOH$, $-NH_2$, and imidazole side chains and form a significant part of the intracellular buffer.

The pH in a buffered solution can be calculated according to Henderson-Hasselbalch:

$$pH = pK + \log \frac{[A^-]}{[HA]} \quad e.g. \quad pH = pK + \log \frac{[protein^-]}{[H^+ \text{ protein}]} \quad \text{Eq. 10}$$

ii) cells need the ability for pH sensing, and the respective signal transduction pathways. It is not completely clear how this functions, but it is well known that certain membrane proteins are involved in pH homeostasis. pH sensitive ion channels (Boron, 2004) are directly functioning as pH sensors and translate the

signal into changes of V_m . Also some H^+ transporters can sense (intracellular) pH, and directly translate pH into H^+ transport. In addition, there are also presumably sensors for increased extracellular CO_2 or HCO_3^- (Boron, 2004).

iii) cells need acid base transport, or in other words 'acid extruders and loaders'.

They can either

- i) try to prevent H^+ from entering the cells, by becoming less permeable,
- ii) transport the protons out, or
- iii) buffer them inside the cell.

The use of ATP-driven pumps, to either extrude H^+ alone or in exchange for e.g. K^+ , is the most expensive way to control pH homeostasis (in terms of cell energy metabolism), however, this is highly efficient and allows large H^+ gradients. Other acid extruding systems are ion coupled cotransporters or antiporters, such as the Na^+/H^+ exchanger, the Na^+ driven Cl^-/HCO_3^- exchanger or the Na^+/HCO_3^- cotransporter, which use the existent Na^+ gradients to either extrude H^+ or take up HCO_3^- to buffer H^+ . This buffering effect can be increased by carbonic anhydrase (CA) which enhances the following reaction:



The direction of the reaction depends on the different concentrations and could be used to produce CO_2 , which is then again either metabolically used (e.g. in photosynthesis) or diffuses out of the cell again, as the carbonate buffer is an open system. The localisation of a CA plays a crucial role for their function in pH homeostasis. There are extracellular and intracellular CA isoforms and some are expressed in the direct proximity to other transporters which themselves remove then one reaction partner (transport metabolon).

Acid base homeostasis on a cellular level is relatively well understood in mammalian tissues.

Fig. 3 shows transporters most important in pH homeostasis. Cells express different combinations of these transporters and pumps in a purpose or organ specific manner. Of course, this is only an excerpt, in nature there are many more, and most likely there are numerous unknown system to be unravelled.

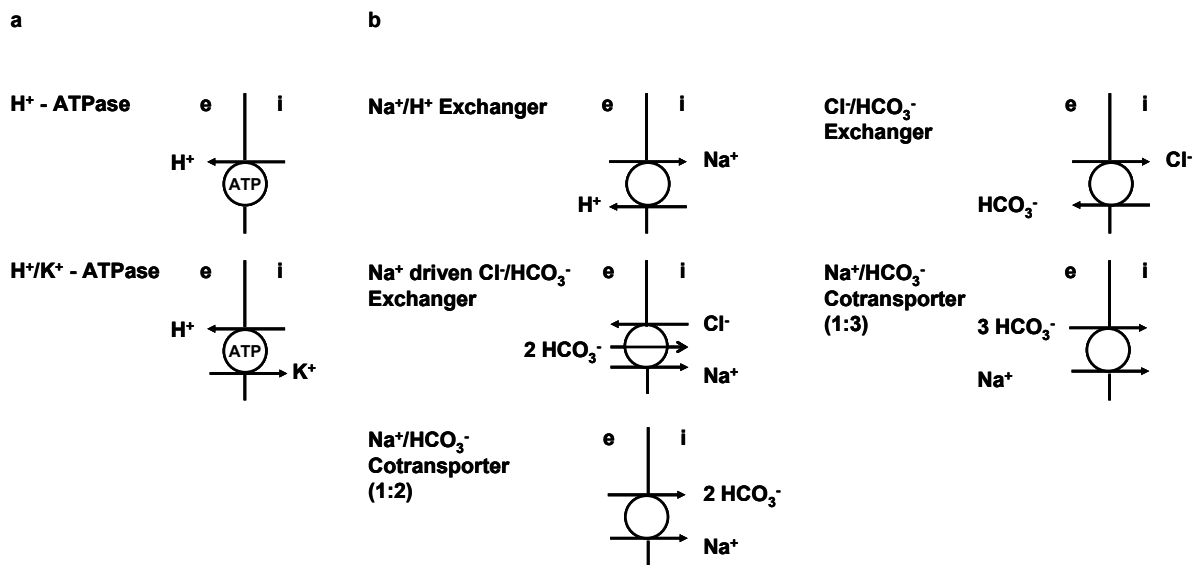


Fig. 3 Compilation of a) ion pumps and b) transporters used in cellular pH homeostasis. e external; i internal

As an example of how pH homeostasis and high transport rates can be combined and controlled in a concerted interplay of different transporters Fig. 4 shows the cell model of a type A intercalated cell in the collecting duct of a nephron.

The task of these cells is H^+ secretion to the lumen and HCO_3^- recovery to the blood. CO_2 passively diffuses into the cell from the basolateral side. There, accelerated by CAII, it reacts with H_2O , to form HCO_3^- and H^+ (according to Eq. 11). A Na^+/HCO_3^- cotransporter (NBC3) is used for additional uptake of HCO_3^- from the lumen. Protons are then extruded to the lumen by H^+ - and H^+/K^+ -ATPases, and HCO_3^- is transported towards the blood by use of Cl^-/HCO_3^- exchangers (AE1).

There are a number of general principles involved in pH regulation and its adaptation. H^+ homeostasis is assured on a short term basis by

- i) pH dependent open permeability and transport rates of membrane proteins themselves,
- ii) modification on the level of protein expression by defining the type and number of transporters by membrane trafficking

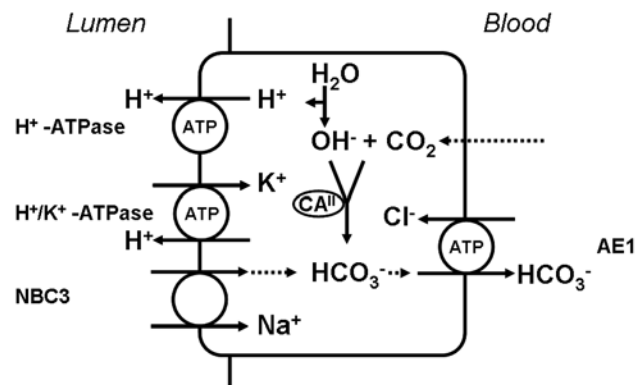


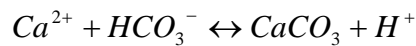
Fig. 4 Cell model of an acid secreting type A intercalated cell. This cell type is found in the collecting duct of a nephron (redrawn after M. Bleich).

- iii) phosphorylation or dephosphorylation of proteins, impacting their functional state.
- iv) modification of V_m , impacting directly the electric driving force of H^+ transport or the structure of voltage sensitive transport proteins.

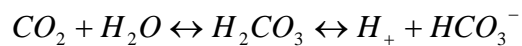
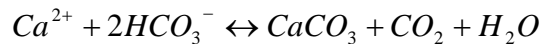
Slower mechanisms include adaptive processes of cells by

- v) regulation of transcription and translation.

All these mechanisms are designed to keep pH_i in a narrow range to protect the cell. However, cells can be subject to severe disturbances in either intracellular or extracellular pH. Actually, this might be the normal situation rather than the exception, as cells produce H^+ in several metabolic processes. Coccolithophores can produce H^+ in significant amounts during calcification. The Ca^{2+} concentrations needed for calcite precipitation were calculated to be between $100 \mu\text{mol l}^{-1}$ (at an intra-coccolith vesicle pH, pH_{CV} , of 8.0) and 10mmol l^{-1} (pH_{CV} of 7.0, respectively), dependent on the pH_{CV} (Anning *et al.*, 1996). As protons are produced in a 1:1 stoichiometry with the Ca^{2+} used during calcification (see Eq. 12), this results in high fluxes of H^+ which the cells have to cope with.



or



Eq. 12

It is an arising question in this regard, whether there is a difference for the cells depending on whether pH_e or pH_i is affected by H^+ challenges: If pH_e decreases, the gradient for H^+ extrusion is decreased, resulting in decreased driving forces. One of the basic questions I wanted to investigate in my studies is whether this causes problems for H^+ extrusion.

3.5 Coccolithophores *Emiliana huxleyi* and *Coccolithus pelagicus*

3.5.1 Coccolithophores

Both model organisms used in our experiments, *E. huxleyi* as well as *C. pelagicus*, are small calcifying marine nanoplankton, and belong to the phylum Haptophyceae, subclass Prymnesiophycidae (Guiry & Guiry, 2010). The species of the orders *Isochrysidales* (*E. huxleyi*) and *Coccolithales* (*C. pelagicus*) are also referred to as

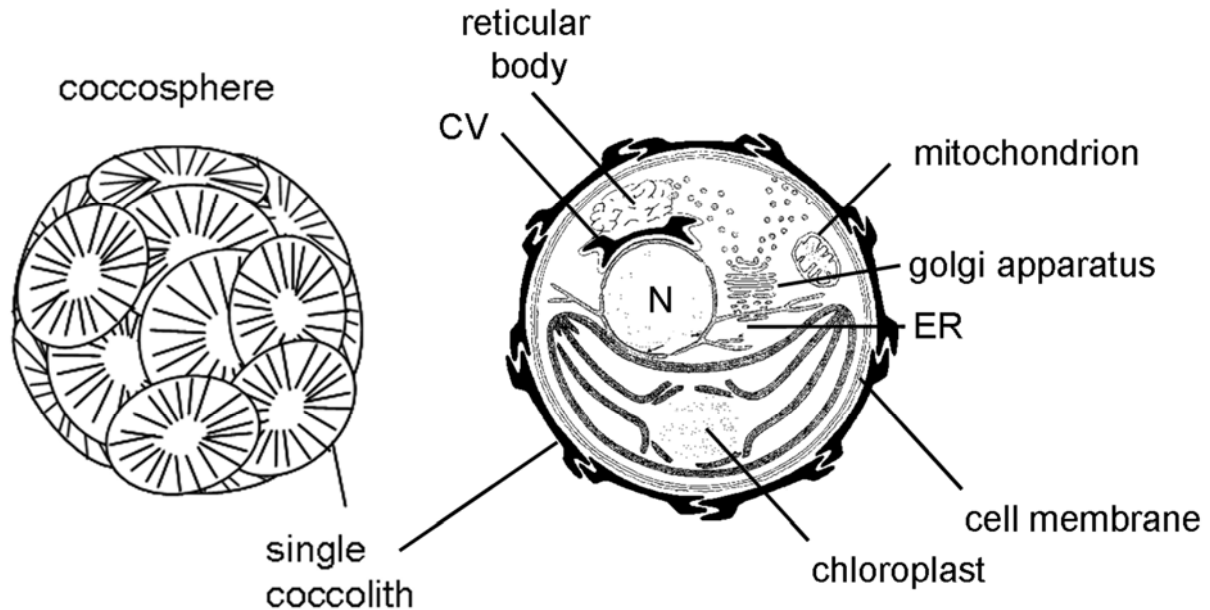


Fig. 5 Schematic drawings of a coccosphere (left) and a section through an *E. huxleyi* cell (right).

Section redrawn after Westbrook, <http://www.noc.soton.ac.uk/soes/staff/tt/eh/cell.html>.

coccolithophores (see Table 1). They are calcite producing flagellates and build polysaccharide scales and in addition calcite plates, so called coccoliths. These coccoliths are composed of calcium carbonate on an organic template matrix in a species specific manner, and are surrounding the cells as a so called coccosphere (Fig. 5).

The coccosphere can be built of holo or hetero coccoliths. Holo coccoliths are usually biomineralised from idiomorph calcite crystals outside the cell, whereas formation of hetero coccoliths occurs intracellularly in so called coccolith (forming) vesicles (CV, Fig. 5), derived from the golgi apparatus. Both species can form hetero coccoliths, which show an elaborate radial disc-like structure, unique for the respective species. The completed coccolith is finally extruded to the coccosphere by exocytosis.

Table 1 Classification of *E. huxleyi* and *C. pelagicus* according to Guiry & Guiry (2010)

Classification:	<i>Emiliana huxleyi</i>	<i>Coccolithus pelagicus</i>
Empire	Eukaryota	Eukaryota
Kingdom	Chromista	Chromista
Subkingdom	Chromobiota	Chromobiota
Infrakingdom	Haptista	Haptista
Phylum	Haptophyta	Haptophyta
Class	Prymnesiophyceae	Prymnesiophyceae
Subclass	Prymnesiophycidae	Prymnesiophycidae
Order	Isochrysidales	Coccolithales
Family	Noëlaerhabdaceae	Coccolithaceae
Genus	Emiliana	Coccolithus

3.5.2 *Emiliana huxleyi* & *Coccolithus pelagicus*

Emiliana huxleyi is the most abundant and cosmopolitan calcifying phytoplankton on earth (Paasche, 2002). It is known to be existent in at least three different cell forms: The coccolith forming immotile C-, the naked immotile N-, and the scaly S-cell form, possessing two flagella. The C morphotype is the generally reported one in the field, with a diameter of 4-5 μm , and found throughout the euphotic zone from cold temperate to tropical waters (Westbroek *et al.*, 1993). It is known to form extensive monospecific blooms covering up to 250,000 km^2 (Balch *et al.*, 2010; Holligan *et al.*, 1983) or annually up to 1.4 million km^2 in total (Brown & Yoder, 1994). It was calculated to be responsible for the production of ca. 50% of calcite on earth (Broecker & Clark, 2009; Westbroek *et al.*, 1989).

C. pelagicus is an always immotile, flagella free species, with a considerably larger mean diameter of $\sim 10 \mu\text{m}$. The larger size is one of the reasons making it a typical laboratory coccolithophore used in many studies - especially in electrophysiology.

3.5.3 Current knowledge on physiology

In the following passages the current knowledge about physiology of these two coccolithophores is summarised. Some findings are general for coccolithophores; others are specific for the respective species. All together, relatively little is known about these organisms' physiology on a cellular level.

3.5.3.1 Internal ion concentrations

Intracellular and especially cytosolic ion concentrations are essential for the calculation of ion gradients and modelling of transport mechanisms.

For *E. huxleyi* published data are summarised in Table 2. The paper by Ho *et al* (2003) also gives elemental quotas (not shown), however not for key players of V_m and coupled transport like Cl^- or Na^+ (see 3.2). Cell homogenate data differ significantly from cytosolic concentrations since they include particulate and compartmentalised matter.

3.5.3.2 DIC uptake and fixation in coccolithophores

Calcification as one of the two main metabolic processes is related to photosynthesis, acid-base metabolism, and the supply of DIC (Paasche, 2002). The same applies for photosynthesis.

Table 2 Ion concentrations of *E. huxleyi* compared to typical algal ion concentrations
a) Cell homogenate (Ho et al., 2003) and cytoplasm concentrations in comparison to cytoplasmic algal ion concentrations (Stewart, 1974).
b) Cell homogenate concentrations (Ho et al., 2003) continued

a	E. huxleyi	Alga	E. huxleyi		b	E. huxleyi
	cell [*1]	cytoplasm [*2]	cytoplasm	ref		cell [*1]
	mmol l ⁻¹	mmol kg ⁻¹ H ₂ O	mmol l ⁻¹			mmol l ⁻¹
K ⁺	110	up to >400	100-200	[*9]	C	31000
			261-322	[*6]		10000 #
Mg ²⁺	18	6			N	1200
Ca ²⁺	19000	10 ⁻⁴ - 10 ⁻⁶	10 ⁻⁴	[*5]	P	130
Na ⁺		up to 60	30	[*9]	S	100
H ⁺		10 ^{-7.0} - 10 ^{-7.3}	10 ^{-7.0}	[*5,7,8]	Sr	44
Cl ⁻		80-150 [*3]	130	[*9]	Fe	0.46
HCO ₃ ⁻		10	0.3-0.5	[*5]	Mn	0.94
V _m [mV]			-60	[*4,5]	Zn	0.05
					Cu	0.0089
					Co	0.039
					Cd	0.048
					Mo	0.0029

*1 Ho T-Y et al 2003, cell homogenate *5 Brownlee et al, 1994
*2 Stewart WDP, 1974 *6 Sikes & Wilbur, 1982
*3 Gorham & Wyn Jones, 1983 *7 Anning et al, 1995
Robinson & Downton, 1985 *8 Dixon et al, 1988
*4 Nimer & Merrett, 1991 *9 Brownlee et al, 1995

Data from HCl treated samples

DIC uptake

A lot of the research has focussed on which inorganic carbon species is used as a substrate for calcification and photosynthesis in *E. huxleyi* (Paasche, 2002). While there is good evidence of existing interactions between the two processes (Buitenhuis *et al.*, 1999; Paasche, 1968a) and while it is generally accepted that HCO₃⁻ can be used as a substrate for calcification, the C species taken up for photosynthesis remains a subject of discussion (Brownlee & Taylor, 2004; Paasche, 2002). In the currently most accepted model HCO₃⁻ can be used as a C source for photosynthesis as well as CO₂ (Buitenhuis *et al.*, 1999; Sikes & Wilbur, 1982). The involvement of calcification in photosynthetic carbon acquisition has been discussed controversially (e.g. Paasche, 2002; Rost & Riebesell, 2004; Young, 1994).

Calcification is handled as an alternative to a classical CCM (carbon concentrating mechanism) for photosynthesis by shifting the equilibrium towards CO₂ (Anning *et al.*, 1996). Nevertheless, more recent results come to the conclusion that calcification and photosynthesis are not closely coupled (Balch *et al.*, 1996; Herfort *et al.*, 2002; Herfort *et al.*, 2004; Leonardos *et al.*, 2009; Rost *et al.*, 2002; Trimborn *et al.*, 2007) as was already postulated by Paasche (1968a).

Results from isotope disequilibrium experiments and the MIMS (Membrane Inlet Mass Spectrometry) approach led to the view of *E. huxleyi* mainly being a HCO_3^- user (Rost *et al.*, 2007; Trimborn *et al.*, 2007). It is relatively well-established that HCO_3^- is the major source of carbon for both photosynthesis (e.g. Paasche, 1964; Nimer & Merrett, 1992; Buitenhuis *et al.*, 1999) and calcification in *E. huxleyi* (Buitenhuis *et al.*, 1999; Paasche E., 1964; Sikes *et al.*, 1980); however the precise mechanisms of uptake remains unidentified (Herfort *et al.*, 2002). Brownlee & Taylor (2004) thus state that there might be significant plasticity with respect to carbon acquisition mechanisms.

It is an ongoing discussion and for a more detailed discussion the interested reader is referred to recent reviews (Brownlee & Taylor, 2004; Paasche, 2002).

Carbon fixation in photosynthesis

As in other algae the primary carbon fixation process in *E. huxleyi* is CO_2 dependent since it is mediated by the enzyme RubisCO (ribulose-1,5-bisphosphate carboxylase/oxygenase) in the Calvin-Benson Cycle, producing C_3 compounds. An active anaplerotic β - carboxylation reaction producing C_4 compounds was also found to be concomitantly operating in *E. huxleyi* (Tsuji *et al.*, 2009).

E. huxleyi were found to have a comparatively low affinity for CO_2 (Nimer & Merrett, 1992). At the low $[\text{CO}_2]$ in today's ocean they are thus believed to be carbon-limited (Riebesell, 2004). The organism was also found to have a relatively inefficient photosynthesis. It was proposed that this could be partly explained by a high leakage for CO_2 , as up to two thirds of the DIC taken up are lost again by CO_2 diffusion (Rost *et al.*, 2006).

Carbonic Anhydrase

E. huxleyi was shown to possess a chloroplast CA (Nimer *et al.*, 1994b; Quiroga & Gonzalez, 1993) and evidence was presented indicating that transcripts of these isozymes are differentially expressed during cell cycle and growth phases (Quinn *et al.*, 2006; Soto *et al.*, 2006).

Only low external CA activities have been observed in *E. huxleyi* under various conditions (Rost *et al.*, 2003; Rost *et al.*, 2006), and results on extracellular CA remain contradictory (Elzenga *et al.*, 2000; Nimer *et al.*, 1994b). This might be

caused by strain specific differences (Elzenga *et al.*, 2000) or by CA dependence on low CO₂ and HCO₃⁻ concentrations (Herfort *et al.*, 2004; Miao & Wu, 2002).

3.5.3.3 Membrane permeability & transport proteins

It is of special interest for pH homeostasis by which mechanisms the cell provides and regulates cell membrane permeability to CO₂, HCO₃⁻ and H⁺.

As mentioned above membrane permeability for a substrate depends on the lipid composition and in addition on the functional expression of membrane proteins like ion channels, transporters, and pumps. Unfortunately, composition of membrane lipids, membrane proteins, and electrical properties are hardly characterised in *E. huxleyi* or *C. pelagicus* likewise.

In *E. huxleyi* CO₂ permeability (Nimer *et al.*, 1992; Rost *et al.*, 2006) and a HCO₃⁻ transport pathway have been suggested.

Concerning HCO₃⁻ transport there are two controversial studies on the role of Cl⁻/HCO₃⁻ exchange using pharmacological tools. Nimer *et al.* (1996) did not find a DIDS (4,4'-Diisothiocyanatostilbene-2,2'-disulfonic acid) sensitive HCO₃⁻ transport in exponentially growing cells. Results by Herfort *et al.* (2002) suggest the existence of a HCO₃⁻ exchanger sensitive to DIDS and the related substance SITS (4-Acetamido-4'-isothiocyanato-stilbene-2,2'-disulfonic acid). Altogether, transport of HCO₃⁻ remains a controversial discussion (Brownlee & Taylor, 2004; Herfort *et al.*, 2002; Nimer *et al.*, 1996; Paasche, 1968b; Paasche, 2002).

For *C. pelagicus* an attractive hypothesis on Ca²⁺ handling for calcification has been generated. In this model the limited space between plasma membrane and the closely attached endoplasmic reticulum is used to shuttle Ca²⁺ through the cytosol without threatening the normally very low cytosolic Ca²⁺ activities (Berry *et al.*, 2002).

In the meantime the *E. huxleyi* genome has been sequenced (<http://genome.jgi-psf.org/Emihu1/Emihu1.home.html>) and thus gene expression analysis (Soto *et al.*, 2006; von Dassow *et al.*, 2009) allows data mining for several genes which could code for candidate proteins involved in membrane permeability for CO₂, HCO₃⁻ and H⁺. Amongst those are aquaporins (Endeward *et al.*, 2006), a variety of HCO₃⁻ - or H⁺ coupled transporters (Boron *et al.*, 2009; Scheel *et al.*, 2005), Ca²⁺ dependent H⁺ transporters and H⁺ channels (Mackinder *et al.*, 2010).

3.5.3.4 Membrane potential & H⁺ gradient

There are no direct electrophysiological measurements of the membrane potential in *E. huxleyi*.

Calculations were done according to Nernst (for details see 3.3) based on either assumptions of pH_i (Dixon *et al.*, 1989) or the distribution of membrane potential probe [³H]TPP⁺ (tetraphenylphosphonium) between cells and medium at a pH_e of 8.0 (Nimer & Merrett, 1992), however in a non-calcifying strain. These approaches resulted in a V_m of -60 mV.

Sikes & Wilbur (1982) estimated V_m with two different methods. Using the dye dis-C3-5 (3,3' - Dipropylthiadiazocarbocyanine iodide) after treatment with valinomycin V_m resulted in -81 mV. Calculations based on intracellular (derived from extracted cellular water) and extracellular [K⁺] resulted in a V_m of -145 mV. All these approaches have different problems: They are either based on relatively vague internal concentrations. Or they are interfering with the V_m itself, directly. Or they interfere indirectly with V_m by influencing e.g. ATP concentration in the cytoplasm, also resulting in changes of the V_m. (Johnstone *et al.*, 1982; Ritchie, 1984; Ritchie, 1999).

Membrane potential in *C. pelagicus* was shown to be between -30 and -60 mV by direct patch clamp measurements. (Taylor & Brownlee, 2003)

The proton electrochemical gradient at a membrane voltage of -60 mV has been calculated to be -19 mV for *E. huxleyi* (Nimer *et al.*, 1994a) according to:

$$\Delta\mu H^+ = E_m + 58 (pH_e - pH_i) = (-60) + 58 (8 - 7.3) = -19mV \quad \text{Eq. 13}$$

This means a relatively small driving force for H⁺ into the cell. Of course these values are variable and depend on the overall activity of all electrogenic transport systems within the cell membrane, which are mainly unknown. Membrane properties and ionic conductances in *C. pelagicus* were investigated by Taylor & Brownlee (2003). A voltage dependent and DIDS inhibitable Cl⁻ current was shown. Also a voltage activated H⁺-conductance is discussed in *C. pelagicus* (Alison R. Taylor, pers. comm.).

3.5.3.5 pH_i in *E. huxleyi*

Concerning pH there are three datasets on the measurement of pH in *E. huxleyi*, reporting a pH integrated for the whole cell between 6.77 ± 0.31 for a low calcifying

strain and 7.29 ± 0.11 for a high calcifying strain (Dixon *et al.*, 1989; Nimer *et al.*, 1994a). In other studies pH for the cytosol was reported to be around 7.0 (Anning *et al.*, 1996; Dixon *et al.*, 1989), pH of the chloroplast 8.0 (Anning *et al.*, 1996), and pH of the coccolith vesicle was measured to be 7.1 ± 0.3 . At a seawater pH of ~ 8.1 the respective H^+ gradient across the plasma membrane is about one order of magnitude. This might reflect either high cytosolic H^+ production at a limited export capacity, or H^+ uptake mechanisms driven by ion gradients or membrane voltage.

3.6 Thesis outline

The experimental studies described in this thesis have been conducted at the Institute of Physiology, CAU Kiel in collaboration with the Leibniz Institute of Marine Sciences (IFM-GEOMAR) in Kiel. The studies were done within the framework of the excellence cluster 'Future Ocean', funded by the DFG.

The overarching theme of the excellence cluster is to improve the restricted knowledge about the current state of the ocean and to gain more knowledge about potential changes in marine systems, and the impact of these changes on physical and biological parameters and variables.

One interest subsidiary to this overarching theme is the investigation of the effect of ocean acidification on marine organisms. It is known by now that the conditions, especially in the surface ocean, and especially in the polar regions, are changing at a fast pace. However, it is known to a much lesser extent, in how far certain organisms might be affected by these changes.

Thereby the effect of changing pH and carbonate chemistry on the organisms can only be projected well if the basic properties like ion transport and pH homeostasis, as well as the adaptive potential are known.

The aim of this thesis therefore was to elucidate some basic properties of ion transport and pH homeostasis in the calcifying unicellular alga *E. huxleyi*. For this, already existing techniques in the physiological department of the medical faculty of the CAU, Kiel were adapted and extended to study marine unicellular photosynthetic organisms.

Here, the experimental studies focussed mainly on pH homeostasis investigated by microfluorimetric measurements.

Results are structured into methodological achievements and achieved measurements. They are presented for microfluorimetric pH_i measurements in *E. huxleyi*, and electrophysiological measurements in *C. pelagicus*.

In the first part of the discussion (6.1) general aspects are discussed. Secondly I discuss different techniques which were tested and applied in order to investigate basic principles in the model organisms (6.2). The techniques involve culture

conditions, microfluorimetry, scanning electron microscopy, the out of equilibrium method and electrophysiology.

In the third part I present effects of manipulated external ion gradients and pharmacological inhibitors on membrane permeabilities of *E. huxleyi*, indicated by changes in pH_i (6.3).

In the fourth part results from electrophysiology in *C. pelagicus* are discussed (6.4).

Finally I synthesise the results and putative transport systems involved in pH homeostasis and present an outlook on further use of the methods established during this thesis (6.5).

Part of the data has been formed into a manuscript and is currently undergoing the review process. In this manuscript I present the new perspective on permeabilities of H^+ , CO_2 , and HCO_3^- and their impact on intracellular pH. This is a first step in understanding mechanistic links between ocean acidification and metabolism in *E. huxleyi*.

The general hypothesis of this thesis was that coccolithophores as calcifying organisms should control their pH_i relatively thoroughly, as the calcification processes are strongly pH dependent. However, little is known about physiological processes in these organisms on a cellular level.

My contribution to these burning questions is some first insight into cellular pH regulation and possibly adaptive mechanisms in *E. huxleyi*. These first results might help in answering the question in how far and to what extent this unicellular calcifying organism might be affected by changes in the marine carbonate system.

4 MATERIALS AND METHODS

4.1 Solutions

4.1.1 Artificial seawater solutions (1-3)

Artificial seawater (ASW) solutions were designed after (Zeebe & Wolf-Gladrow, 2001), giving typical concentrations of the major components in seawater. The carbonate system was chosen according to concentrations at typical conditions (see 3.1). Osmolality and salinity were chosen according to measurements of natural seawater (NSW). All experimental solutions (Table 3) were adjusted to an osmolality of 1070 ± 10 mosm kg^{-1} , either at the expense of NaCl or by addition of Na-Gluconate. Osmolality was measured with an automatic cryoscopic osmometer (Osmomat 030, Gonotec GmbH, Berlin, Germany). pH, if not indicated otherwise, was 8.08 ± 0.05 . Calculations for the carbonate system were performed using

Table 3 Artificial seawater solutions (1-3)

ASW solutions were designed according to values of pH, osmolality and salinity measured in North Sea water. Standard seawater composition was modified after Zeebe & Wolf-Gladrow (2001). All solutions were allowed to equilibrate and, if necessary, adjusted to the exact pH at 20°C (NaOH or HCl).

[mmol kg^{-1}]	Seawater	1 ASW _{culture}	2 ASW _C	3 ASW _{strip}
Na ⁺	469	491	491	435
K ⁺	10	10	10	10
Mg ²⁺	53	52	52	49
Ca ²⁺	10	10	10	0
Sr ²⁺	0.09	0.09	0	0
Cl ⁻	546	530	531	541
SO ₄ ²⁻	28	27	27	0
Br ⁻	0.84	0.80	0	0
F ⁻	0.07	0.07	0	0
H ₃ BO ₃	0.42	0.41	0	0
HCO ₃ ⁻	---	2.3	2.3	1.9
HEPES	---	0	0	0
Gluconate	---	37	37	0
EGTA	---	0	0	24
<i>calculated values (CO2SYS)</i>				
HCO ₃ ⁻	2.03	2.14 ± 0.01		1.80
CO ₃ ²⁻	0.25	0.19 ± 0.02		0.19
CO ₂	0.01	0.02 ± 0.00		0.01
pCO ₂ [µatm]	400	592 ± 60		363
pH	8.1	8.08 ± 0.03		
Osmolality	1070	1070 ± 10		
Salinity	35	35 ± 1		

CO2SYS (Lewis & D.W.R.Wallace, 1998), based on pH measurements and total carbon. Dissociation constants (K_1 , K_2) for carbonic acid were taken from Roy *et al.* (1993), $K_{SO_4^-}$ from Dickson (1990). pH was measured and calculations are given on the NBS scale.

All chemicals were purchased at highest grade of purity from Merck and Sigma, Germany. DIDS was dissolved in Dimethyl sulfoxide (DMSO) at a stock concentration of 0.1 mol l^{-1} and added at a final concentration of 0.1 mmol l^{-1} to the respective experimental solutions, unless indicated otherwise. DMSO did not exceed a concentration of 0.1%. DIDS auto fluorescence did not interfere with BCECF fluorescence at the selected wavelengths.

4.1.2 Modified ASW solutions (4-8)

Modified artificial seawater solutions (Table 4) were designed to change concentrations of single ions, thereby keeping typical concentrations of the other major components in seawater as close as possible. The osmolality was adjusted to be 1070 ± 10 on the expense of Na^+ and/or by addition of gluconate or N-Methyl-D-glucamine (NMDG).

The carbonate system was added in the form of HCO_3^- and the solution was allowed to equilibrate with CO_2 under stirring conditions and assumed to be in the standard equilibrium state thereafter:

Table 4 Modified ASW solutions (4-8)

Solutions were designed to mimic NSW osmolality and pH (if not indicated otherwise). Single ion concentrations were decreased or increased to change physical driving forces over the plasma membrane.

	4	5	6	7	8
	ASW	0 ASW	ASW	ASW	ASW _{Nig}
	HCO_3^-	100 K^+	90 Cl^-	0 Na^+	
[mmol kg^{-1}]					
Na^+	475	460.2	498.8	0.0	436.8
K^+	10	97.4	9.6	9.6	97.4
Mg^{2+}	52	51.9	51.9	51.9	51.9
Ca^{2+}	10	10.1	9.7	10.1	9.7
Cl^-	554	527.3	87.7	561.9	531.5
SO_4^{2-}	27	27.3	27.3	27.3	27.3
HEPES	4.9	0.0	0.0	0.0	4.9
Gluconate	0.0	97.4	487.1	0.0	71.4
NMDG	0.0	0.0	0.0	485.2	0.0
HCO_3^-	0.0	2.3	2.3	2.3	0.0
pH	<i>(as ind.)</i>		8.00 ± 0.1		<i>(as ind.)</i>
Osmolality	10		1070 ± 10		

pH was measured and, if not indicated otherwise, was 8.0 ± 0.1 . No calculations for the carbonate system were performed in solutions 4-8 as the relations between normally conservative ions were not kept constant and thus assumptions in the program were not fulfilled. Nevertheless, the assumption was made that the carbonate system was close to natural conditions in solutions 5-7.

4.1.3 Out of equilibrium solutions (9-10)

OOEs were designed to investigate the effects of either comparatively high $[\text{CO}_2]$ and low $[\text{HCO}_3^-]$, or high $[\text{HCO}_3^-]$ and very low $[\text{CO}_2]$ in an isolated manner at a typical surface ocean pH of 8.0 ± 0.1 . The enzymatically catalysed equilibration of experimental solutions directly at the extracellular surface of the cells was neglected since low external CA activity has been reported (see 3.5.3). No CA inhibitors were applied to avoid dampening of cytosolic reactions in pH homeostasis.

A chemical model of the carbonate system, including all important reactions in seawater together with HEPES (N-2-Hydroxyethylpiperazine-N'-2-ethanesulfonic acid) buffer kinetics was implemented by Kai Schulz according to Schulz *et al.* (2006).

The resulting seven differential equations, were integrated numerically with the

Table 5 Out-of-equilibrium (OOE) solutions (9-10).
OOE solutions a and b were adjusted or aerated to the measured pH value at 20°C. Solutions were generated acutely before application within the experiment.

	9a	9b	9	10a	10b	10
[mmol kg ⁻¹]	High CO ₂		(a+b) OOE	High HCO ₃ ⁻		(a+b) OOE
Na ⁺	484	415	450	563	361	462
K ⁺	10	10	10	10	10	10
Mg ²⁺	52	52	52	0	103	52
Ca ²⁺	10	10	10	0	19	10
Cl ⁻	563	494	528	530	508	519
SO ₄ ²⁻	27	27	27	0	55	27
HEPES	0	63	31.7	0	63	31.7
HCO ₃ ⁻	0	0	0	43	0	21
CO ₂ (%)	5	0	2.4	0	0	0
<i>calculated values</i>						
HCO ₃ ⁻	0.1	0	0.05	10.6	0	20
CO ₃ ²⁻	0	0	0	33.4	0	2
CO ₂	1.72	0	0.86	0	0	0
(%)	5.0	0	2.5	0	0	0
pH	4.90	8.07	8.08	9.24	7.69	8.07
Osmolality	1070±10					
Salinity	35±1					

matlab 'ode15s' solver for 'stiff' problems (Shampine & Reichelt, 1997), and used to calculate the reaction kinetics in carbonate chemistry speciation upon mixing of two different artificial seawater solutions.

Furthermore, the model also allows estimating the degree of disequilibrium at any given point in time and deriving the actual concentrations of $[H^+]$, $[CO_2]$ and $[HCO_3^-]$.

4.1.4 Intracellular solutions (11-13)

Intracellular solutions (IS) were designed to adapt presumed cytosolic concentrations of ions and mimic pH_i (Table 6a). Different compositions were tested.

4.1.5 Enzymatic stripping solution (14)

An enzymatic cocktail (EL, sol.14, Table 6) was tested to produce clean protoplasts. The enzymatic cocktail modified after Lemtiri-Chlieh (2003) was only used with cells prepared for electrophysiological measurements.

10 mU chitinase per 200 μ l highly dense *E. huxleyi* suspension was tested in addition (Chitinase from *Trichoderma viride*, Sigma C8241-25UN).

Table 6 Intracellular solutions (11-13) and enzymatic solution (14)
Solutions were used for electrophysiology (a) and preparation of protoplasts for electrophysiology (b). Solution 14 adapted after Lemtiri-Chlieh et al, 2003.

a				b	
	11	12	13	14	
[mmol kg ⁻¹]	IS _{KS}	IS	IS _{spec}	EL	
				% (w/v)	[mmol l ⁻¹]
Na ⁺	9.9	9.7	0.0	Cellulase	2.5
K ⁺	97.4	97.4	194.9	Pectinase (S)	2.0
Mg ²⁺	4.9	4.9	4.9	Pectolyase	0.026
Ca ²⁺	0.7	0.0	0.0	BSA	0.26
Cl ⁻	11.2	9.7	9.7	CaCl ₂	1
SO ₄ ²⁻	4.9	0.0	0.0	Na-Ascorbat (S)	10
HEPES	0.0	4.9	97.4	pH	6.5 ± 0.05
Gluconate	97.4	107.2	194.9	Osmolality	1070 ± 10
Sorbitol	818.4	812.5	535.9		
EGTA	1.0	4.9	4.9		
ATP	1.0	1.0	0.0		
HCO ₃ ⁻	0.2	0.0	0.0		
pH	7.00 ± 0.2				
Osmolality	1070 ± 10				

4.2 Cell culture

The *E. huxleyi* strain was previously isolated in 2005 during the PeECE III mesocosm study in the Raune Fjord (Norway) and kindly provided by M. N. Müller (Riebesell *et al.*, 2007). *C. pelagicus* (PLY 182G, Plymouth Culture Collection) was kindly provided by Alison R. Taylor.

The *E. huxleyi* cultures were grown in artificial seawater (ASW_{culture},

Table 3) modified from Kester *et al.* (1967), with an initial pH of 8.05 ± 0.05 , and enriched with nutrients according to f/20-Si, modified after Guillard (1975). *C. pelagicus* cultures were grown under the same conditions with higher nutrient concentrations according to f/2.

Nutrients were measured on one occasion at the IFM-GEOMAR with the help of P. Fritsche. PO_4^{3-} , NO_3^- , and NO_2^- were analysed after Hansen & Koroleff (1999) on one occasion to verify nutrient limitation in the sampling time frame.

[DIC] was analysed with a $[\text{CO}_2]_{\text{total}}$ analyser (Corning 965, Ciba Corning Diagnostics Ltd, GB) on different occasions to verify the state of the carbonate system, especially in the OOE solutions (Data not shown).

Cells were exposed to daylight (Osram Lumilux L 18W/950 Color Proof Daylight G13) in a simulated diurnal cycle (Fig. 6) with a maximum photosynthetically active radiation (PAR, 400-700 nm; QSL-2101, Biospherical Instruments) of $170 \mu\text{mol photons m}^{-2} \text{ s}^{-1}$ for 6 h, framed by a 6h increment and a 6h decrement in 3 steps, respectively.

The mean PAR during the illumination phase was $100 \mu\text{mol photons m}^{-2} \text{ s}^{-1}$. Cells were kept at 17°C in a growth chamber (KBWF 240, Binder) in 50 ml PE culture flasks (Sarstedt).

Cell density was monitored by cell counting in a counting chamber (Neubauer improved) according to:

$$\text{cell density} = \frac{n}{A \cdot D} \quad \text{Eq. 14}$$

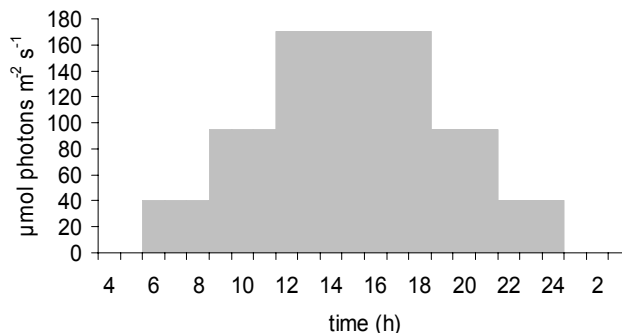


Fig. 6 Scheme of simulated diurnal cycle in the growth chamber.

Mean PAR was $100 \mu\text{mol photons m}^{-2} \text{ s}^{-1}$ during the illumination period of 12 h.

- n** number of counted cells
- A** area of counted major squares (square = 1 mm²)
- D** depth in mm (Neubauer improved: 0.1 mm; Jessen chamber: 0.4 mm)

4.3 Viability tests

For viability testing trypan blue (0.4% \equiv 458 $\mu\text{mol l}^{-1}$) was added to the concentrated cell suspension after protoplast production or dye loading in a 1 : 10 relation. This was done under visual control at the microscope. After a short incubation time (< 5 min) cell viability was evaluated according to the cells' ability of dye exclusion.

In a second approach decalcified and stripped cells were recultivated to monitor their viability. Therefore the same number of cells as in the respective standard cell culture was used for seeding and cells were cultured as described within section 4.2.

4.4 Adhesiveness of the bath bottoms

Adhesion of cells for experiments on glass was supported by poly-D-lysine coating. The bath bottoms were coated with poly-D-lysine (Sigma-Aldrich, 1 mg ml⁻¹ in deionised water) for ~30 s before rinsing thoroughly with deionised water.

4.5 Microfluorimetry

4.5.1 Decalcification and Protoplast Isolation for Microfluorimetry

The respective decalcification protocol for *C. pelagicus* protoplasts according to Taylor & Brownlee (2003) was modified to produce *E. huxleyi* protoplasts (Fig. 7). 10-15 ml of a dense *E. huxleyi* cell culture were centrifuged at 1882 x g for 5 minutes and the supernatant was discarded. The cell pellet was resuspended in the Ethylene glycol-bis(2-aminoethylether)-*N,N,N',N'*-tetraacetic acid (EGTA) containing solution 3 (ASW_{strip}) by gentle mixing with a plastic transfer pipette and then incubated for 15 minutes. Cells were centrifuged again and incubated in ASW_{strip} for

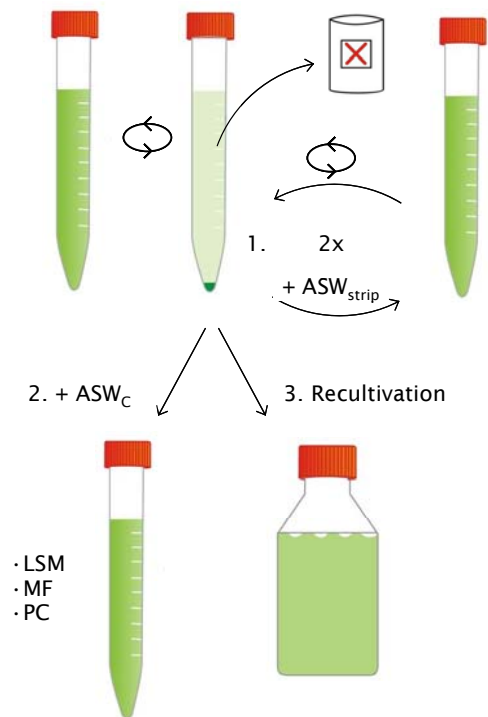


Fig. 7 Schematic protoplast production for microfluorimetry.
X Disposal; LSM Laser Scanning microscopy; MF microfluorimetry; PC Patch clamp

another 10 minutes. Thereafter, cells were mechanically agitated by a series of rapid aspirations and expulsions through a PE tubing (i. d. 350 μm) attached to a 1 ml syringe to remove remnants of coccospheres. After another centrifugation step the cells were transferred to solution 2 (ASW_c, pH 8.05 \pm 0.05). Cells were allowed 2 hours in ASW_c for recovery before dye loading for microfluorimetry was started. Apart from centrifugation, all steps were performed under illumination. Viability was tested by recultivation on different occasions (data not shown).

4.5.2 General principles in microfluorimetry at the example BCECF

Fluorescent dyes change their fluorimetric characteristics depending on a specific factor, e.g. $[\text{H}^+]$ or $[\text{Ca}^{2+}]$.

BCECF, the dye used in this study, decreases fluorescence intensity when binding a H^+ . It has been used since the 1980s (Rink *et al.*, 1982) to measure intracellular pH and can be used as a dual excitation ratiometric pH indicator. For this, pH dependent emission ratio at 535 nm is detected after excitation at ~ 490 nm and ~ 440 nm (isosbestic point). At the isosbestic point the indicator is insensitive to changes in pH. Ratiometric pH indicators have the advantage of reduced signal errors due to variations in concentration, leakage or photo bleaching.

BCECF is brought into the cell in its esterified form BCECF-AM (2',7'-bis-(2-carboxyethyl)-5-(and-6)-carboxyfluorescein-acetoxymethyl ester), where it is hydrolysed by cellular esterases to the free acid. This free acid form has four to five negative charges at pH 7 – 8, which helps retaining it inside the cell. Its pK_a is 6.98,

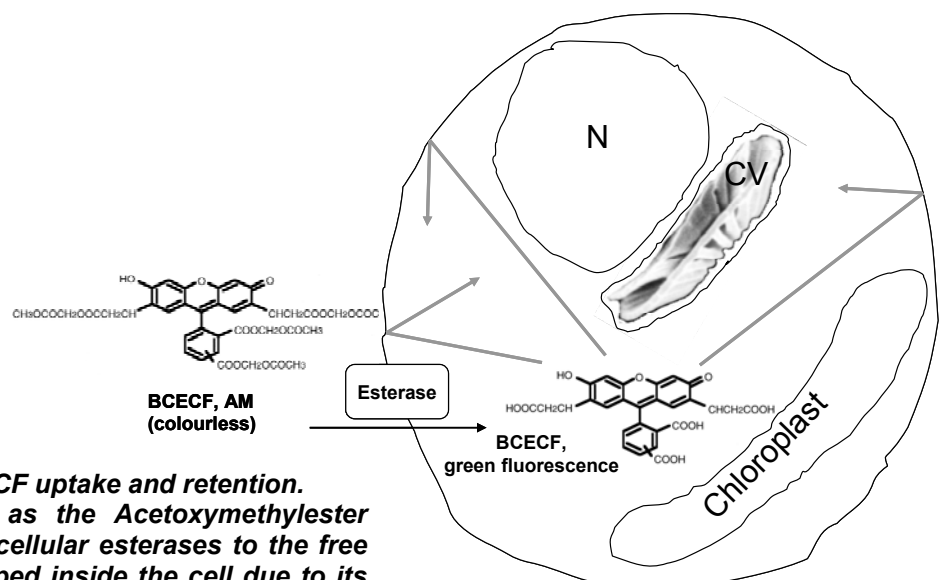


Fig. 8 Schematic BCECF uptake and retention. BCECF is taken up as the Acetoxymethylester (AM) and cleaved by cellular esterases to the free acid. The acid is trapped inside the cell due to its charges.

making it ideal for typical intracellular pH measurements.

BCECF can be used for an in situ calibration of the pH_i of living cells by the nigericin method (4.5.6).

4.5.3 Dye loading (BCECF) in *E. huxleyi*

Stock solutions of BCECF-AM (10 mmol l^{-1} in dimethyl sulfoxide, B1150, Invitrogen), and a detergent, Pluronic F-127 (10% in H_2O , Invitrogen), were prepared and stored dark in aliquots at $-20 \text{ }^\circ\text{C}$ until use. Different dye concentrations ($5 - 50 \text{ } \mu\text{mol l}^{-1}$) and loading times (10 – 240 min) were tested. Also loading conditions were varied concerning light ($0 - 170 \text{ } \mu\text{mol photons m}^{-2} \text{ s}^{-1}$) and temperature ($17 - 25 \text{ }^\circ\text{C}$).

Best results were achieved when cells were incubated at $17 - 20 \text{ }^\circ\text{C}$ with a final concentration of $50 \text{ } \mu\text{mol l}^{-1}$ BCECF-AM and 0.5 % Pluronic in solution 2 (ASW_c) for ~120 minutes. Cells then were centrifuged and the supernatant was discarded. After resuspension in solution 2 (ASW_c) cells were transferred into the bath chamber and allowed to settle and adhere to the poly-D-lysine coated bottom cover slip for at least 30 minutes.

After this dye loading procedure I achieved a signal to noise relation for the emission signal >10 throughout a 1 hour experimental period in most cells. Cells with weak dye loading below this threshold or showing signs of overloading (intensity > 800) were excluded from the analysis.

4.5.4 Experimental procedure and devices

The bath chamber was mounted on an inverted microscope (Zeiss Axiovert 35M), equipped with an A-Plan 100x/1.25 Oil objective (100x, Zeiss). The microscope again was mounted on a vibration isolation table (RG Breadboard, Newport, Irvine, CA, USA).

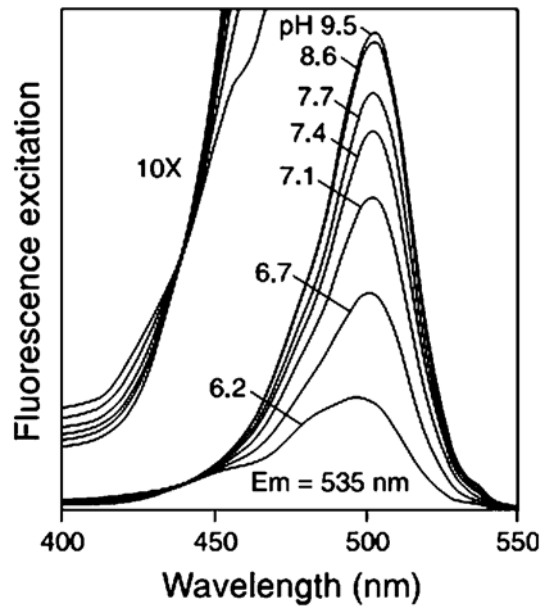


Fig. 9 pH-dependent fluorescence excitation spectra of BCECF. The 10X enlargements of the region below 470 nm clearly illustrate the excitation isosbestic point at ~439 nm. Source: Invitrogen, BCECF manual.

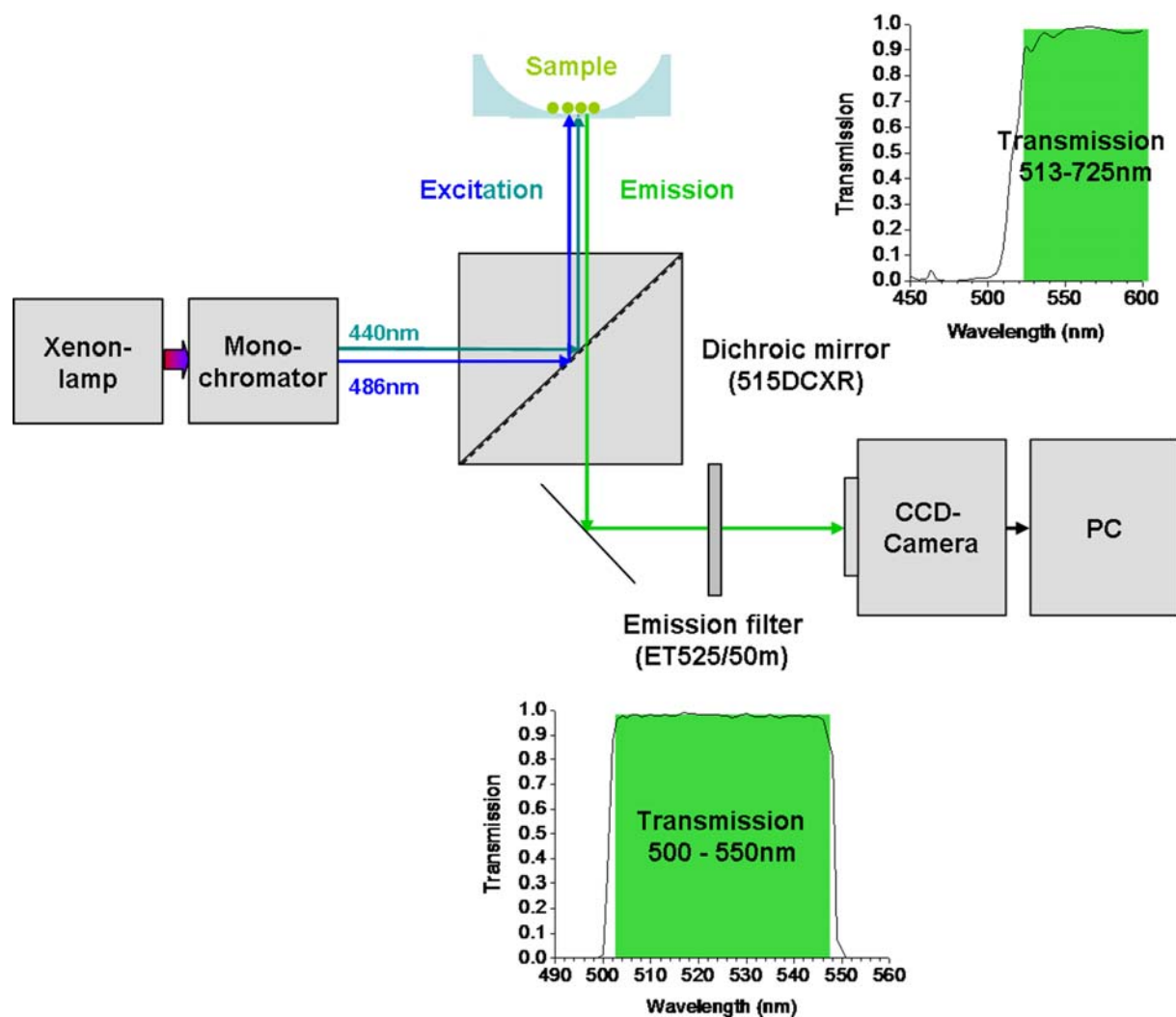


Fig. 10 Scheme of the microfluorimetric detection system.
CCD Charge Coupled Device; PC Personal Computer

Light was fed in by a VisiChrome Polychromatic Illumination System (Visitron systems GmbH, Puchheim, Germany) consisting of a 75W Xe short arc lamp (UXL-75XE, Ushio Inc., Japan) and a subsequent monochromator, defining wavelength by a galvo controlled grid decreasing the time needed to switch between 2 wavelength to <2 ms.

Fluorescence was monitored with the Visitron Imaging Software (MetaFluor, Visitron systems GmbH, Puchheim, Germany) using a CCD-camera (CoolSNAP HQ², Photometrics).

At a rate of 0.2 Hz the dye was alternately excited at 486 nm and 440 nm (± 10 nm bandwidth) for 24 and 60 ms, respectively. Acquisition settings were set on gain 2 and binning 3. With this binning 3 x 3 pixels are integrated, leading to a higher signal on the expense of spatial resolution. The pixel in this system has an edge length of

6.45 μm , with binning 3 the edge length increases to 19.35 μm . The actual resolution can be calculated according to

$$\text{pixel size} = \frac{\text{edge length } [\mu\text{m}]}{\text{objective magnification}} = \frac{19.35 \mu\text{m}}{100} = 0.1935 \mu\text{m} \quad \text{Eq. 15}$$

Emission was recorded at 525 nm (emission filter ET525/50 nm, Chroma Technology Corp) and the ratio of the emission intensities at the two excitation wavelengths integrated over the whole cell was calculated after subtraction of system immanent camera offset and background signal (MetaFluor Meta Series Software 7.6.1, Meta Imaging System).

Cells were checked for auto fluorescence after excitation at the experimental wavelengths 486 and 440nm, known to induce chlorophyll auto fluorescence.

However, no auto fluorescence is induced in the detection range of 525 nm \pm 25 nm.

4.5.5 Experimental procedure: General

For all experiments the bath chamber (350 μl volume) was mounted on the stage of the inverted microscope and perfused by gravity at a rate of 6 to 8 ml min^{-1} at 17 $^{\circ}\text{C}$, ensuring rapid bath exchange rates.

The sequence of bath solution exchanges is described in detail for each series in the respective results section.

4.5.6 Calibration of pH_i with nigericin

Nigericin has been used since the mid seventies (Pressman, 1976) to calibrate internal pHs of living cells. For this purpose cells which have been loaded with a pH indicator like BCECF are exposed to a solution containing between 10 – 50 $\mu\text{mol l}^{-1}$ nigericin in the presence of 100-150 mmol l^{-1} K^+ , reflecting the organisms' cytosolic $[\text{K}^+]_i$. Nigericin is an ionophore and acts as a mobile K^+/H^+ exchanger. $[\text{K}^+]_e$ has to be adjusted to $[\text{K}^+]_i$ to depolarise the cell to zero and to remove the K^+ gradient. Under these conditions internal and external $[\text{H}^+]$ will equilibrate.

Changes in the ratio of the intracellularly trapped pH sensitive dye, e.g. BCECF, due to changes in pH_e can then be directly assigned to changes in pH_i .

For a pH calibration a stock solution of nigericin (Nigericin sodium salt, 72445, Fluka, Sigma Aldrich, 10 mmol l⁻¹ in ethanol) was prepared and stored in aliquots at -20 °C until use. *E. huxleyi* cells were exposed to 10 μmol l⁻¹ nigericin in the presence of 100 mmol l⁻¹ K⁺, an estimate of the organism's cytosolic [K⁺] (solution 8, Table 4). Solutions with a known pH_e were applied to the cells and the change in ratio was monitored. A calibration curve was calculated (Fig. 21), allowing an estimate of the relation between the detected emission ratio of BCECF and the respective change in pH_i.

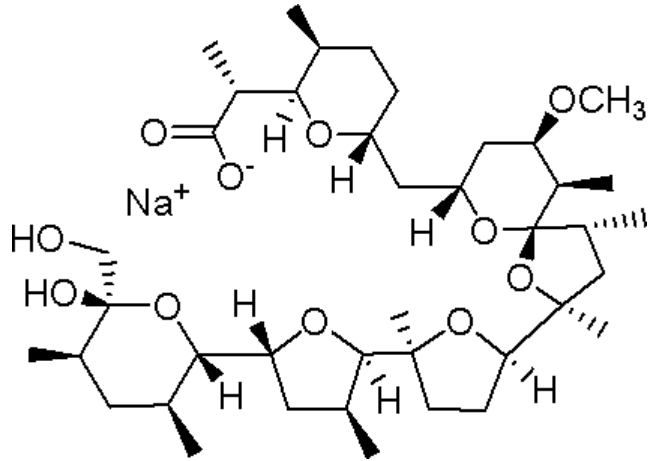


Fig. 11 Chemical structure of nigericin.
Source: Sigma Aldrich.

4.5.7 Application of OOE solutions

OOE solutions were directly applied to the investigated cells by a micro-manipulated superfusion pipette system. During application of the OOE solutions the bath was continuously rinsed by solution 2 (ASW_c), securing a permanent removal of the OOE solution.

Dual-syringe pumps (50 ml, Perfusor Secura, B. Braun) were used to drive solution pairs A and B (Table 2) at a constant rate of 7-10 ml h⁻¹ to a Teflon mixing unit (Fig. 12) with six inlets, each secured with a unidirectional restrictor valve, for a consecutive application of up to 3 OOE solutions. Stainless steel inlet pairs for the 1:1 combination of A and B solutions were situated opposite to ensure optimal mixing.

In addition, mixing was improved and dead space was minimised by a nylon mesh (60 μm pore size nylon filter, Millipore NY60) mounted inside the mixing unit in front of the outflow canula. The opening of this canula was positioned left and above the cells in a 30° angle (Fig. 12b), directly facing the cells of interest under investigation, to ensure a laminar superfusion and to prevent any mixing with bath perfusion solutions in the vicinity of the cells.

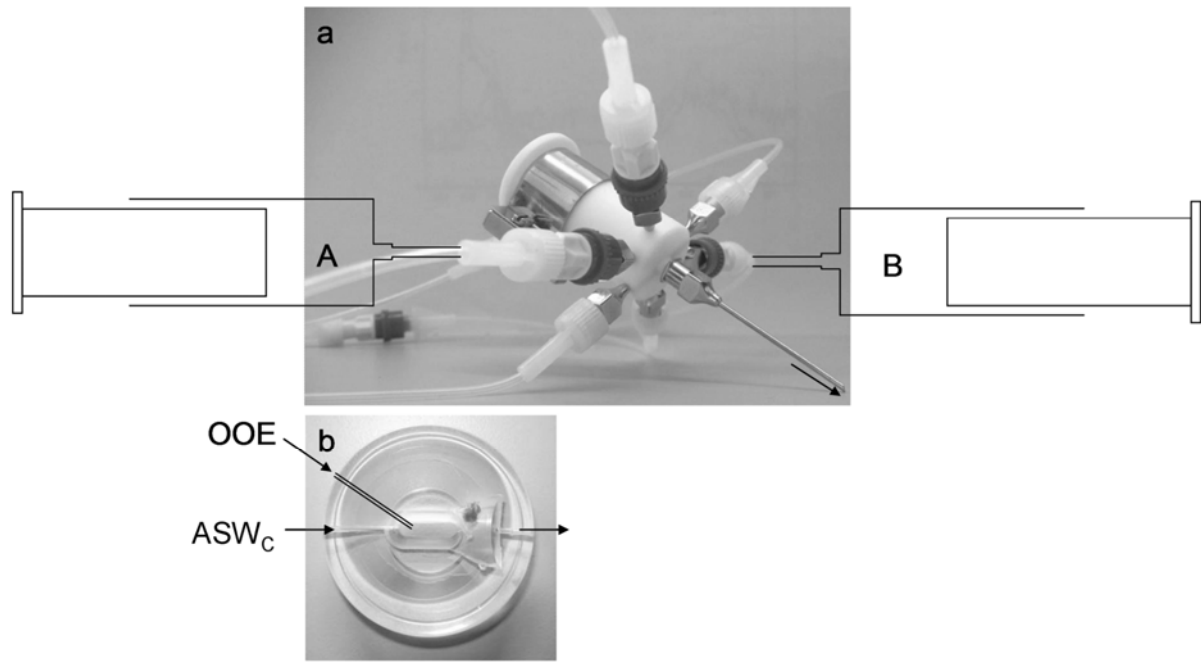


Fig. 12 Picture of a) the OOE mixing unit and b) the experimental bath chamber. The mixing unit in a) was attached to a micro-manipulated superfusion pipette system to ensure rapid bath exchange rates. Solutions A and B were mixed 1:1 with a dual-syringe pump to the respective final OOE solution and directly applied through a canula onto the investigated cells attached to the bottom of the bath chamber, as indicated in b). Control solution 2 (ASW_c) was supplied continuously to the bath chamber to secure a rapid and permanent removal of the OOE solutions.

The total dead space volume of the system after mixing was $\sim 20 \mu\text{l}$. In consequence the time between mixing and supply of OOE solutions to the cells was 7 - 10 s, and thus well within the time required to prevent any significant equilibration (see Fig. 23).

4.5.8 pH measurements in experimental solutions

pH was measured with a pH sensitive single-rod measuring cell (Blueline 16pH, Schott Instruments) with a micro probe. This enabled me to measure the pH directly at the outlet of the OOE mixing unit to check for target pH. pH values are presented on the NBS scale and a pH of 8.05 ± 0.05 was defined as the control pH.

4.6 Electrophysiological measurements

4.6.1 Patch Clamp Method

The patch clamp method was originally invented by E. Neher & B. Sakmann (1976). For this achievement they received the noble price for medicine and physiology in 1991. It grounds on the voltage clamp technique, already invented in the 1930s by K. Cole & H.J. Curtis, where sharp electrodes were used to impale cells. The great

advantage of the patch clamp method was the possibility of measuring small currents through ion channels with a high spatial and temporal resolution (Sakmann & Neher, 1984). This provided the opportunity to analyse the function of ion channels in different experimental settings.

For a successful experiment an electrically tight seal with a resistance on the order of $10^9 - 10^{11}$ ohms between a glass pipette and the clean plasma membrane of a cell has to be established. This so called gigaseal results in a reduction of noise, and also of leakage currents, and thus a good signal to noise ratio.

Once a gigaseal has been established, typically four different patch clamp configurations can be achieved.

- Cell-attached or on-cell (OC)
- Inside-out (IO) by excising the patch under the pipette
- Whole cell (WC) by breaking the patch under the pipette
- Outside-out (OO) by resealing of the membrane after excision, starting from WC configuration

Cell-attached, Inside-out and Outside-out configurations are used to characterise individual channels, as only the membrane patch sealed to the pipette opening is measured. Whole cell configuration is used to characterise the electrical properties of the entire cell.

Currents through the area under the pipette, the patch, or the whole cell can then be analysed in two basic modes:

- Voltage clamp (VC)
- Current clamp (CC)

In VC mode voltage can be either kept to a constant value or changed intentionally by applying a step wise or transient change. The current measured correlates to the ion current through all open channels in the patch or whole cell. The magnitude of the current depends on the number of channels (in the order of 0.5 - 100 pA for single channels). Due to the gigaseal the leak current is very small.

$$\text{Example: } i = \frac{100mV}{100G\Omega} = \frac{10^{-1}V}{10^{11}\Omega} = 10^{-12} A \equiv 1pA$$

In the VC mode current voltage relationships can be generated. To do so a range of defined holding potentials is set and the corresponding currents are measured. Subsequently the currents are plotted against the holding potentials (I/V curve). An

I/V curve characterises how the relation between the membrane potential and the current is voltage dependent. In single channel measurements (patch clamp) it characterises how the conductance and open probability of a certain ion channel are voltage dependent. The slope of the I/V curve (usually in pA/mV = nS) gives the conductance, the extrapolated intersection with the abscissa gives the zero current potential, an indicator of the ion species carrying the respective current. For an ion specific channel the zero current potential corresponds to the respective Nernst potential (3.3).

In the CC mode the resting potential of a cell is measured at zero current (CC₀) or any other command current (CC_x).

The most important electrical properties measured and/or calculated are:

- Resting potential (V_m in CC₀)
- Dynamic voltage changes (action potentials)
- Ion currents
- Conductance (G_m)

The conductance is the reciprocal of the resistance (G=1/R) and by application of Ohm's law (U=R·I) can be calculated according to:

$$G = \frac{I}{U} \quad (\text{S}) \quad \text{Eq. 16}$$

Measurements on *C. pelagicus* in this study were done cell attached in VC mode.

4.6.2 Experimental procedure and devices

Electrical measurements were performed with an amplifier system (EPC 7, HEKA electronics, Germany) under an inverted microscope (Zeiss Axiovert 25). The microscope was equipped with an A-Plan 100x/1.25 Oil objective (Zeiss). The measuring station (schematic drawing in Fig. 13), consisting of the microscope, the pre-amplifier with an integrated pipette holder (EPC 7, HEKA electronics, Germany), and micro manipulators, was assembled onto a vibration isolation table to minimise vibration artefacts.

The setup on the vibration isolation table was protected by a Faraday cage to avoid electrical disturbance by the environment.

The patch clamp amplifier signal was filtered (Low pass filter 902, Frequency devices, USA), and recorded and analysed with a computer software (pClamp 9 acquisition & analysis software, Axon instruments, USA).

A digital-to-analogue converter (Digidata 1322A, Axon instruments, USA) was interconnected between amplifier and computer to translate analogue into digital signals and vice versa. In addition an oscilloscope (Analog Digital Scope HM507, HAMEG Instruments, USA) was connected for direct optical control of current and voltage.

Glass micropipettes were made with an automated puller (DMZ Universal Puller, Zeitz) from filamented borosilicate glass blanks (GB 150 F-8T, 0.86 x 1.50 x 80 mm, Science products, Germany). The blanks were polished to protect the chlorinated silver wires and O-ring seals from damage by sharp edges. Pipettes were polished a second time to achieve smooth tips and subsequently filled by use of a carbon fibre with either sterile filtrated solution 2 (ASW_c) or internal solution 12 (IS) and connected to the pipette holder of the pre-amplifier. Resistance of the pipette vs. the bath solution (ASW_c vs. ASW_c) was around 1 to 4 MΩ, corresponding to an opening diameter of 0.5 - 1.5 μm.

Pipettes were connected by tubing to a syringe system for the application of (positive or negative) gauge pressure. Before immersing the pipette into the bath solution constant positive pressure was applied to avoid intrusion of bath solution into the pipette solution.

Electrical connection between pipette and pre-amplifier was supplied by a Ag/AgCl-wire. Contact between pre-amplifier and bath solution was established by a chlorinated Ag/AgCl bath electrode.

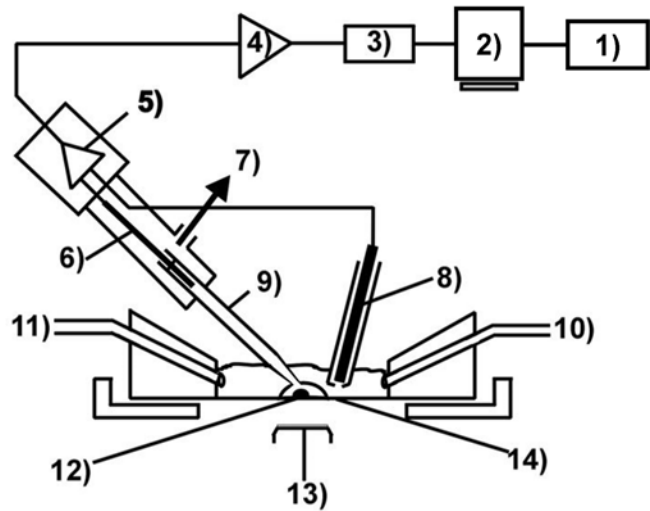


Fig. 13 Scheme of the patch clamp measuring system

1) oscilloscope 2) computer 3) low pass filter 4) amplifier 5) pre-amplifier 6) measuring electrode/pipette holder 7) gauge pressure system 8) reference bath electrode 9) glass micropipette 10) bath outflow 11) bath inflow 12) protoplast 13) inverted microscope 14) cover slip

The bath chamber was fabricated of a round acrylic glass disk, $\text{\O} 38$ mm and 10 mm high, which tapered towards the centre to leave an opening of $\text{\O} 10$ mm and resulting in a bath volume of ~ 1 ml. Underneath this opening a round cover slip ($\text{\O} 1$ cm) could be attached by mounting wax, on which the cells were allowed to settle. The bath chamber was equipped with in- and outflow ports, situated opposite each other, on which tubing for solutions were attached. Temperature of the solutions was kept constantly at 17°C (measured directly in the bath chamber by use of a handheld probe thermometer, Checktemp1, HANNA Instruments, USA) by a F25-MB Refrigerated/Heating Circulator (Julabo, USA).

For all experiments the bath chamber was mounted on the stage of the microscope and perfused by gravity at a rate of 6 to 8 ml min^{-1} , ensuring rapid bath exchange rates. Flow rates of the bath solutions, however, were reduced in some cases to improve seal formation. The reference bath electrode was immersed into the solution together with the measuring electrode.

4.6.3 Decalcification and Protoplast Isolation for Electrophysiology

Cells for electrophysiological measurements need to have a freely accessible plasma

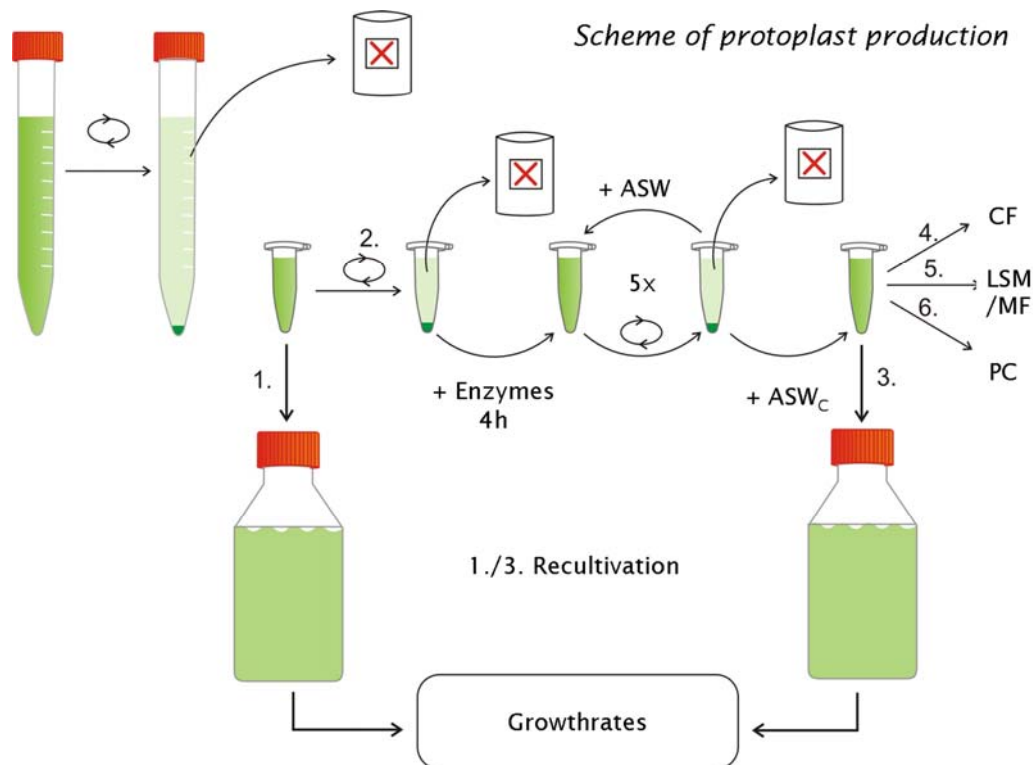


Fig. 14 Scheme of *E. huxleyi* protoplast production for electrophysiology. An enzymatic cocktail (see Table 6b) was used to produce cleaner protoplasts. X Disposal; CF Calcifluor; LSM/MF Laser Scanning microscopy / Meta Fluor microfluorimetry setup; PC Patch clamp

membrane. To achieve this cells were treated either according to the protoplast isolation protocol (Fig. 7) or underwent a protocol as given in Fig. 14. In these cases 200 μ l highly dense *E. huxleyi* cells were treated with 200-1000 μ l of the enzymatic cocktail (solution 14, Table 9) for up to 240 min.

If the enzymatic cocktail was used, after incubation for up to 240 min in different temperatures (17, 25, and 35 °C) cells were again vigorously sucked through a PE tubing (inner diameter \sim 350 μ m) and then washed 3 - 5 times with solution 2 (ASW_c). Cells were then resuspended in solution 2 (ASW_c) and on different occasions cells were also recultivated under normal culture conditions to check for viability (see 4.3). Accordingly I tested the addition of 10 mU chitinase (*Trichoderma viride*, Sigma C8241-25UN) to solution 14 or directly to 200 μ l highly dense *E. huxleyi* suspension.

4.6.4 Sealing procedure with *E. huxleyi* protoplasts

After protoplast isolation cells were resuspended in solution 2 (ASW_c). Cells were then transferred into the bath chamber and allowed to settle and adhere to the poly-D-lysine (see 4.4) coated bottom cover slip for at least 30 minutes. Suspended cells were removed and the bath flow was started to check for settled, attached cells.

A clean micropipette under positive pressure was approached close to the cell surface. Positive pressure was taken away at the instant of touching, and a slight negative pressure was applied. A gigaseal formation was detectable by a decrease in the current pulse and correspondingly an increase in the resistance.

4.7 Confocal laser scanning microscopy

An inverted microscope (Axiovert 200M, Zeiss, Jena, Germany) equipped with a 40x objective (Plan-Neofluar 40x/1.30 Oil, Zeiss, Jena, Germany) was mounted on a vibration isolation table (TS 140, Herzan LLC, Laguna Hills, Ca, USA).

Confocal laser scanning microscopy was performed on a LSM 510 (Zeiss, Jena, Germany). I used the confocal system for microfluorimetric measurements to assess the dye distribution of BCECF. For this the 488 and the 458 nm laser lines of the Ar Laser (Lasos Laser Technique, Jena, Germany) were used in combination with a band pass (505-530 nm or 530-560 nm, Zeiss, Jena, Germany) for emission.

Chloroplast auto fluorescence was induced at an excitation wavelength of 488 nm and detected with a 650 nm emission long pass. Pictures were merged by software

LSM 510 (version 3.2 SP2, Zeiss, Jena, Germany) to verify differential localisation of fluorescence signals.

4.8 Cellulose staining

Cellulose staining was applied to check for remnants of extracellular matrix in isolated protoplasts. After protoplast preparation as described in 4.6.3 cells were transferred to the microscope in a bath chamber, and a drop of Calcofluor White Stain (Fluka, 18909) was added. 415 - 440 nm fluorescence emission was recorded with Visitron Imaging Software (MetaFluor, Visitron systems GmbH, Puchheim, Germany) after excitation at 355 nm to check for remnants of 'cell walls' (cellulose and/or chitin: green to blue fluorescence).

4.9 Statistics

In the microfluorimetric measurements from each experiment 5-35 cells were selected for analysis. Each cell was analysed individually for changes in emission ratio and the resulting changes are shown as a mean \pm SEM. The change in fluorescence ratio represents ΔpH_i , an estimation of the magnitude in change was done by nigericin calibration (5.1.4).

Data were pooled from multiple cells from different experiments where (n, m) indicate the number of cells (n) from m experiments. Paired students t-test was applied, and a p-value <0.05 was accepted for statistical significance. Statistics and calculations were performed either in Excel 2003 (Microsoft) or OriginPro 7.5G (OriginLab Corporation, MA, USA).

For electrophysiology and laser scanning microscopy only qualitative data are given.

5 RESULTS

5.1 Fluorimetric measurements of intracellular pH

5.1.1 General remarks

For the fluorimetric approach used it was necessary to have high cell numbers, to be able to strip and load cells, and to have cells adhering the glass bath bottoms, to enable fast fluid exchange. Cells grown to high densities (up to $1.8 \cdot 10^6$ cells ml^{-1} , achieved at day 7-10) fitted best to these requirements.

Fig. 15a shows a typical growth pattern over 14 d. After an initial lag phase a relatively short exponential growth phase starts, followed by a stationary phase leading to a death phase. The short duration of the exponential growth phase is due to adapted cultural conditions (nutrient limitation starting from day 3-4 onwards after Shiraiwa (2003), as shown in b) The sampling time span is indicated in grey.

Nutrients were checked on one occasion to verify nutrient limitation during the sampling time span (Fig. 15b). Concentrations of NO_3^- and PO_4^{3-} as the major nutrients are shown for a typical culture. It can be clearly shown that cells were nutrient limited during the experimental time span.

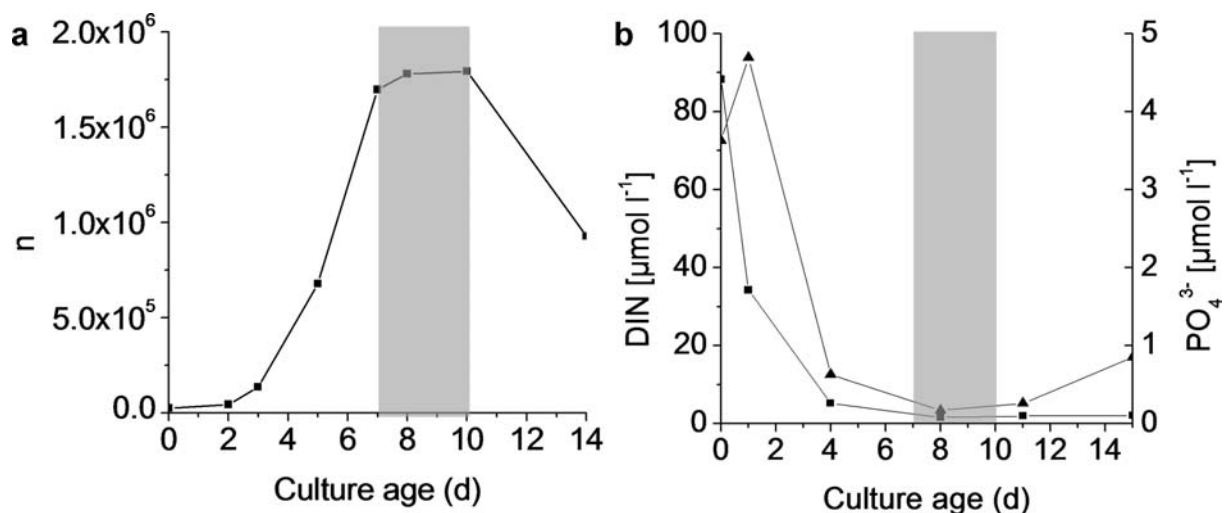


Fig. 15 Development of abundance (a) and nutrient concentration (b) during cell culture. a) Typical growth curve of a calcifying *E. huxleyi* culture generated under nutrient limitation. After an initial lag phase an exponential growth phase starts, followed by a stationary phase before death phase. b) Nutrient status in cell cultures (f/20) of different age under the same conditions. ■ on left axis, indicating NO_3^- plus NO_2^- , ▲ on right axis, indicating PO_4^{3-} . Grey areas indicate sampling time span (d 7 – 10).

5.1.2 Viability tests

Cells were monitored for viability by light microscopy. In Fig. 16a-d characteristic micrographs of cells generated in the described manner are depicted. Fig. 16c documents the loss of coccoliths due to treatment. Stripped naked cells (protoplasts) are smoothly shaped and circular, and often show clearly distinguishable (twin) chloroplasts.

Fig. 16d confirms viability of the protoplasts in a Trypan Blue staining. Exclusion of the dye was accepted for intact protoplasts and observed in >90 % of the tested cells.

In a second approach I tested the ability of subsamples of cells treated as described (4.5.1, 4.6.3) to recalcify under normal cell culture conditions (4.3). Virtually all of the observed cells were able to recalcify within the observation period of 2 days and the culture did not show any significant change in growth rate compared to control (data not shown).

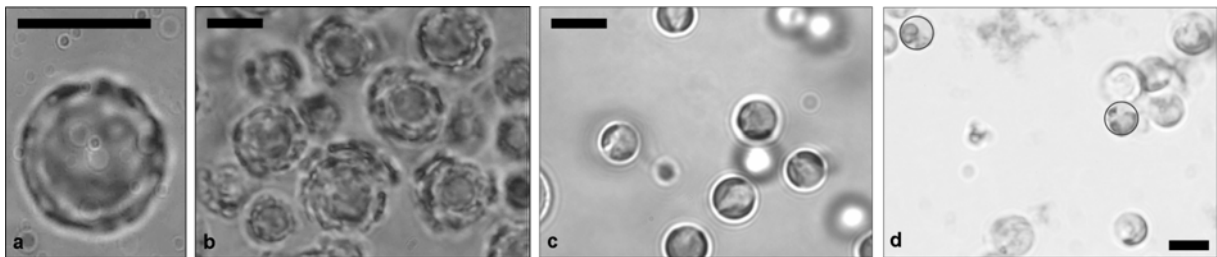


Fig. 16 Characteristics of highly calcified *E. huxleyi* cells before and after protoplast preparation.

a) Single cell, b) Cells with up to three layers of coccoliths c) Pure protoplasts after preparation d) Trypan blue staining (circles) of non viable cells. Scale bar 5 μm

5.1.3 Dye loading and basal BCECF fluorescence properties

Dye distribution within the cell was visualised by LSM. Confocal imaging of *E. huxleyi* showed an intracellular dye distribution excluding the chloroplast (Fig. 17).

At BCECF excitation wavelengths *E. huxleyi* cells showed no significant auto fluorescence at the emission band of 515 - 535 nm (Fig. 18).

Most consistent results in microfluorimetric measurements were achieved when *E. huxleyi* was allowed to equilibrate for a few minutes under control conditions after dye loading, before start of the measurements.

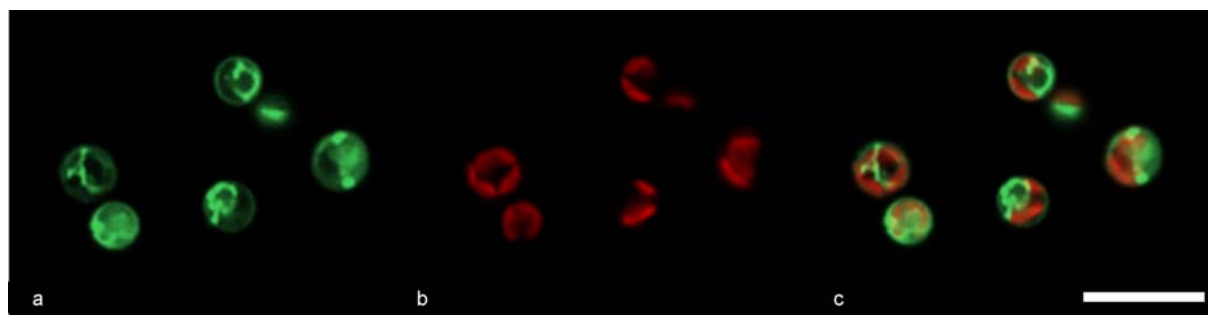


Fig. 17 Confocal false colour image of *E. huxleyi* cells loaded with BCECF-AM
 a) BCECF fluorescence intensity, green (Excitation 488nm, band pass 530-550 nm). b) Chloroplast auto fluorescence intensity, red (Excitation 488 nm, Emission long pass 600 nm). c) Merged image indicates differential localisation of fluorescence signals. No BCECF loading of chloroplast. Picture courtesy of M. Gutowska. Scale bar 10 μ m.

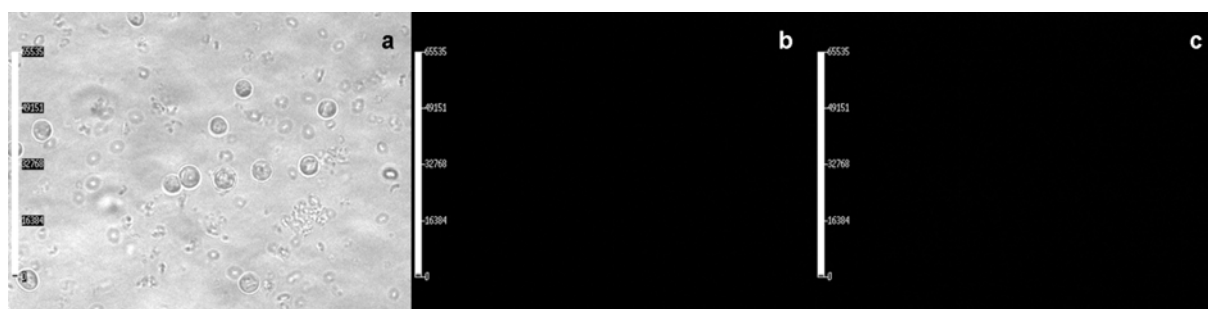


Fig. 18 Absence of detectable auto fluorescence in *E. huxleyi* in the experimental setup
 a) Transmission light micrograph b) and c) no detectable auto fluorescence emission after excitation at 486 nm and 440 nm, respectively at the emission band 515 – 535 nm.

BCECF fluorescence ratio as a measure of pH_i resembled a Gaussian distribution over all analysed experiments (Fig. 19). This was also observed for batches of cells within one experiment, indicating different individual starting pH_i values.

The mean ratio values under control conditions in the experimental series were between 2.49 and 2.54. In some experiments I observed a decline in ratio over time.

Analysed cells of all experiments under control conditions had a ratio between 2 and 3.

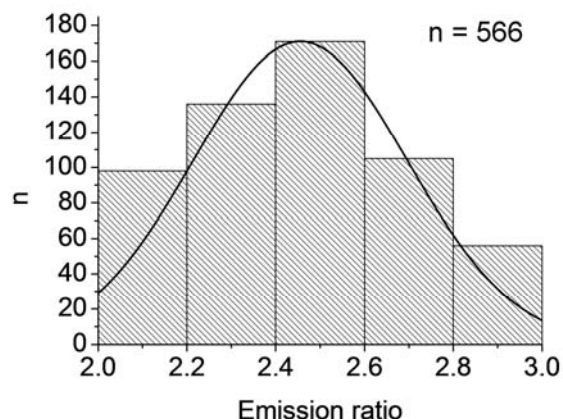


Fig. 19 Frequency distribution of measured emission ratios
 BCECF fluorescence of single cells under control conditions before start of the respective experiment. Analysis of the distribution of measured emission ratios of $n = 566$ cells displayed as absolute number in clusters of 0.2.

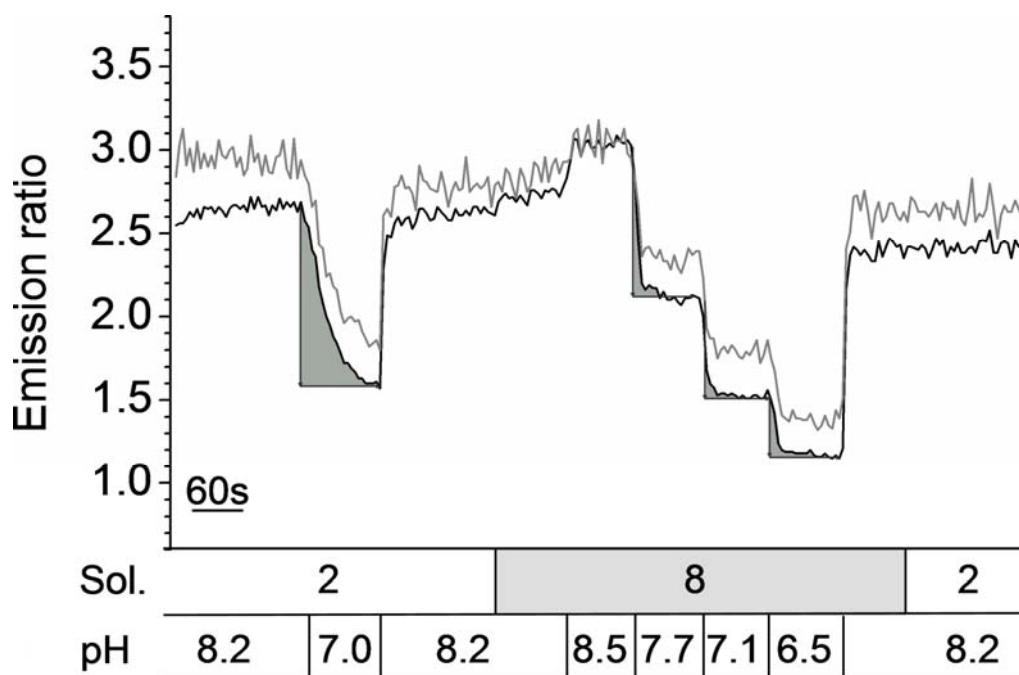


Fig. 20 Typical trace of a pH_i calibration experiment with nigericin. Shown is the change in emission ratio of BCECF in two *E. huxleyi* cells. in solution 2 (ASW_c) and calibration solution 8 with nigericin at different pH_e .

5.1.4 Calibration of pH_i with nigericin

I was able to establish calibration experiments with nigericin (4.5.6). In a first step cells were exposed to a more acidic pH_e to test their general behaviour. For this solution 2 (ASW_c), pH 8.2 was exchanged for solution 2 (ASW_c), pH 7.0, and back.

Cells followed instantaneously. Afterwards solution 2 (ASW_c), pH 8.2 was exchanged for solution 8 (ASW_{Nig}) at the same pH_e (Fig. 20). Cells showed a slight increase in emission ratio, indicating that pH_i was below pH_e before nigericin permeabilisation. Afterwards the pH of solution 8 (ASW_{Nig}) was varied between pH 8.5 and 6.5. pH_e in the calibration experiments equals pH_i . The ratio followed the external pH changes fast and instantaneously, and recovered to almost initial values upon return to pH_e 8.2.

Data of several experiments ($n = 10$, $m = 6$) were used to calculate a calibration curve (Fig. 21). A direct comparison of the effect of extracellular acidification in the absence and presence of nigericin on fluorescence ratio shows that the change in ratio induced by a pH_e change is greater and faster in the presence of nigericin. This demonstrates the additional H^+ permeability introduced into the plasma membrane by nigericin at high $[K^+]$. The calibration curve was linear in the investigated pH range between 6.5 and 8.5. Changes in 0.78 fluorescence ratio units corresponded to a

change of one unit in pH_i (Fig. 21). Caveats of the method used with *E. huxleyi* cells are discussed later (6.2.3), and I will stay with the relative changes in emission ratio for this manuscript.

5.1.5 Effect of $[\text{H}^+]$ on pH_i

In a first series of experiments I investigated the effect of acidic seawater on pH_i , represented by the absolute change in emission ratio.

Fig. 22a shows an original experiment where solution 2 (ASW_c) was rapidly changed from pH_e 8 to pH_e 6. The emission ratio of *E. huxleyi* cells declined instantaneously with bath exchange. The kinetics of acidification was fast and presumably close to the bath exchange rate.

I did not observe any compensation of pH_i during the acid challenge. When the acidified ASW was again exchanged for solution 2 (ASW_c), pH_i increased again, however, in some cells the effect was not completely reversible.

To differentiate between CO_2 and H^+ effects on pH_i I repeated these experiments in the absence of HCO_3^- and CO_2 (HEPES buffered solution 4). Again I observed the same pattern of cytosolic acidification (Fig. 22b): pH_i decreased instantaneously responding to pH_e and reached a new stable pH_i (Table 7).

Even if the length of the exposure to the increased $[\text{H}^+]$ was extended I did not observe any cellular compensation mechanism to re-establish the initial pH_i while under acid challenge (data not shown). Only upon return to control conditions the pH_i effect was reversible.

A concentration response curve for the dependence of pH_i on pH_e is shown in Fig. 22c as an original recording. The relationship (Fig. 22d) was linear over the physiological range between pH_e 6.5-9.0. The change in pH_e of one unit induced a change in ratio of 0.44 relative units. Data of the reported changes in ratio in response to changes in pH_e are summarised in Table 7.

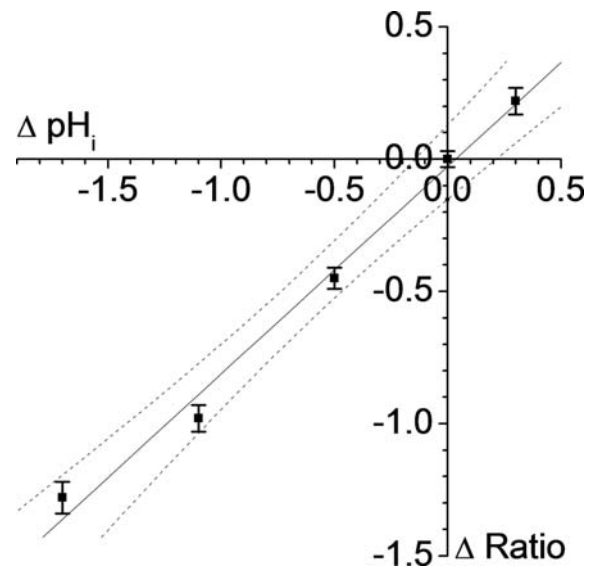


Fig. 21 Calibration curve for BCECF emission ratio
Absolute ratio deltas were achieved at five pH_e values between 8.5 and 6.5. Shown is the linear fit for the absolute deltas with 95% confidence intervals. A change of 1 in the pH corresponds to a change of 0.78 in emission ratio.

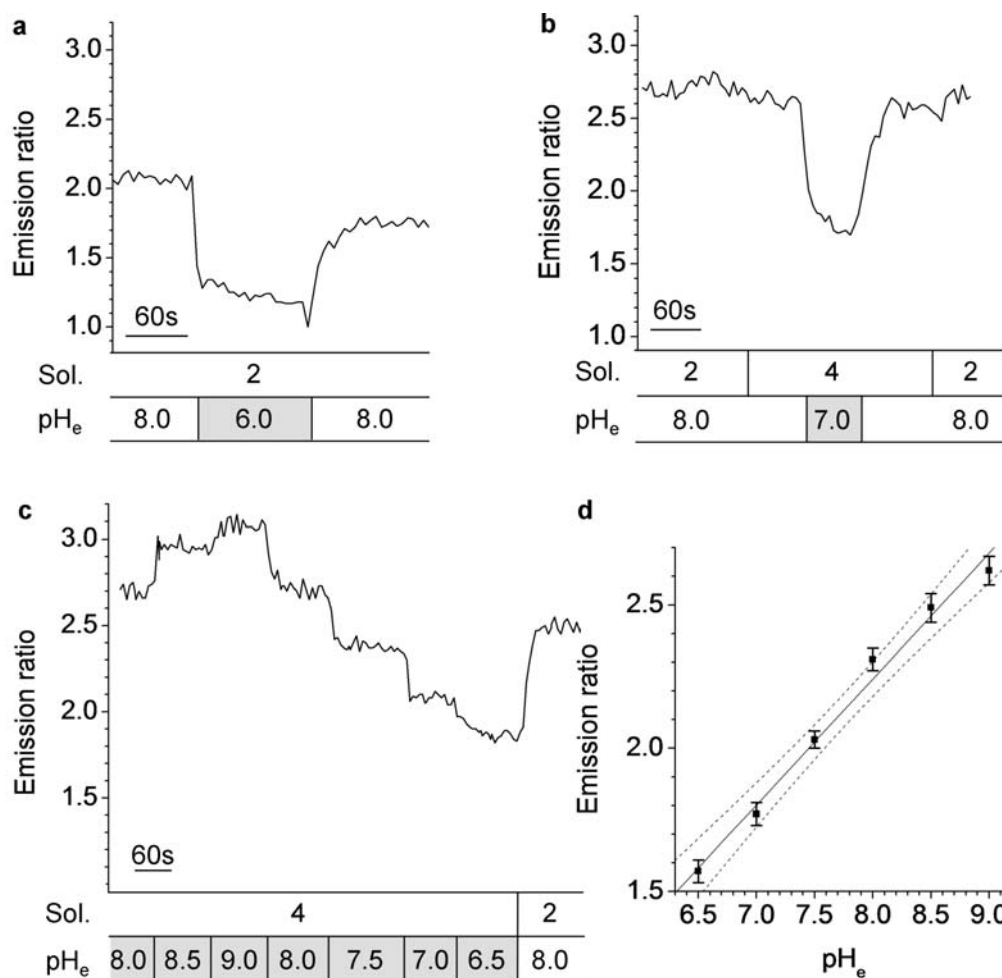


Fig. 22 Effect of $[H^+]_e$ on fluorescence emission ratio as a measure of pH_i . Original recordings of fluorescence ratio in representative single cells. a) Effect of change from pH_e 8 to 6 in control ASW (ASW_c). b) Effect of change from pH_e 8 to 7 in the absence of HCO_3^- (solution 4). c) Concentration response in a representative single cell. d) Summary of 31 cells ($m = 6$). pH_i followed pH_e in a linear relationship ($y = 0.44x$) over the physiological range ($R^2 = 0.99$) Confidence intervals 95%

Table 7 Effects of changes in external $[H^+]$ on pH_i . Control solution ASW_c was exchanged by the respective experimental solution. Mean values give fluorescence ratio as a measure of pH_i . Concentration response of pH_i to changes in pH_e . Ratio changes were calculated relative to the previous pH_e step. n number of individual cells; m : number of experiments; mean: average ratio; d_{abs} : change ratio; d [%]: relative change; $p < 0.01$ indicates significant difference versus the respective previous pH step

solution	pH_e	H^+ [mol kg ⁻¹]	n	m	mean	d_{abs}	d [%]	p
4	9.0	1E-09	31	6	2.62 ± 0.05	-0.13 ± 0.02	-5 ± 0.7	<0.01
	8.5	5E-09			2.49 ± 0.05	-0.18 ± 0.03	-7 ± 1.3	<0.01
	8.0	1E-08			2.31 ± 0.04	-0.28 ± 0.02	-7 ± 1.3	<0.01
	7.5	5E-08			2.03 ± 0.03	-0.27 ± 0.02	-12 ± 0.9	<0.01
	7.0	1E-07			1.77 ± 0.04	-0.20 ± 0.02	-11 ± 1.0	<0.01
	6.5	5E-07			1.57 ± 0.04			

In a further series of experiments using OOE solutions I tested the effects of isolated changes in CO_2 and HCO_3^- on pH_i .

5.1.6 Out of equilibrium solutions

The present experiments with OOE solutions were performed in the time range of 7-10 s after mixing of the respective solution pairs A and B. Reaction kinetics for the carbonate chemistry were calculated and kindly provided by Kai Schulz (as in Schulz *et al.*, 2006) to ensure that the cells under investigation were in fact exposed to solutions which were still out of equilibrium, Fig. 23.

I generated two OOE solutions with high CO_2 or high HCO_3^- , respectively. The two solutions are depicted as solid line (high CO_2) and dashed line (high HCO_3^-). The development of the solutions can be identified easily in Fig. 23d and e which show

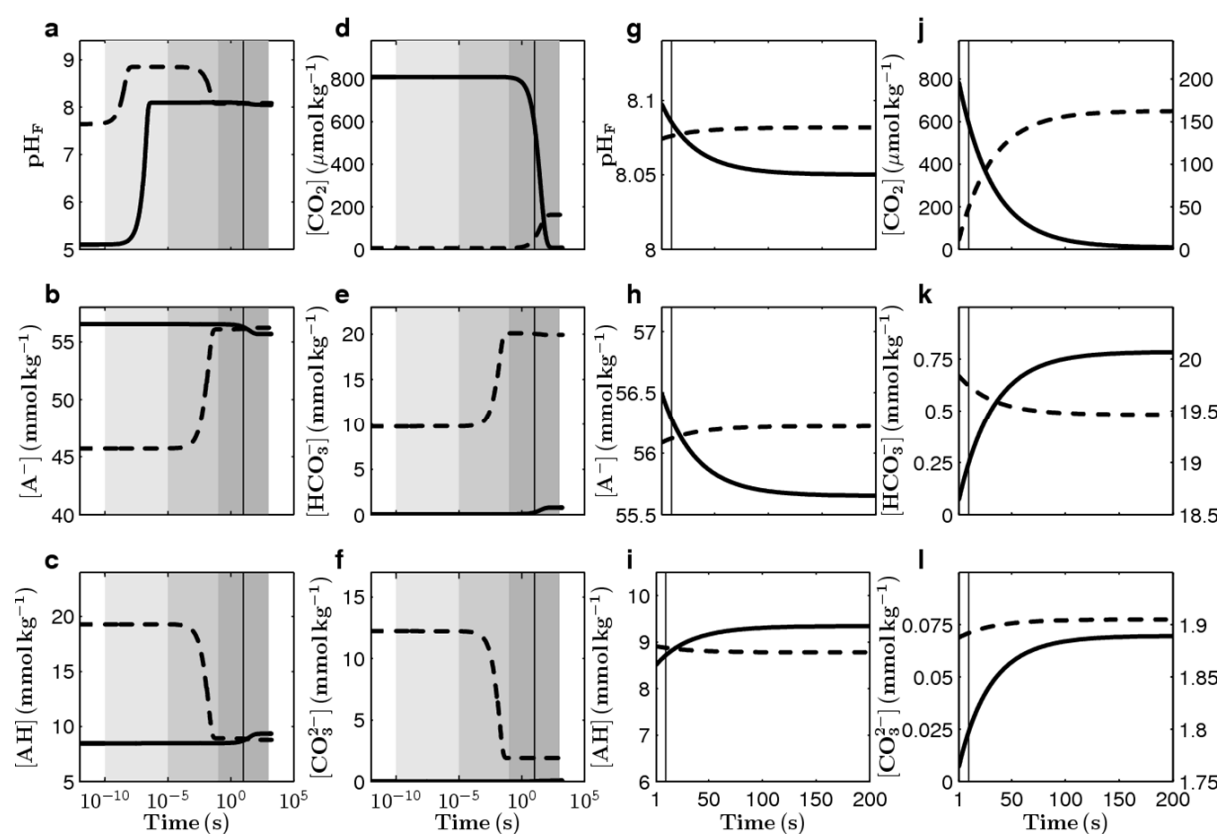


Fig. 23 Reaction kinetics upon mixing of OOE solutions (K. G. Schulz)
Changes in concentrations against time upon mixing of two solutions (see Table 5) with different carbonate chemistry; a-f) on a logarithmic scale (10^{-10} to 10^5 s), g-l) on a linear scale (0 to 200 s). Solid lines illustrate evolution of carbonate chemistry speciation in solution 9 (high CO_2). Dashed lines show carbonate chemistry kinetics in solution 10 (high HCO_3^-). Calculations of carbonate chemistry speciation were done at salinity of 35 and at 20°C . All pH values are given on free scale, pH_F . The vertical line represents the experimental time range of 7-10s after mixing. [A⁻]: unprotonated form of HEPES buffer; [AH]: protonated form of HEPES buffer. Light, intermediate and dark grey shaded areas mark the time ranging from 10^{-10} to 10^{-5} , 10^{-5} to 10^{-1} , and 10^{-1} to 1000 s, respectively.

Note: the additional right ordinate in j-l) gives the values for the dashed lines (high HCO_3^-).

the concentrations of CO_2 and HCO_3^- versus time.

The time axis is logarithmic and covers the whole period from initial mixing to equilibrium. The time range of the experiment is indicated as a vertical line.

The high CO_2 solution (solution 9, solid line) shows a virtually constant CO_2 concentration until approximately 1s (Fig. 23d) and even at the time of experiment $[\text{CO}_2]$ is still above $\sim 600 \mu\text{mol kg}^{-1}$. The formation of HCO_3^- at the same time is negligible (Fig. 23e). Only after minutes the solution reaches equilibrium with the conversion of CO_2 into HCO_3^- . The target pH value in this solution is reached already 10 μs after mixing (Fig. 23a).

The high HCO_3^- solution (solution 10, dashed line) shows a substantial increase in HCO_3^- concentration to the target value in the time range of ms (Fig. 23e) by the protonation of CO_3^{2-} (Fig. 23f). This value stays virtually constant until the time of the experiment. CO_2 formation in this solution does not exceed $50 \mu\text{mol kg}^{-1}$. In this solution the target pH value is reached within ms after mixing (Fig. 23a). The initial pH changes reflect buffering and the protonation of CO_3^{2-} . Fig. 23b and c show the respective changes in HEPES buffer components.

For a higher time and concentration resolution of the equilibration phase refer to Fig. 23g-l. Please note the linear time axis. The left ordinate (Fig. 23j-l) gives the scale for high CO_2 solution 9, the right ordinate shows the numbers for high HCO_3^- solution 10.

Taken together, the carbonate chemistry allows the use of OOE solutions in the time frame between 0.1s and 10s after mixing without relevant equilibration. Even after 10s the most obvious change in $[\text{CO}_2]$ in the high CO_2 solution (Fig. 23j) leaves a $[\text{CO}_2]$ which is 30-fold above equilibrium.

5.1.7 Effect of high $[\text{CO}_2]$ on pH_i

To challenge the cell with a high CO_2 concentration and to monitor the respective changes in pH_i I exchanged solution 2 (ASW_c , $\text{pH } 8.05 \pm 0.05$) for high CO_2 solution 9 (Table 5).

No significant effect on pH_i could be detected (Fig. 24b, Table 8) in the time range of up to 3 min exposure to high CO_2 .

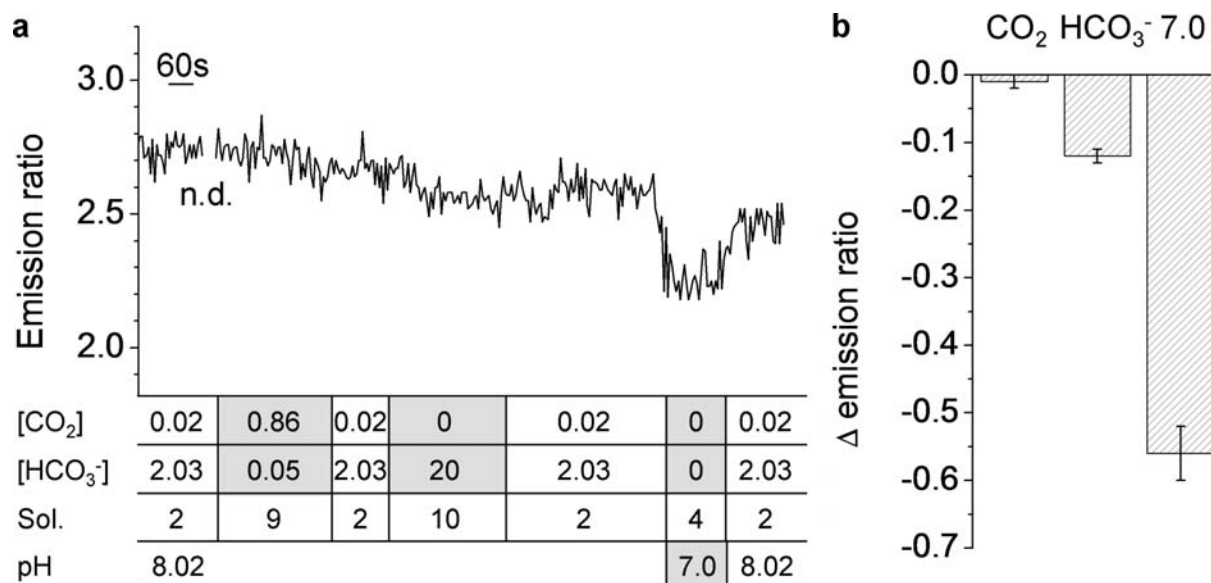


Fig. 24 Effect of high [CO₂] or high [HCO₃⁻] out of equilibrium in comparison to a change in [H⁺]
a) Original recording of fluorescence ratio as a measure of pH_i in a representative single cell.
b) Absolute change in ratio. High CO₂ (sol. 9): $n = 148$, $m = 8$, $p = 0.15$; High HCO₃⁻ (sol. 10): $n = 54$, $m = 5$, $p < 0.01$; pH 7, (sol. 4): $n = 42$, $m = 3$, $p < 0.01$; C: ASW_c. (n.d. data points not determined in this experiment.)

5.1.8 Effect of high [HCO₃⁻] on pH_i

In the same manner I challenged the cells by high extracellular HCO₃⁻ concentrations. Control solution 2 (ASW_c) was exchanged for OOE solution 10 (Table 5) and pH_i of *E. huxleyi* cells was monitored again (Fig. 24a).

Interestingly, the ratio decreased significantly (Fig. 24b, Table 8). The effect of HCO₃⁻ was reversible upon return to control solution 2 (ASW_c). To confirm the normal behaviour of the cells to changes in pH_e I challenged the cells again with pH_e 7.0 (Fig. 24a).

Table 8 Effects of changes in [CO₂], and [HCO₃⁻] on pH_i
Control solution 2 (ASW_c) was exchanged by the respective experimental solution. Mean values give fluorescence ratio as a measure of pH_i, $p < 0.01$ indicates significant difference versus the respective control value. Relative changes in ratio differed significantly ($p < 0.01$). n number of individual cells; m : number of experiments; mean: average ratio; d_{abs} : change ratio; d [%]: relative change; $p < 0.01$ indicates significant difference versus the respective previous pH step

solution		[mol kg ⁻¹]	n	m	mean	d_{abs}	d [%]	p
9	CO ₂	0.0017	148	8	2.42 ± 0.02	-0.01 ± 0.01	-1 ± 0.4	0.18
10	HCO ₃ ⁻	0.0220	85	5	2.31 ± 0.02	-0.12 ± 0.01	-5 ± 0.3	<0.01

5.1.9 Effect of DIDS on pH_i

To investigate whether there is a DIDS inhibitable transport system expressed and functionally relevant in *E. huxleyi* I measured the effect of DIDS on pH_i . Application of DIDS in solution 2 (ASW_c) acidified the cell (Fig. 25a).

This effect on pH_i was concentration dependent (Fig. 25b, $n = 11$, $m = 2$). The effect of DIDS, however, was irreversible, and even after a washout period of more than

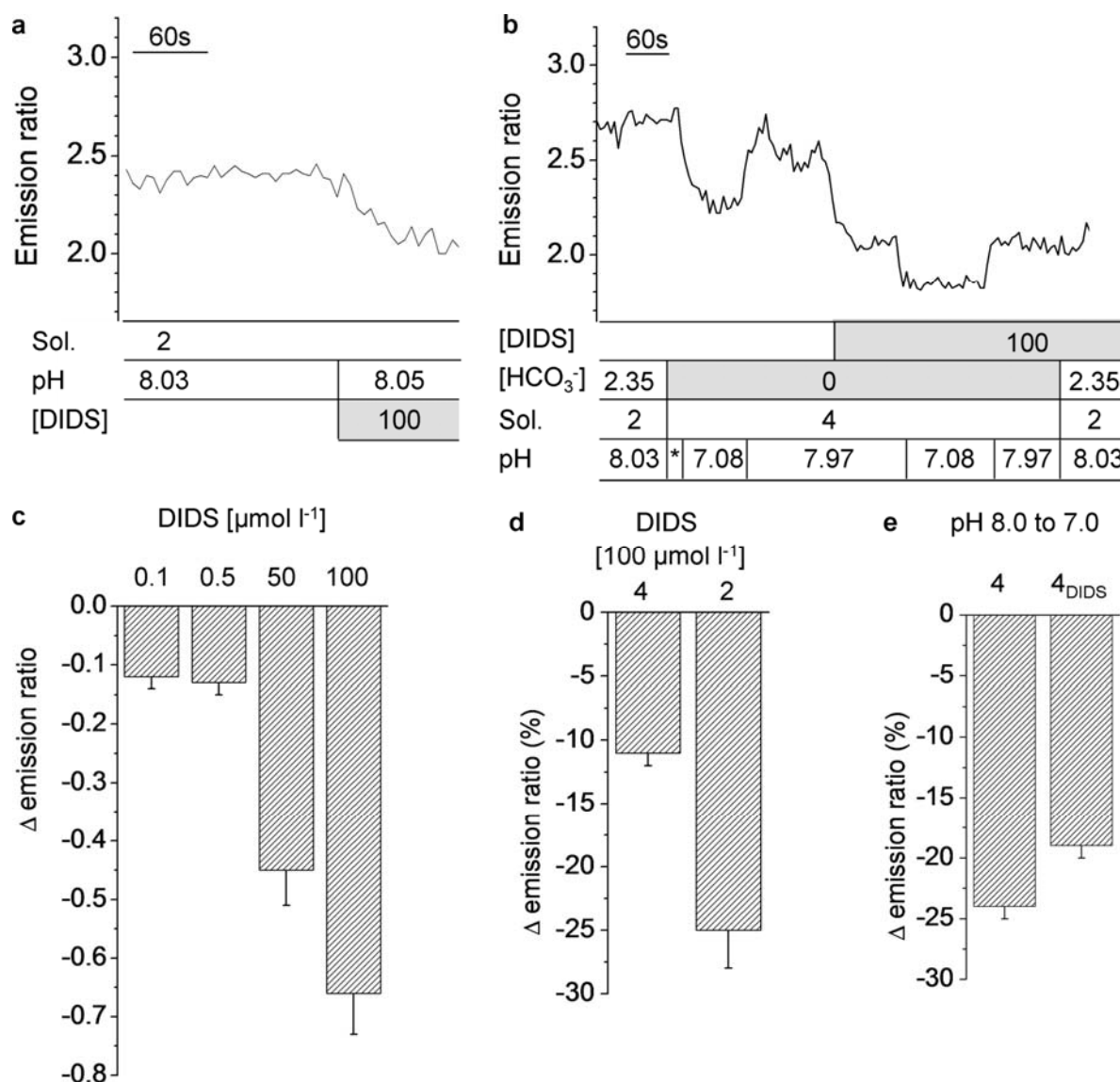


Fig. 25 Effect of DIDS on fluorescence ratio as a measure of pH_i

a) Original recording of fluorescence ratio as a measure of pH_i in a single cell. Effect of DIDS ($100 \mu\text{mol l}^{-1}$) in the presence of HCO_3^- . **b)** Original recording of the effect of DIDS ($100 \mu\text{mol l}^{-1}$) in the absence of HCO_3^- . Comparison of the effect of pH_e 7 in the absence and presence of DIDS. * pH 7.97 **c).** Concentration response for the effect of DIDS on pH_i in the presence of HCO_3^- given as absolute change in fluorescence ratio (Δ); $m = 2$, $n = 11$. **d)** relative change in fluorescence ratio by DIDS in the absence of HCO_3^- and presence of HCO_3^- ($m = 3$, $n = 46$ and $m = 2$, $n = 11$, respectively, $p < 0.01$). **e)** relative change in fluorescence ratio by pH_e 7 in the absence and presence of DIDS; $m = 3$, $n = 46$. Relative changes in ratio differed significantly ($p < 0.01$).

solution		ΔH^+	n	m	mean	d_{abs}	d [%]	p
4	H^+	9E-07	46	3	1.93 ± 0.03	-0.62 ± 0.04	-24 ± 1.3	<0.01
4	H^+_{DIDS}	9E-07			1.70 ± 0.04	-0.40 ± 0.02	-19 ± 1.0	

Table 9 Effects of changes in H^+ on pH_i under control conditions and in the presence of DIDS. Control solution 2 (ASW_c) was exchanged by the respective experimental solution. Mean values give fluorescence ratio as a measure of pH_i . Changes by H^+ (ΔH^+) were compared to pre control (pH 8) with and without DIDS ($100 \mu\text{mol l}^{-1}$), respectively. Relative changes in ratio differed significantly ($p < 0.01$). n: number of individual cells; m: number of experiments; mean: average ratio; d_{abs} : change ratio; d [%]: relative change

15min, pH_i of *E. huxleyi* cells did not show signs of recovery (data not shown).

In a second series of experiments I tested whether the acidification by DIDS was dependent on external HCO_3^- . For this DIDS was applied in solution 4 (0 HCO_3^-). As shown in Fig. 25b and d, DIDS ($100 \mu\text{mol l}^{-1}$) still decreased pH_i under HCO_3^- free conditions. However, the effect was significantly smaller than in the presence of HCO_3^- , indicating that this effect did not completely depend on external HCO_3^- .

Finally I investigated whether DIDS influenced the effect of pH_e on pH_i of *E. huxleyi* cells. In the absence of HCO_3^- I compared the effect of pH_e 7 on pH_i (see also 5.1.4) in the presence and absence of DIDS ($100 \mu\text{mol l}^{-1}$). As shown in Fig. 25e the effect of pH_e 7 was slightly but significantly reduced in the presence of DIDS (Table 9).

5.1.10 Effect of decreased $[\text{Cl}]_e$ on pH_i

5.1.10.1 Effect of decreased $[\text{Cl}]_e$ alone

The fact that DIDS decreased pH_i in *E. huxleyi* indicated a potential involvement of an anion transporter or channel in pH homeostasis. As DIDS also acted in the absence of HCO_3^- I continued my experiments investigating the effect of seawater with a decreased concentration of Cl^- on pH_i . Fig. 26 shows an original trace of an experiment, in which the control bath solution 2 (ASW_c, $540 \text{ mmol l}^{-1} \text{ Cl}^-$) was rapidly exchanged for solution 6 at the same pH_e , containing only $90 \text{ mmol l}^{-1} \text{ Cl}^-$ (Table 4). The cells reacted instantaneously with an acute acidification. The emission ratio decreased sharply by 0.47 ± 0.02 , corresponding to a relative decrease of $19 \% \pm 0.8 \%$ ($n = 148$, $m = 14$). Nevertheless, the cells counter

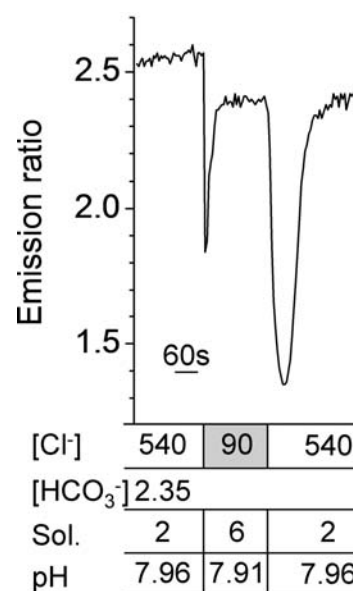


Fig. 26 Effect of low $[\text{Cl}]_e$ on pH_i . Reduction of $[\text{Cl}]_e$ results in a short and transient acidification, followed by a plateau. Upon return to control $[\text{Cl}]_e$ the cell again acidified transiently within a longer time range.

regulated under decreased $[Cl^-]$ to almost the initial pH_i (-0.13 ± 0.01 absolute difference to precontrol (solution 2); this corresponds to a relative difference of $5 \% \pm 0.3 \%$).

Even more astonishing was the finding, that upon return to control solution 2 (ASW_c) the ratio, indicating pH_i of the cells, decreased again, and to an even more acidic value (-0.87 ± 0.03 absolute difference to precontrol (solution 2); this corresponds to a relative difference of $36 \% \pm 1,0 \%$).

This reaction showed a slower time course and was also reversible, with the cells re-establishing the initial pH_i to almost the initial ratio within minutes (-0.21 ± 0.01 absolute difference to precontrol (solution 2); this corresponds to a relative difference of $9 \% \pm 0.5 \%$).

Table 10 Effect of decreased $[Cl^-]_e$ on pH_i
Shown are data for the 1st acidification and the following plateau phase under low $[Cl^-]$, and the 2nd acidification, followed by the re-alkalinisation under control conditions. Absolute (d_{abs}), and relative (%) changes in comparison to pre control values (ASW_c), $n = 148$, $m = 14$

	90 Cl^-		ASW_c	
	IIa	IIb	Va	Vb
	1 st ta	Plateau	2 nd ta	Recovery
d_{abs}	-0.47 ± 0.02	-0.13 ± 0.01	-0.87 ± 0.03	-0.21 ± 0.01
%	-19 ± 0.8	-5 ± 0.3	-36 ± 1.0	-9 ± 0.5
p	<0.01	<0.01	<0.01	<0.01

5.1.10.2 Effect of HCO_3^- and Na^+ on the Cl^- induced pH effect

I tested which other ions could interfere with the acidification upon return to control. The first ion tested was HCO_3^- , also shown in Fig. 27. For this solution 6 (90 Cl^-), which again induced a sharp acute but transient acidification, was not washed out by solution 2 (ASW_c), but by solution 4 (0 HCO_3^-). No acidification could be observed.

Only upon return to the regular control solution 2 (ASW_c), containing HCO_3^- and Cl^- at normal seawater concentrations, the acidification again took place. This led to the hypothesis that a Cl^-/HCO_3^- exchanger might be part of the mechanism behind the observed pH_i effect.

From literature it is known that there are Na^+ dependent and independent Cl^-/HCO_3^- exchangers (e.g. solute carrier 4 family, SLC4, Romero *et al.*, 2004).

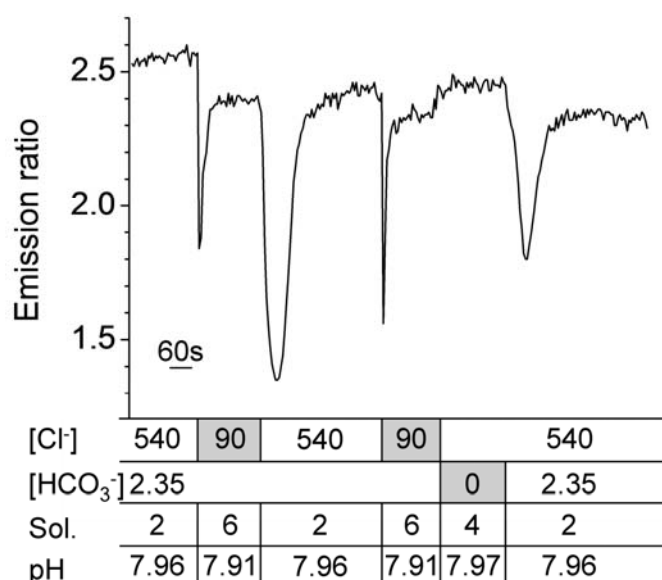


Fig. 27 Effect of low [HCO₃⁻] on the 2nd Cl⁻ induced transient acidification
Reduction of [Cl⁻]_e results in a short and transient acidification. This also occurs in the repeated experiment. However, upon return to control [Cl⁻]_e the cell does not acidify in the absence of [HCO₃⁻]_e. The transient 2nd acidification only occurs upon re-establishing normal [Cl⁻]_e and [HCO₃⁻]_e.

On this background I started a new experimental series to test whether a decrease in [Na⁺]_e affects the observed effect (Fig. 28). The same protocol was repeated (Fig. 28a), but after solution 4 (0 HCO₃⁻) and before return to solution 2 (ASW_c) I additionally exchanged for solution 7 (nominally 0 mmol l⁻¹ Na⁺, Fig. 28c).

Again I did not observe a transient acidification, but only upon return to solution 2 (ASW_c), Fig. 28.

Table 11 Effect of [HCO₃⁻] and [Na⁺] on the 2nd Cl⁻ induced transient acidification
Shown are data for the 1st acidification and the following plateau phase under low [Cl⁻], and the 2nd acidification, followed by the realkalinisation under control conditions. Absolute (*d*_{abs}), and relative (%) changes in comparison to pre control values (ASW_c), *p* significance level vs. pre ASW_c values *p*¹ significance level vs. the respective paired experiment (e.g. % change due to 90 Cl⁻ in the short and extended version of the experiment) (Ia) transient acidification (IIa) 1st low [Cl⁻]_e induced transient acidification (IIb) re-alkalinisation under low [Cl⁻]_e (III) low [HCO₃⁻] (IV) low [Na⁺] (Va) low [Cl⁻]_e induced acidification upon return to ASW_c and (Vb) re-alkalinisation The 2nd acidification only occurs upon return to ASW_c with normal Cl⁻, Na⁺, and HCO₃⁻ concentrations. *n* = 47, *m* = 4 The grey area corresponds to the grey area in Fig. 28
* significantly more acidic vs. IIb (*p* < 0.01), # non significant vs. IIb (*p* = 0.24), § significantly more alkaline vs. IIb (*p* < 0.01)

	90 Cl ⁻		0 HCO ₃ ⁻	0 Na ⁺	ASW _c	
	IIa 1 st ta	IIb Plateau	III	IV	Va 2 nd ta	Vb Recovery
<i>d</i> _{abs}	-0.35 ± 0.03	-0.12 ± 0.01	-0.07 ± 0.02 #	-0.03 ± 0.02 §	-0.67 ± 0.04 *	-0.24 ± 0.03
%	-15 ± 1.1	-5 ± 0.6	-4 ± 0.9 #	-1.0 ± 1.0 §	-29.0 ± 1.6 *	-10 ± 1.1
	-18 ± 1.5	-4 ± 0.6			-23.0 ± 0.9 *	-9 ± 1.0

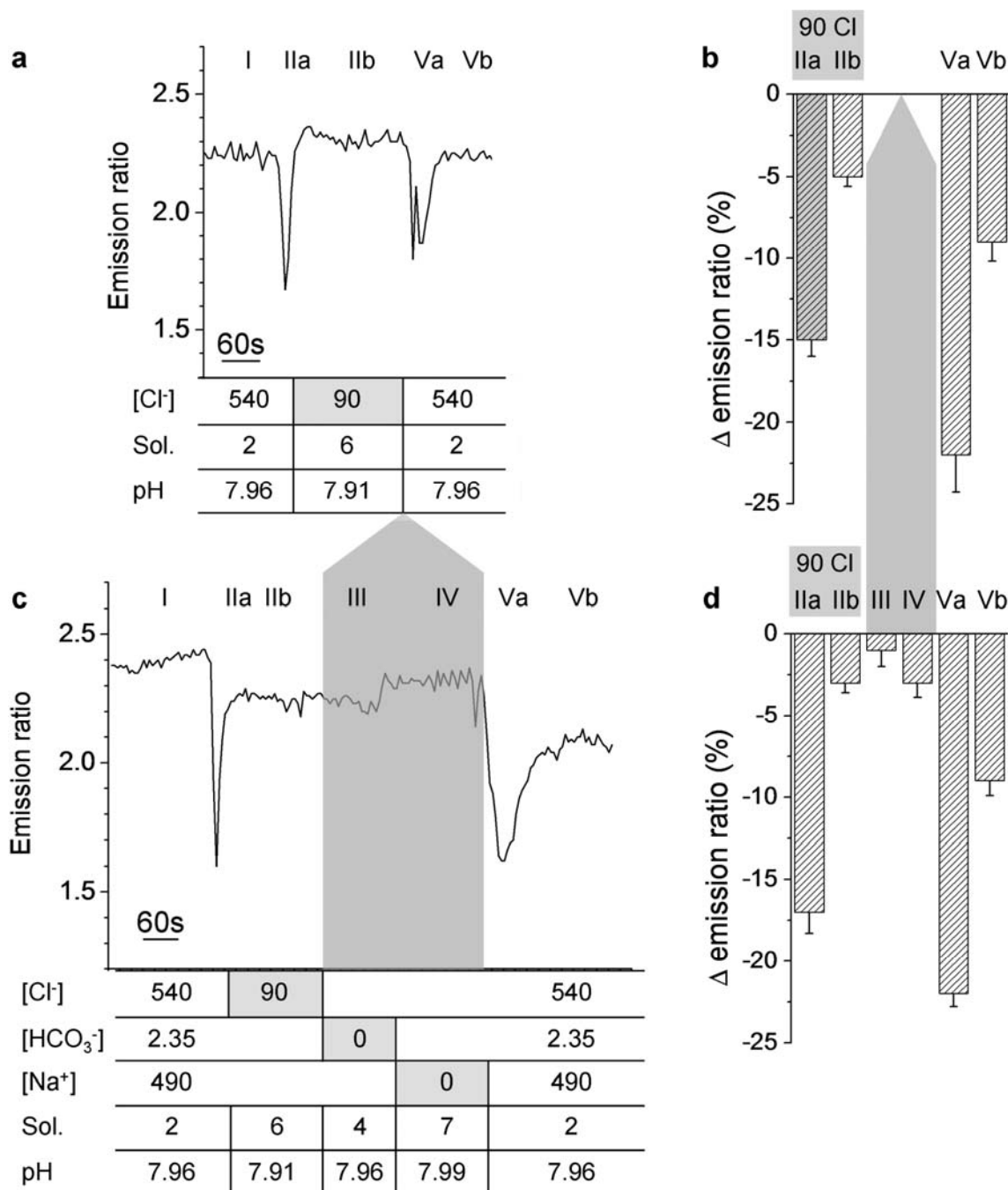


Fig. 28 Effect of $[\text{HCO}_3^-]$ and $[\text{Na}^+]$ on the 2nd Cl⁻ induced transient acidification

a) Representative original experiment showing the direct decrease in emission ratio upon removal of Cl⁻: I ASW_C, IIa low $[\text{Cl}]_e$ induced acidification, and IIb re-alkalinisation under low $[\text{Cl}]_e$. Va low $[\text{Cl}]_e$ induced acidification upon return to ASW_C and Vb re-alkalinisation upon return to ASW_C. **b)** Relative decreases of the emission ratio ($n = 54$, $m = 4$). All values are significantly lower compared to pre control ($p < 0.01$).

c) Representative original experiment showing the direct decrease in emission ratio upon removal of Cl⁻, and the effect of low $[\text{HCO}_3^-]$ (III) and low $[\text{Na}^+]$ (IV). The 2nd acidification only occurs upon return to ASW_C with normal $[\text{Cl}]_e$, $[\text{Na}^+]_e$, and $[\text{HCO}_3^-]_e$. **d)** Relative decreases of the emission ratio in the extended experiments ($n = 54$, $m = 4$). All values are lower compared to pre control (Table 11, p) apart from low $[\text{Na}^+]_e$ ($p = 0.24$), but relative change are the same (Table 11, p₁).

5.1.11 Effect of increased $[K^+]_e$ on pH_i

5.1.11.1 Effect of $[K^+]_e$ alone

To elucidate the potential involvement of V_m to the regulation of pH_i I investigated the effect of seawater with an increased $[K^+]_e$ on pH_i . For this, solution 2 (ASW_c) was rapidly exchanged for solution 5 (100 mmol l⁻¹ K⁺). Surprisingly, as with decreased $[Cl^-]_e$ the cells reacted instantaneously with an acute acidification (Fig. 29, 1st transient). As the results were so similar to the experiments with decreased Cl⁻, I decided to test the effect of 0 HCO₃⁻ and 0 Na⁺ on second transient acidification (Fig. 29; Table 12).

5.1.11.2 Effect of HCO₃⁻ and Na⁺ on the K⁺ induced pH effect

For this the 100 mmol l⁻¹ K⁺ solution was exchanged for a solution 7 (0 Na⁺) and solution 4 (0 HCO₃⁻), respectively, in analogy to the experiment described in 0. Again no transient acidification occurred under these conditions, independent of the order, but only upon return to solution 2 (ASW_c) with all three respective concentrations re-established. I could thus show that this second transient acidification again is HCO₃⁻ and Na⁺ dependent.

The 100 mmol l⁻¹ K⁺ induced acidification decreased in the ratio by 0.64 ± 0.03 absolute difference to precontrol (solution 2); this corresponds to a relative difference of $27 \% \pm 1.4 \%$ (n = 96, m = 4). This acidification was followed by a rapid return to almost the initial emission ratio. (-0.05 ± 0.01 absolute difference to precontrol (solution 2); this corresponds to a relative difference of $2 \% \pm 0.3 \%$).

Comparable to the effect in the 90 Cl⁻ experiments the cells

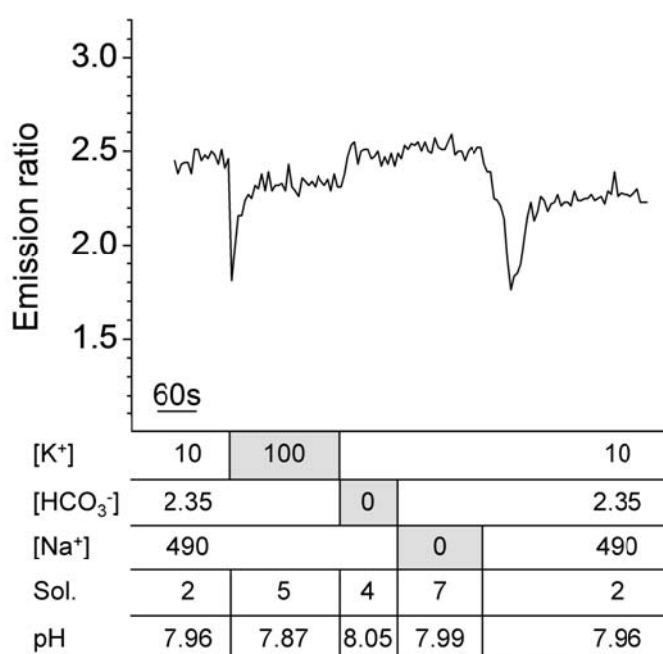


Fig. 29 Effect of low $[Na^+]$ and low $[HCO_3^-]$ on the 2nd K⁺ induced transient acidification
Again, the 2nd transient acidification only takes place upon return to normal K⁺, Na⁺, and HCO₃⁻ concentrations.

again acidified upon return to control solution 2 (ASW_c, 10 mmol l⁻¹ K⁺, -0.53 ± 0.02 absolute difference to precontrol (solution 2); this corresponds to a relative difference of 22 % ± 0.8 %), and then slowly recovered to almost the initial pH (-0.19 ± 0.01 absolute difference to precontrol (solution 2); this corresponds to a relative difference of 8 % ± 0.6 %, Table 12).

5.1.11.3 Effect of Ba²⁺ on the K⁺ induced pH effect

In a next step I tested the effect of 100 μmol l⁻¹ Ba²⁺, a K⁺ channel blocker, on *E. huxleyi* pH_i.

No effect was detected when Ba²⁺ was applied alone (Fig. 30, 1st grey column; n = 9, m = 1). When the cells were first challenged by an increase in the [K⁺]_e, application of Ba²⁺ or return to HCO₃⁻ induced a transient acidification (Fig. 30, 2nd grey column; -0.57 ± 0.04 absolute difference to precontrol (solution 2); this corresponds to a relative difference of 24 % ± 1.5 %;). This acidification was followed by a 2nd transient acidification upon removal of Ba²⁺ from control solution 2 (ASW_c, -0.66 ± 0.03 absolute difference to precontrol (solution 2); this corresponds to a relative difference of 27 % ± 1.1 %, correspondingly).

Afterwards the emission ratio increased again, with a remaining difference to pre control of -0.26 ± 0.01, corresponding to a relative difference of -10 % ± 0.5 %.

The Ba²⁺ dependent acidification was thus dependent on a preceding K⁺ pulse, inducing changes for a transport system sensitive to inhibition by Ba²⁺.

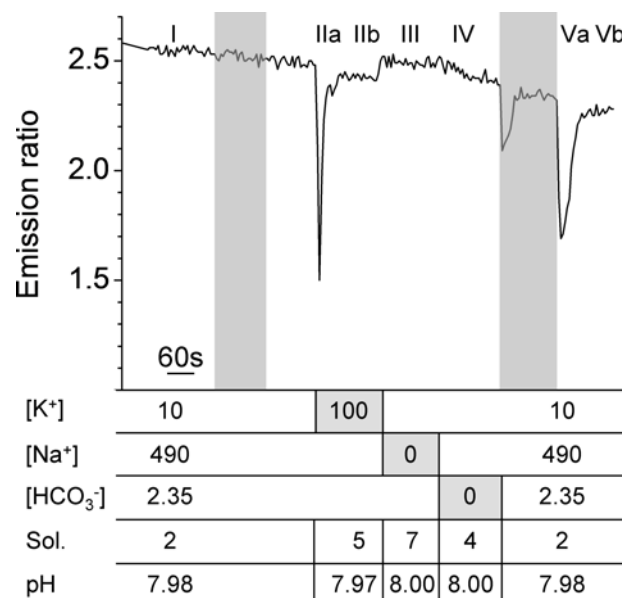


Fig. 30 Effect of Ba²⁺ on the acidification upon return to ASW_c with normal [K⁺]_e concentrations
 I ASW_c IIa high [K⁺]_e induced acidification and IIb re-alkalinisation under high [K⁺]_e III low [Na⁺]_e IV low [HCO₃⁻]_e Va high [K⁺]_e induced acidification upon return to ASW_c and Vb re-alkalinisation. Columns (green) indicate the effect of 100 μmol l⁻¹ Ba²⁺ before (left, n = 9, m = 1) and after (right) application of high [K⁺]_e. n = 23, m = 3

	100K ⁺		0 HCO ₃ ⁻		0 Na ⁺		ASW _c + Ba ²⁺		ASW _c	
	IIa 1 st ta	IIb Plateau	III	IV	Va Ba ²⁺ ta	Vb Recovery	Va 2 nd ta	Vb Recovery		
d _{abs}	-0.67 ± 0.04	-0.05 ± 0.01	-0.04 ± 0.02 #	0.00 ± 0.01 §					-0.53 ± 0.02 *	-0.19 ± 0.01
	-0.81 ± 0.05	-0.08 ± 0.01	-0.06 ± 0.01 #	-0.01 ± 0.01 §	-0.57 ± 0.04 *	-0.19 ± 0.02			-0.66 ± 0.03 *	-0.26 ± 0.01
%	-27 ± 1.4	-2 ± 0.3	-2 ± 1.0 #	0.0 ± 1.0 §					-22 ± 0.8 *	-8 ± 0.6
	-34 ± 2.0	-3 ± 0.3	-2 ± 0.4 #	0.0 ± 0.3 §	-24 ± 1.5 *	-8 ± 0.6			-27 ± 1.1 *	-10 ± 0.5

Table 12 Effect of increased [K⁺]_e on pH_i and effects of HCO₃⁻, Na⁺, and Ba²⁺ on the reacidification upon return to control (ta) transient acidification; (IIa) 1st high [K⁺]_e induced transient acidification; (IIb) re-alkalinisation under high [K⁺]_e; (III) low [HCO₃⁻]; (IV) low [Na⁺]; (Va) acidification upon return to ASW_c; (Vb) recovery
The 2nd acidification only occurs upon return to ASW_c with normal K⁺, Na⁺, and HCO₃⁻ concentrations. Experiments with (n = 23, m = 3) and without (n = 96, m = 4) Ba²⁺. * significantly more acidic vs. IIb (p<0.01); significantly more alkaline vs. IIb (p<0.05); significantly more alkaline vs. IIb (p<0.01)

5.2 Electrophysiological measurements

Until now there is no information about membrane voltage measurements or ion channel expression in *E. huxleyi* available. Since membrane voltage is the major driver of ion movements in addition to concentration gradients, it is of particular importance to characterise the electrophysiological properties of these cells.

E. huxleyi, however, offers limited access to investigations by its small size, the robust and tight cell cover (organic matrix) and by calcite shells. Nevertheless, we established several approaches to prepare clean protoplasts and to obtain electrical access to the intracellular space. As a control organism we used *C. pelagicus*, where such measurements have been published (Taylor & Brownlee, 2003).

5.2.1 General remarks

The different protocols applied in *E. huxleyi* consisted of two steps: 1. removal of coccoliths as for optical measurements, and 2. mechanic or enzyme assisted removal of the organic scales. A range of different protocols for the production of clean protoplasts in *E. huxleyi* was tested; however during these experiments I found that it was impossible to produce protoplasts accessible to patch clamp investigation. The protoplasts produced by the extended stripping protocol (see 4.6.3) looked clean (Fig. 31). To verify the effect of the enzymes used (cellulase, pectinase, pectolyase and sometimes chitinase in addition, 4.1.5) I performed cellulose staining (see 4.8) and could show cells without any detectable surroundings left (Fig. 31c).

Nevertheless, the cells were relatively stiff, and did hardly react towards suction, or in

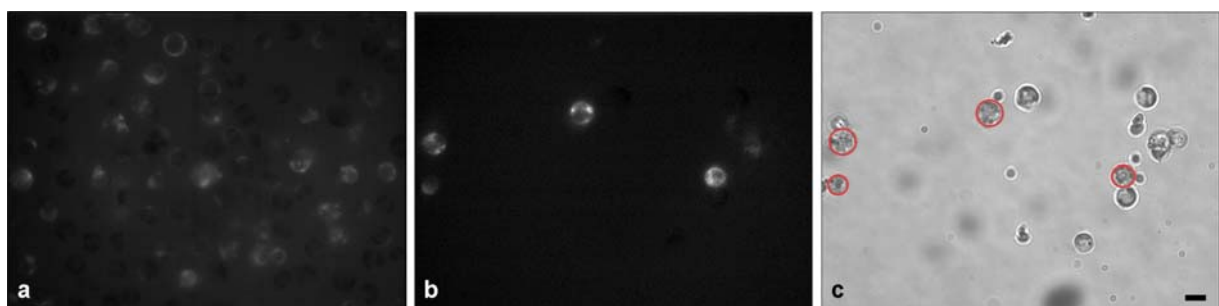


Fig. 31 Representative images of cellulose staining in *E. huxleyi*
 a) Staining of cellulose with Calcofluor White stain before digestion with solution 14 (enzymatic digestion, see 4.6.3). 415-440 nm Fluorescence emission at 355 nm excitation b) Staining of cellulose with Calcofluor White stain after protoplast preparation. 415-440 nm Fluorescence emission at 355 nm excitation c) Bright field image of 3 reveals about 50% cellulose free protoplasts. Red circles indicate incomplete digestion, visible in b). Scale bar 5 μm .

the other extreme, ruptured immediately upon slightest suction (data not shown).

In contrast, measurements in *C. pelagicus*, which was used as the test species, were successful.

5.2.2 *C. pelagicus*

Protoplast production was feasible in this species, even if not regular or in large quantities. Cellulose staining as well as optical control (Fig. 32 c) showed clean protoplasts with only marginal leftovers of the surrounding organic covering (arrows in Fig. 32). Cells were soft and reacted properly towards suction.

I was able to improve the technique to the extent that I was able to establish gigaseals by applying tender suction (Fig. 33 shows one example). Sealing was slow (minutes) and often resulted in larger parts of cell membrane covering the inside of the micropipette.

I succeeded in achieving gigaseals and on cell configurations (11 out of 196 cells) and was able to detect and record channel openings in few occasions (example shown in Fig. 34).

The respective current voltage relation for this channel is shown in Fig. 35.

5.2.3 Electric properties of *C. pelagicus*

The recording of channel openings in the example shown revealed 4 channel opening niveaus. This indicates either 4 channels of the same type opening up or 4 conductance states of one channel type.

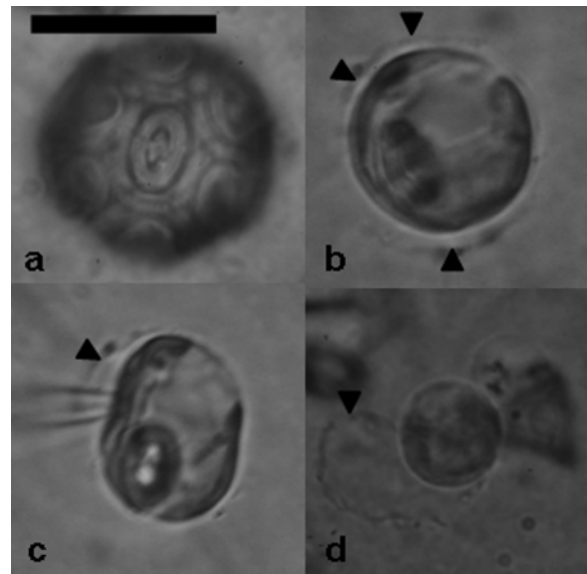


Fig. 32 *C. pelagicus* cell during protoplast production and experiment. a) *C. pelagicus* cell with coccosphere before treatment b) protoplast with leftovers of organic cover (arrows) c) protoplast deformed by micropipette; some organic cover is still visible d) Cell after intentional disruption. Scale bar 10 μ m



Fig. 33 Exemplary picture of a patch pipette sealed to a protoplast of *C. pelagicus*. Scale bar 10 μ m

In the experiment shown the respective currents were measured in 10 mV steps of the holding potential between -30 and 0 mV.

As shown in Fig. 35a extrapolated through the abscissa the data result in a zero current potential of 41 mV. The slope of the I/V curve, representing the single channel conductance, was calculated to be 19 pS ($n, m = 1$). The linear I/V curve derived from these values indicates a voltage independent, non rectifying channel.

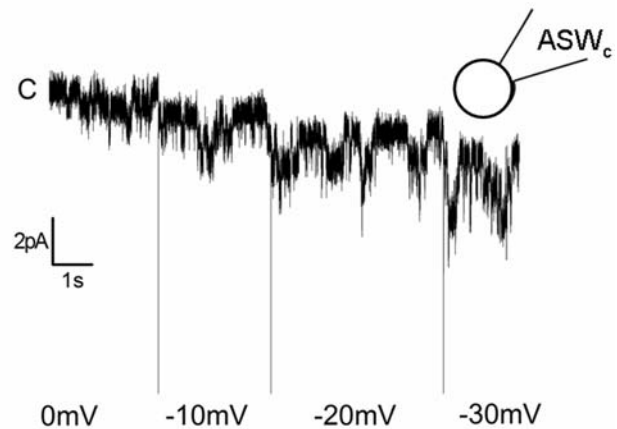


Fig. 34 Current traces of an ion channel in *C. pelagicus* at different clamp voltages. 4 voltage dependent niveaus of channel openings are visible, indicating 4 open channels of the same type

A channel measured in another example (Fig. 35b) revealed 5 channel opening niveaus, indicating either 5 channels of the same type opening up or 5 conductance states of one channel type. In this experiment the respective currents were measured in 10 mV steps of the holding potential between -100 and -20 mV. Extrapolated through the abscissa these data result in a zero current potential of 5.5 mV. The single channel conductance was calculated to be 26 pS ($n, m = 1$) in this case.

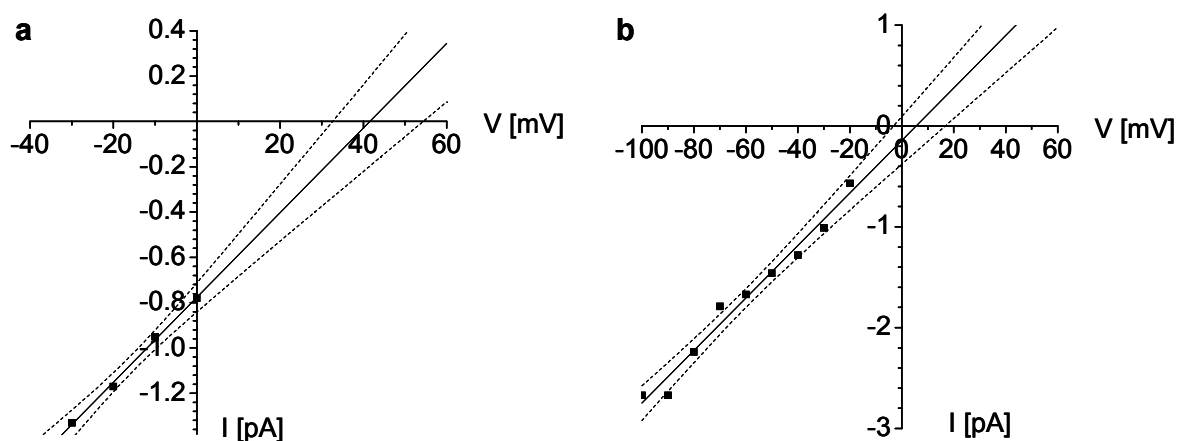


Fig. 35 I/V curves of two *C. pelagicus* experiments
 a) The slope of the curve was 19 pS and the zero current potential was 41 mV; $R^2 = 0.99$. $n, m = 1$ (corresponding to data shown in Fig. 34).
 b) The slope of the curve was 26 pS and the zero current potential was 5.5 mV; $R^2 = 0.98$. $n, m = 1$

6 Discussion

6.1 General

During this thesis I managed to successfully achieve pH_i (BCECF) measurements and first steps in electrophysiological measurements in coccolithophores. This complementary approach, bringing the findings from field experiments into physiological context, will enable us to move on from description to a better understanding of the underlying mechanisms.

6.2 Methodological

6.2.1 Culture conditions for microscopy

The cultural conditions used in these studies provided large numbers of cells. With an increasing age of the cell culture the stickiness of the cells increased. The conditions of cell culture were optimised for experimental requirements like cell number, cell adhesion, and dye loading. Compared to field conditions this culture protocol was characterised by the following aspects:

Cells were rapidly nutrient depleted under the given conditions, and for most of the culture time (from d 4 onwards), still growing, but at a decreased rate, and still calcifying at a comparatively high rate. Also they might change the carbonate system in their environment under the given circumstances. Table 13 gives an overview on different physiological states of *E. huxleyi* in comparison to the selected culture conditions. The culture conditions most likely represent the stationary phase of *E. huxleyi* cells. In most experiments done on *E. huxleyi* cells are kept at low cell numbers, under nutrient replete and stable carbonate system conditions, to represent more natural conditions. However, when cells were kept under more optimised conditions of nutrient repletion in semi-continuous batch culture they did neither take

Table 13 overview on characteristics of different physiological states of *E. huxleyi*
Best indicator of the physiological state is the cell division rate, reflecting whether the cells are still growing exponentially.

Growth phase	exponential	stationary	decay
Nutrients	+++	(+)	-
Cell division [doublings d ⁻¹]	2-3	1	-
Calcification	+	++	(+)
Abundance [cells ml ⁻¹]		>1000000	

up dye properly, nor were adhesive enough to the bath bottom for a fast fluid exchange.

The experiments discussed in this thesis thus are considered a first step in understanding the cellular properties of *E. huxleyi* with respect to ion transport over the plasma membrane and pH homeostasis. Nevertheless, the cultural conditions must be taken into consideration when discussing homeostatic mechanisms and ion transport properties of these cells in general. I expect quantitative differences for different cellular states, possibly resulting in a modified set of transport and regulatory proteins being synthesised. The results stated in this thesis are thus quantitatively valid only for these conditions, but it is likely that the findings qualitatively also can be confirmed in other stages of *E. huxleyi*. This has to be further investigated in exponentially growing, unlimited cultures or in cells living under natural conditions.

A second important point concerning the validity of the results is the duration of the whole protoplast producing procedure. Stripping, recovery phases and settling times were in the range of hours, thus resulting in cells being out of natural conditions for a considerable time. Cells might have had enough time to express transport systems and / or homeostatic mechanisms not active under normal conditions. Nevertheless, systems expressed under these conditions are part of the species' transport and regulatory tool box, and can give valuable hints about possible adaptation mechanisms in these unicellular organisms.

Summarised, we are aware of the constraints; however do accept them on the background of working with an organism representing a black box on the physiological level in combination with methods which had to be applied of scratch.

Nevertheless, the results achieved are considered to be valuable for the scientific community.

6.2.2 Microfluorimetry

A stable ratio with a mean value around 2.4 of fluorescence emission was established regularly, with loading intensities (at 486nm) between 150 and 600 arbitrary units. However, there was considerable scattering and I often observed cells which were higher or lower in ratio as well as in the absolute intensity.

It is known, that metabolism in *E. huxleyi* varies substantially during certain phases of the cell cycle, e.g. calcification is restricted to the G1 phase (Müller *et al.*, 2008). This

might also hold true for the expression of certain enzymes, e.g. esterases needed for the conversion of BCECF-AM to the free acid. In general the cells used in this study are assumed to have been in the G1 phase, predominantly, i) as they were always harvested at approximately the same time during the light phase, when >85% of the cells are in G1, and ii) as they arrest in the G1 phase when they are PO_4^{3-} or NO_3^- limited (Müller *et al.*, 2008). In this phase the cells can be considered to be in a PO_4^{3-} scavenging mode, with a considerable expression of alkaline phosphatase. As BCECF has to be taken up and then cleaved by esterases, I think that e.g. an increase in alkaline phosphatase activity with increasing P-limitation might be one explanation for the observed improved dye uptake with increasing culture age and increased nutrient limitation.

In this study I recorded BCECF fluorescence in *E. huxleyi* as a measure of cytosolic pH and managed to get a first insight into the membrane permeability properties with respect to CO_2 , HCO_3^- and H^+ . The use of pH sensitive dyes is a long used approach to analyse transport processes and pH homeostasis on a single cell level, with BCECF as the most widely used indicator dye (Rink *et al.*, 1982). In these pH_i measurements the interpretation of data is straight forward as long as the concentration of a single ion species, e.g. Na^+ or Cl^- , is experimentally modified or pharmacological tools are used. BCECF measurements of pH_i in *E. huxleyi* have already been established before (Dixon *et al.*, 1989) and values for overall pH_i were recorded in the range of 7.1 - 7.3 in the presence of $2 \text{ mmol l}^{-1} \text{HCO}_3^-$.

A direct translation of our calibration measurements into pH_i resulted in a more alkaline pH of around 8. As already mentioned in the materials and methods section, there are considerable limitations with respect to the absolute calibration of pH_i . In the study of Dixon *et al.* the ion composition of the extracellular space for example was completely different from our or physiological conditions. In addition dye loading and distribution within the cell have a strong influence on the contribution of pH_i as the cytosolic to the whole signal. We excluded dye loading of the chloroplast and could show at confocal resolution that the fluorescence signal did not origin from specific intracellular organelles. In line with Anning *et al.* (1996), our observations confirm the unequal dye loading intensity between cells within the same batch.

In addition, I observed a larger scatter of resting emission ratios (Fig. 19) for the individual cells of the same batch which was independent of dye loading. This could

be caused by real differences in pH_i values between cells and caused by their individual functional state. However, since the relation between pH_i and fluorescence ratio depends on the intracellular composition, it could also originate from different individual BCECF calibration curves for each cell.

I did not observe a dye signal from the chloroplast (c.f. confocal image, Figure 2b).

The detected fluorescence signal thus resembles an integrated signal of the whole cell with a major contribution by the cytosol. However, I cannot exclude a partial contribution of otherwise compartmentalised dye to the integrated signal. In some cases I observed a slight decrease in the ratio over time. At present I have no clear explanation for this. I might speculate that it indicates an acidification of the cells over the time course of the experiment, or a change in the contribution of compartmentalised dye to the integrated signal.

6.2.3 Calibration of pH_i with nigericin

I was able to calibrate cells with the nigericin approach.

In the nigericin / high K^+ calibration experiments cells followed pH_e in a linear fashion. Under calibration conditions change in pH_i was fast and reached a stable plateau at the rate of bath exchange. Comparison of the slopes of delta emission change due to pH_e alone ($\Delta \text{pH}_i = 0.44 \Delta \text{ratio}$) or pH_e with nigericin ($\Delta \text{pH}_i = 0.78 \Delta \text{ratio}$; see Fig. 21, Fig. 22) shows that *E. huxleyi* physiological H^+ permeability is still limited and that *E. huxleyi* is able to buffer the influx of H^+ by further $\text{H}^+/\text{HCO}_3^-$ metabolism.

Given these results one would be tempted to give absolute pH_i values and transform the changes in emission ratio directly to changes in pH_i , to compare them to values from the literature. However, there are a few caveats.

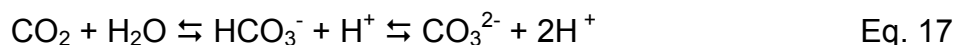
The detected emission ratio (Fig. 19) corresponds to individual dye loading, and compartmentalisation within the cells. In favour of an optimal time window for the experiments with respect to fluorescence intensity and cell viability I decided not to perform an individual calibration for each cell. For a clear statement about the actual pH_i in *E. huxleyi*, however, exactly this would have been necessary.

I focussed on relative changes of pH_i , shown here as changes in the emission ratio. Hence, it remains open how close our cells were to the reported pH_i values when entering the experiments. In fact, they could be different since previous calibrations using BCECF were performed with *E. huxleyi* in a minimal medium consisting of 100

mmol l⁻¹ K⁺, 30 mmol l⁻¹ NaCl, 500 mmol l⁻¹ mannitol, 25 mmol l⁻¹ 2-(N-morpholino) ethanesulfonic acid (Mes), and 25 mmol l⁻¹ HEPES buffer (Dixon *et al.*, 1989). Properties of our experimental control solutions were derived from natural seawater. The main differences were the presence of high Na⁺ and Cl⁻. This might significantly influence pH_i and the capability of the cells to maintain pH homeostasis since it is likely that Na⁺ and Cl⁻ dependent mechanisms are involved in H⁺ and HCO₃⁻ transport. In addition, membrane voltage also in coccolithophores strongly depends on either K⁺ or Cl⁻ conductances (Sikes & Wilbur, 1982; Taylor & Brownlee, 2003) and the respective electrochemical driving forces (i.e. ion gradients).

6.2.4 OOE_s

With the OOE approach we advanced an elegant method to test H⁺, HCO₃⁻ and CO₂ separately of another. This always is the challenge in a HCO₃⁻ buffered system like seawater. Under steady state conditions it is impossible to solely alter any of the 3 species as they are inter-dependent (Eq. 17).



Different approaches have been applied to solve this problem, taking advantage of the slow reaction rates between CO₂ and HCO₃⁻. The isotopic disequilibrium technique (Endeward *et al.*, 2006; Rost *et al.*, 2002) uses radioactive or stable isotopes of the CO₂ and HCO₃⁻ pools and mass spectrometry of the resulting metabolites. I could show with the out-of-equilibrium approach (Zhao *et al.*, 1995) that the impact of any of the 3 species on pH_i can be monitored online and on a single cell level in a repeatable manner. Calculations confirmed that the time frame of the experiments was well within the out of equilibrium range.

For this I had to develop a mixing unit which allowed a fast supply and exchange of the non equilibrated solutions and a visible control of the direction of the filament towards the cells in focus. At the same time flow rate had to be adapted to ensure the adhesion of the cells to the glass bath bottom. By the much appreciated help of the workshop of the physiological institute this was achieved in a simple prototype, and further developed into the OOE mixing unit, designed for 3 OOE solutions (4.5.7).

6.3 Membrane properties and pH homeostasis of *Coccolithophores*

6.3.1 Membrane H⁺ permeability and effect on pH_i

E. huxleyi followed pH_e over a broad pH range linearly. This is surprising, as a lipid bilayer per se is impermeable to H⁺ ions. Pore forming structures like channels or facilitated transport proteins like transporters or pumps are needed to allow movement of ions over the membrane in sufficient amounts. In mammalian cells one would rather expect cells to be relatively tight for H⁺, as pH homeostasis is so essential. At the least, one would expect the cell to control the in- or efflux of H⁺ tightly.

Diffusion of protons across biological membranes can be facilitated by a number of specialised proteins which could support the observed effect directly or indirectly:

- i) facilitated CO₂ influx via aquaporins and subsequent formation and dissociation of carbonic acid in the presence of CA.
- ii) carrier proteins which use the trans membrane gradient for one substrate (e.g. Cl⁻) for the transport of another substrate (e.g. HCO₃⁻) against its concentration gradient.
- iii) ion channels providing a direct conductive permeability (e.g. H⁺).
- iv) artificial membrane damage resulting in unspecific pores.

The results discussed in the following speak against a ruptured and disintegrated membrane but for a specific channel.

I observed a dramatic and instant change in pH_i with a change in the external pH. The kinetics of this effect was close to the range of the bath exchange rate (6-8 ml min⁻¹ at a bath volume of 350 µl, corresponding to an exchange time of ~ 2.4 s). However, with nigericin there the pH effect was even faster. Nigericin therefore introduced a further H⁺ permeability into a plasma membrane which already displayed a distinct but still limited H⁺ permeability.

The effect of acidic pH_e was most likely directly via the influx of acid equivalents or the impairment of the efflux of continuously produced H⁺, or a combination of both effects. Any indirect effects using more complex intracellular metabolic events would have been expected on a slower time scale. From personal communication it is known that also in the working group of A.R. Taylor & C. Brownlee a H⁺ conductance is discussed for *C. pelagicus*.

If one considers pH changes during a bloom, which occur regularly and rather fast (on the order of days to weeks), these cells will have different internal pH values under these circumstances. During an *E. huxleyi* bloom, when CO₂ is used for photosynthesis, pH_e can rise to values as high as 8.8 (Dong *et al.*, 1993). Later, when nutrients are suboptimal, increase of calcification can lead to an increase in pCO₂ (Delille *et al.*, 2005) according to 3.4, Eq. 11, and thus to a decrease in pH_e.

To distinguish among the possibilities mentioned beforehand I generated the OOE solutions. Our results clearly show that a conductive or carrier mediated H⁺ pathway underlies the high proton permeability of the membrane. Since I did not observe any saturation or nonlinear behaviour within the investigated pH range a proton conductance via H⁺ channels is the most likely explanation.

I did not observe a pH_i recovery under the continuous challenge by acidic pH_e. After return to control conditions the cells again followed passively pH_e and did not show any sign of overcompensation. Some cells, however, remained slightly more acidic after the experiment.

On the first sight this would suggest a cell with low pH regulatory capacity or even low metabolism. On the other hand, since calcifying *E. huxleyi* produce large amounts of H⁺ (see estimate based on Anning *et al.* (1996) and Dong *et al.* (1993)) the existence of an almost unlimited H⁺ export pathway would make perfect sense. This pathway would mask regulatory mechanisms with lower transport capacity. Also, turning around the gradient and thus the driving force for H⁺ by acidifying the extracellular fluid, a situation which has never happened in seawater since the evolution of *E. huxleyi*, might simply overburden any given buffering capacities of the cells.

Assuming a conductive H⁺ pathway, membrane voltage in *E. huxleyi* would gain a predominant role in pH_i homeostasis and become decisive for the export of H⁺ and hence for the ability to calcify. These results are encouraging for establishing electrophysiological measurements and K⁺ / Cl⁻ perturbations.

6.3.2 Membrane CO₂ permeability and effect on pH_i

The isolated increase in CO₂ did not cause any detectable change in pH_i. This was surprising since a considerable CO₂ permeability of *E. huxleyi* cell membrane is very likely and a consecutive acidification of the cytosol would then be expected after

intracellular formation and dissociation of carbonic acid. Most cell membranes show intrinsic CO₂ permeability and in addition there are membrane proteins which facilitate CO₂ diffusion like aquaporins (Musa-Aziz *et al.*, 2009). In fact the *E. huxleyi* genome reveals several candidate aquaporins (von Dassow *et al.*, 2009 and also <http://supfam.cs.bris.ac.uk/superfamily>) which might be functionally relevant. On the other hand there are examples of membranes with very limited CO₂ permeability like luminal membranes of epithelia in mammalian kidney and gastrointestinal tract (Bleich *et al.*, 1995; Hasselblatt *et al.*, 2000). In any case acidification by an extracellular CO₂ increase would only be visible at a significant activity of CA and at limited membrane permeability for H⁺. In fact, in our experiments I show high H⁺ permeability and the expression of CA has been discussed to be low at our cell culture conditions (Herfort *et al.*, 2002; Nimer *et al.*, 1994b).

Finally, CO₂ could be trapped immediately by photosynthesis, bypassing metabolic conversion within the cytosol. However, our experimental conditions render this alternative unlikely.

Illumination times in the experimental setup were kept very short (24 and 60 ms at 486 and 440nm, respectively), and illumination only took place every 5 seconds. These conditions should not drive photosynthesis significantly.

li) Even if photosynthesis was activated by the conditions, at 600 μmol kg⁻¹ CO₂ RubisCo is well saturated even at highest light.

On this background and given our observations on H⁺ permeability it is not surprising that an isolated change in CO₂ did not affect pH_i. However, I am not able to give an estimate of the plasma membrane CO₂ permeability at this stage.

6.3.3 Membrane HCO₃⁻ permeability and effect on pH_i

The isolated increase in extracellular HCO₃⁻ concentration led to a decrease in pH_i. This was surprising since one would expect rather an alkalisation at a typical cellular pH_i since uptake of HCO₃⁻ and subsequent cytosolic H⁺ buffering would increase pH_i. The observed decrease in pH_i might be caused by immediate metabolism of HCO₃⁻ to CO₃²⁻ and H⁺ (Anning *et al.*, 1996). *E. huxleyi* continuously requires high amounts of CO₃²⁻ for coccolith formation and the respective metabolism of HCO₃⁻ would generate H⁺ and decrease pH_i, irrespective of whether CO₃²⁻ formation occurs within the cytosol or inside the coccolith vesicle. Another alternative

would be cotransport of HCO_3^- with H^+ or antiport of HCO_3^- vs. OH^- or Cl^- . If any of these transporters were electrogenic the increased exchange could result in a change in membrane voltage which directly would influence the proton current through putative proton channels.

Why, on the other hand, is the respective H^+ load by metabolism or cotransport not short circuited by the observed H^+ permeability? In contrast to the experiment with an isolated increase in $[\text{CO}_2]$, providing $0.6 \text{ mmol kg}^{-1} \text{ CO}_2$, the isolated increase in $[\text{HCO}_3^-]$ provides $19.7 \text{ mmol kg}^{-1} \text{ HCO}_3^-$ at the experimental time slot, resulting in 33fold higher substrate concentration for the respective generation of H^+ . Under these conditions the H^+ pathway might become limiting.

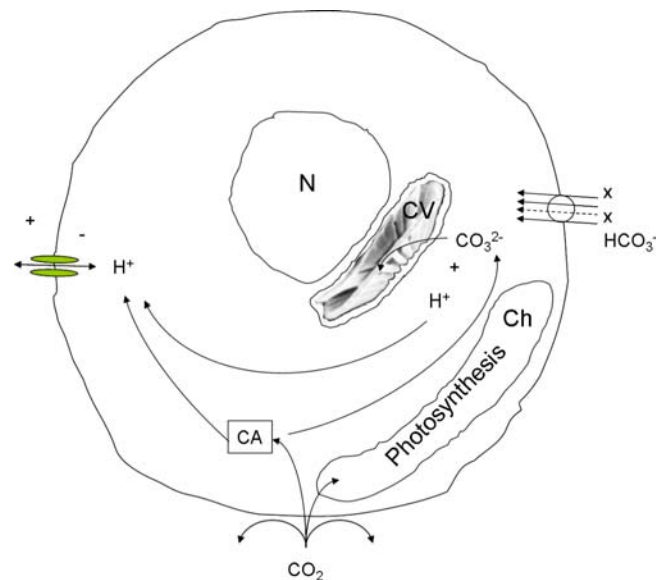


Fig. 36 Schematic *E. huxleyi* cell model I
First simple model, showing putative H^+ , HCO_3^- , and CO_2 permeabilities and their possible interactions. N nucleus, CV coccolith vesicle, Ch chloroplast, CA carbonic anhydrase

6.3.4 Cell model for membrane permeabilities

Taken together the experiments with isolated H^+ , CO_2 , and HCO_3^- yielded in a first cell model of membrane pathways in *E. huxleyi* (Fig. 36).

Isolated increase in $[H^+]$ ions shows a direct effect on pH_i , with a linear response of the cell's pH_i over the physiological range. Due to the instantaneous changes it is tempting to speculate about a H^+ channel (Fig. 36). Still, the cells seem to reach a steady pH_i state above pH_e , as shown by the increase in speed and magnitude of H^+ influx in the nigericin experiments.

Isolated increased $[CO_2]$ shows hardly any effect. This might be either due to CO_2 not passing the plasma membrane because of a tighter than speculated membrane and absence of a CA, or due to direct use in photosynthesis. Also, protons produced by CA activity might also leave the cells too fast to be detected, if so supporting the H^+ pathway hypothesis.

Isolated increase in $[HCO_3^-]$ shows the unexpected effect of slightly decreasing pH_i . This might be due to CO_3^{2-} formation in the course of calcification and subsequent H^+ production. However, this process would have to be significantly faster than any CA activity, resulting in significant amounts of protons, if detected in these settings. Activity of CA is viewed as the fastest enzymatic activity known, however. A substantiated HCO_3^- uptake pathway has to be hypothesised as well. This was

further investigated with ion gradients and DIDS - influencing classical HCO_3^- transporters.

6.3.5 DIDS effect on membrane H^+ permeability and pH_i

A variety of transporters, pumps and channels can be involved in pH homeostasis, as shown in Table 14. The SLC4 family, one large group of transporters, can be divided functionally into 3 groups: Na^+ independent $\text{Cl}^-/\text{HCO}_3^-$ exchangers, $\text{Na}^+/\text{HCO}_3^-$ cotransporters, and Na^+ driven $\text{Cl}^-/\text{HCO}_3^-$ exchangers (Pushkin & Kurtz, 2006). These transporters work either electroneutral or electrogenic, have different stoichiometries (1:1 up to 1:3), and therefore can function as acid loaders or extruders. Also Ca^{2+} transporters and ion channels for K^+ , Cl^- , or Ca^{2+} influence acid base transport.

Single amino acid substitution in the proteins can induce different stoichiometries (Pushkin & Kurtz, 2006), and by this turn electroneutral into electrogenic transport. This can cause various diseases in humans (Alper, 2006; Pushkin & Kurtz, 2006). An increase in internal $[\text{Ca}^{2+}]$ was also shown to induce changes in the stoichiometry, and even the transport direction of the involved ions can reverse, also dependent on the stoichiometry and membrane voltage, turning acid loaders into acid extruders or vice versa (Pushkin & Kurtz, 2006).

Among the transport systems putatively involved in pH homeostasis are a number of DIDS sensitive transporters and channels, which belong to different transport types (exchangers, cotransporters and channels). DIDS has been used as a blocker for a variety of transporters involved in pH homeostasis and HCO_3^- transport (Romero *et al.*, 2004). It has been shown to interact on different reaction motifs, the interaction can be reversible or irreversible (Lu & Boron, 2007; Romero *et al.*, 2004) and shows biphasic kinetics in some tissues (Gallemore & Steinberg, 1989; Nakhoul *et al.*, 1998; Wehner *et al.*, 1993). Also for the CIC family of Cl^- coupled H^+ transporters, DIDS inhibition has been reported, with intra- and extracellular binding sites (Pusch *et al.*, 2006).

In contrast to Nimer *et al.* (1996) which did not find a DIDS sensitive HCO_3^- transport in exponentially growing *E. huxleyi* cells, Herfort *et al.* (2002) found a DIDS and SITS inhibitable HCO_3^- sensitive system and postulated an anion exchanger (AE1). In *C. pelagicus* DIDS sensitivity of an inward Cl^- rectifier channel has been shown (Taylor & Brownlee, 2003). This channel might be involved in balancing H^+ and HCO_3^- transport directly or indirectly via membrane voltage regulation. Transcriptome

analysis by von Dassow (2009) revealed several candidates for pH homeostasis, of which again the AE1 is DIDS sensitive.

In our hands DIDS itself led to a substantial acidification of the cells, which was only partially dependent on extracellular HCO_3^- . This indicates that, apart from the postulated H^+ permeability, DIDS sensitive processes are involved in pH homeostasis and HCO_3^- metabolism in these cells. Combination with the isolated H^+ experiments revealed that H^+ loading was also sensitive to DIDS. As the effect of acidic pH_e on pH_i was decreased in the presence of DIDS it might interfere directly with the H^+ permeability in *E. huxleyi*. On the other hand it might also be a less specific effect on the H^+ current, e.g. by affecting the Cl^- conductance and the membrane potential, respectively.

At this stage it is completely open which membrane proteins provide the H^+ pathway, how it is regulated, and what other transport systems it might be dependent on.

Table 14 could be a starting point for the search of candidate proteins involved in *E. huxleyi* membrane H^+ transport. Good candidates in our eyes are HCO_3^- transporters of the SLC4 family.

Further experiments to characterise the involvement of DIDS sensitive transporters in pH homeostasis would require inhibitors of the H^+ pathway, of photosynthesis and a reassessment of CA activity.

In any case, both effects of DIDS described above speak against the cells being H^+ permeable by artificial membrane damage, but favour the existence of actively regulated homeostatic mechanisms.

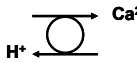

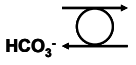
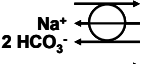
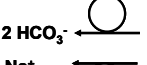
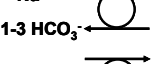
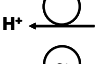
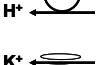
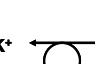
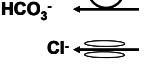
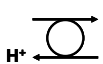

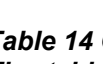
Protein	Type	Cl ⁻	K ⁺	Na ⁺	HCO ₃ ⁻	V _m	OH ⁻	H ⁺	Ca ²⁺	DIDS	EC	Reference
 VCXI (CAX _{homologue})	Ex							+	+		+	von Dassow, 2009
 HVCN1	Ch					+		+			+	von Dassow, 2009
 AE1(-3) (SLC4A1)	Ex	+			+		(+)	(+)		+	+	van Dassow, 2009; Herfort, 2002; Romero, 2004
 NBCe1(-2) (SLCA4)	Co			+	* ¹	+				+		Romero, 2004; Boron, 2004; Lu & Boron, 2006
 NDCBE (SLC4A8)	Ex	+		+	* ¹					+		Romero, 2004
 NCBE (SLC4A10)	Ex	+		+	+					+		Romero, 2004
 NHE	Ex			+				+				Boron, 2004
 V-H ⁺ ATPase (subunit)	P							+			+	von Dassow, 2009
 K ⁺ channel	Ch		+			+				+		Hill, 1999 ² ; Wehner, 1993 ²
 K ⁺ /HCO ₃ ⁻ , n	Co		+		+					+		Leviel F, 1992
 Cl ⁻ channel	Ch	+				+				+		Taylor & Brownlee, 2003
 ClCec1	Ex	+						+		+		Matulef & Maduke, 2005; Pusch, 2006
 Cl ⁻ channel	Ch	+	+			+				+		Gallemore & Steinberg, 1989

Table 14 Overview of cellular transport systems involved in pH homeostasis

The table shows a collection of transport systems involved in pH homeostasis. It is indicated which ions are (putatively) essential for transport of the respective system and if membrane voltage is affected. Data are from different organisms, direct measurements. e electrogenic; n electroneutral; Type transport type; Ex exchanger; Ch channel; Co cotransporter; P pump; DIDS DIDS sensitivity; EC *E. huxleyi* transcriptome; ² activation of Ba²⁺ sensitive inward rectifying K⁺ channel by DIDS; * HCO₃⁻ or CO₃²⁻ as a substrate is not clarified, yet.

6.3.6 Effect of decreased $[Cl^-]$, increased $[K^+]$, the role of V_m and co- or antiporters

Experiments with a lowered Cl^- and K^+ driving force and thus decreased E_m for the respective ions show similar effects. With both ions an acute acidification upon application of the respective solution and a prolonged acidification upon washout was observed. In both cases show Na^+ and HCO_3^- dependency of the onset of the second acidification could be shown.

Both manoeuvres significantly disturb V_m by introducing depolarisation. If pH homeostasis is dependent on V_m dependent transport systems this could explain the influence on pH_i .

$[Cl^-]_i$ in algae is low, ($\sim 90 \text{ mmol l}^{-1}$, Stewart (1974)) compared to $[Cl^-]_e$ in seawater ($546 \text{ mmol l}^{-1} Cl^-$). At a temperature of $17^\circ C$ (290.16 K), the Cl^- gradient translates into an equilibrium potential of -45 mV . A decrease in $[Cl^-]_e$ leads to a decrease in this gradient and thus a reduction in driving forces and membrane depolarisation.

The same might be true for K^+ , the other major player defining V_m . Due to the Na^+K^+ -ATPase the intracellular concentration of K^+ , $[K^+]_i$, is high, up to $>400 \text{ mmol l}^{-1}$ for algae, (Stewart, 1974) when compared to the extracellular concentration, $[K^+]_e$ ($10 \text{ mmol l}^{-1} K^+$). At a temperature of $17^\circ C$ the respective Nernst potential would be -58 mV . Again, if $[K^+]_e$ is increased also 100 mmol l^{-1} E_{K^+} will be 0 mV , and in analogy to the Cl^- experiment cells will undergo depolarisation.

In both cases depolarisation could now influence voltage dependent H^+ channels, resulting in a sharp decrease of pH_i by either decreasing the export of internally produced H^+ (e.g. due to calcification) or by increasing the import of external protons. The last is relatively unlikely, as with a depolarisation also the driving force for a positively charged ion towards the cytosol would be diminished, and the $[H^+]_e$ at a pH of ~ 8.1 is potentially lower than the $[H^+]_i$, resulting in an outwardly directed transport direction for protons following the concentration gradient.

Unfortunately neither the actual cytosolic $[K^+]$ of *E. huxleyi* is known, nor to what percentage E_{K^+} or E_{Cl^-} define V_m in this and other coccolithophore species. At least for K^+ the effect of Ba^{2+} supports the existence of a K^+ channel involved in this phenomenon.

An alternative for the V_m dependent H^+ transport system being responsible for the pH_i decrease could be a K^+ or Cl^- dependent H^+ transport system.

6.4 Electrophysiology

6.4.1 General (methodological) remarks

Electrophysiological data i.e. information about membrane voltage, membrane conductance, selective permeabilities and finally the analysis of ion channels and electrogenic transporters is mandatory to complement the picture collected by fluorescence techniques. For *E. huxleyi*, however, there are no data available.

By use of the electrophysiological approach we aimed to supplement results from the microfluorimetric experiments. Unfortunately considerable difficulties were experienced. A range of different protocols for the production of clean protoplasts in *E. huxleyi* was tested. In my hands, it was impossible to produce protoplasts clean enough for electrophysiology. The protoplasts produced by the extended stripping protocol (see 4.6.3) looked clean and the absence of cellulose and chitin could be shown (see Fig. 31c). However, the cells still seemed to be surrounded by a robust envelope. Even if a cell looked like a clean protoplast and was attached to a micropipette it was not possible to seal in. The cells were relatively stiff, and did hardly react towards suction by the micropipette, or in the other extreme, ruptured immediately upon slightest suction.

Another reason attributed to the observed difficulties is the small size in addition to the robust and complex cell.

6.4.2 Electric measurements in *C. pelagicus*

To reproduce the methodological approach, we changed the species to *C. pelagicus*. Protoplast production was found more feasible, even if not regular or in large quantities. Cellulose staining as well as optical control (Fig. 32 b, c) showed clean protoplasts with only marginal leftovers of the surrounding organic covering (arrows in Fig. 32). Cells were soft and reacted properly towards suction. Sealing was slow (minutes) and often resulted in protrusions of cell membrane into the micropipette. Patch clamp studies in native cells often are characterised by a high number of attempts to seal in comparison to the number of successful recordings. Many factors like temperature, cell culture conditions, protoplast preparation, etc. influence the

success and have to be optimised. I improved the technique to the extent that I was able to establish several gigaseals (Fig. 33) in *C. pelagicus* by applying tender suction. The sealing process was very slow, and in rare occasions I could detect channel activity. Successful ion channel recordings on cell (Fig. 33) nicely support whole cell measurements in *C. pelagicus* described by Taylor & Brownlee, 2003. They described a Cl^- conductance as the major ion pathway. We found single channel currents which were most likely carried by Cl^- . In fact, the single channel conductance found in our recordings is well in agreement with Cl^- channels described in other algae. Also the zero current voltage in cell attached configuration is compatible with the membrane voltages and Cl^- gradients reported by Taylor & Brownlee, 2003. In the cell attached configuration the zero current or reversal potential in our settings was measured to be 5 to 40 mV. It was measured at normal ion concentrations, with ASW_c in the pipette vs. intracellular concentrations in the intact cell. If we take this reversal potential and the Cl^- concentrations we can calculate a membrane voltage between -30 mV to -65 mV. At the given assumptions a Cl^- channel is the most likely candidate.

The on cell recording of one channel revealed 4 opening niveaus. These are equivalent to 4 channels. As the niveaus were of the same magnitude, they most likely result from the same type of channel, forming a cluster within the patched membrane area. The linear behaviour of the I/V curve indicates a voltage independent channel in the investigated voltage range. The single channel conductance was calculated to be 19 – 26 pS. However, the critical range of voltage dependence as described by Taylor & Brownlee, 2003 was not investigated (clamp voltage > 0 mV).

Since the aim was to measure *E. huxleyi* we did not further invest in optimisation of *C. pelagicus* patch clamping. The electrophysiological approach was thus deferred in favour of the microfluorimetric measurements after a considerable amount of time and trials. In a separate future effort alternative approaches to measure membrane voltage in *E. huxleyi* have to be established systematically.

6.5 Synthesis & Outlook

In this study we present first insights into pH regulation and ion fluxes over the plasma membrane in *Emiliana huxleyi*. With the methods established during the course of this thesis we now have tools at hand to further illuminate the transport and pH homeostatic properties of *E. huxleyi*.

This is extremely valuable, as we want to understand how these organisms will respond to environmental changes in pH and carbonate speciation. Furthermore, we are interested in how these changes will manifest themselves on a physiological level, and in identifying the underlying cellular mechanisms.

We present changes in BCECF fluorescence ratio as a measure of changes in pH_i , elicited by changes in external pH or ion concentrations. We did not calibrate for absolute pH_i values, as absolute ratio values were variable between different experiments and cells. However, the pH_i changes were comparable and consistent. Nigericin calibrations revealed the relation between ratio changes and changes in pH_i .

Seawater $[\text{H}^+]$, $[\text{HCO}_3^-]$ and $[\text{CO}_2]$ were increased independently using out of equilibrium solutions (OOE) to illuminate proton equivalent transport over the plasma membrane and to discriminate between their effects on pH_i .

We could show that physiological investigations on a cellular level are feasible with *E. huxleyi*, being a small, unicellular, photoautotrophic organism.

For the first time we could demonstrate a proton permeability in *E. huxleyi*. When the cells were subjected to changes in pH_e , pH_i followed in a linear fashion, and reached a steady state which was still above pH_e . The decrease of pH_i by an increase in extracellular $[\text{HCO}_3^-]$ suggests a predominant conversion of HCO_3^- to H^+ and CO_3^{2-} . In contrast, an increase in extracellular $[\text{CO}_2]$ did not significantly affect pH_i in our settings. This impedes conclusions about CO_2 permeability, as we cannot state whether CO_2 did or did not enter the cells. We can only conclude that even if CO_2 permeated the membrane, no significant pH_i change was measurable.

The effects of DIDS, a relatively unspecific inhibitor of anion exchange, on pH_i suggest the involvement of at least two different DIDS-sensitive transport systems in pH homeostasis. DIDS on the one hand acidified the cells, a process being partially dependent on $[\text{HCO}_3^-]$. On the other hand DIDS minimised the intracellular

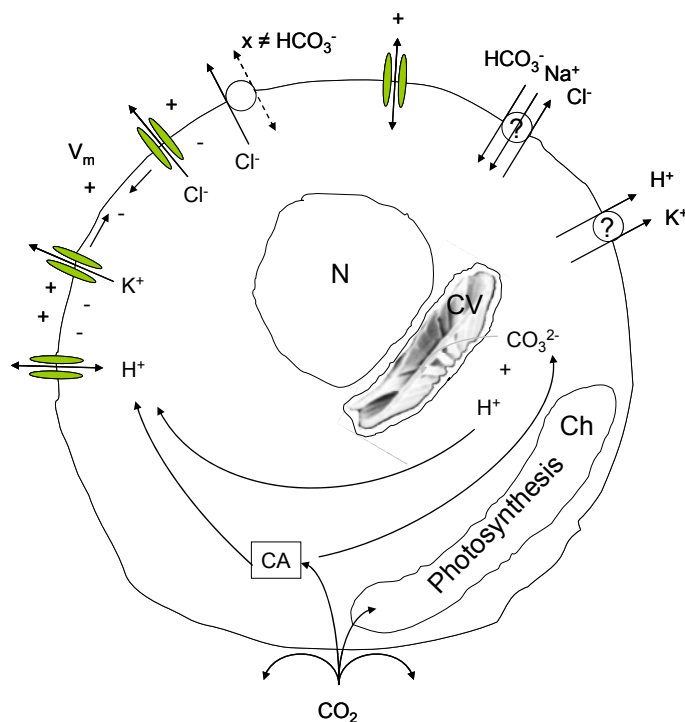


Fig. 37 Schematic *E. huxleyi* cell model II

Compilation of all putative transport systems impacting pH_i found in this study, with addition of the putative unspecific cation channel found in *C. pelagicus*.

acidification due to a decrease in pH_e . It can thus be used as a tool to further examine the properties of H^+ transport in *E. huxleyi*.

Ion manipulation experiments with altered $[Cl^-]$ and $[K^+]$ were performed in order to illuminate dependencies of pH homeostasis on specific ion gradients. Decreased seawater $[Cl^-]$ and increased seawater $[K^+]$ both induced a transient acidification of the cells, and a 2nd transient acidification upon return to control conditions was observed. The appearance of this 2nd transient was HCO_3^- and Na^+ dependent. In the high $[K^+]$ experiments we could further show a Ba^{2+} dependent transient acidification. The observed pH_i effects suggest $[K^+]_e$ and $[Cl^-]_e$ being involved in H^+ homeostasis. This could be explained either by a direct dependence of pH_i on membrane voltage or by an effect of ion gradients of $[K^+]$ and $[Cl^-]$ on transport systems coupled to these respective ions.

The methods developed during this thesis and the experimental tools characterised can be used in the future to understand pH_i homeostasis in more detail. It might be used to answer important research questions such as

- i) how *E. huxleyi* cells react after pre-adaption to decreased pH_e and an altered carbonate system speciation.
- ii) how great the variability in pH homeostasis is in different *E. huxleyi* strains.

The schematic model of *E. huxleyi* in Fig. 37 shows a compilation of all putative transport systems discussed in this study. These proteins are a good starting point for further investigation of mechanisms putatively involved in ion and pH_i homeostasis. Also, on the background of the sequenced genome and progressing annotation, the microfluorimetric approach is a promising tool. If dependencies of transport proteins involved in pH homeostasis on certain ions are known, this approach can be used as an assay to specifically test for expressed transporters or channels. Also the transcriptomic approach by von Dassow *et al.* (2009) resulted in a number of targets, such as homologs of aquaporins, anion exchanger 2, or a Cl⁻/HCO₃⁻ exchanger, which could be investigated by the established methods. A large number of inhibitors is available, e.g. HgCl₂ (aquaporin), omeprazole (H⁺K⁺-ATPase), gadolinium (H⁺ channel), or NPPB (Cl⁻ channel). It would be a good starting point to test whether these inhibitors, which have mainly been used in mammalian cells and tissues, are also useful in unravelling transport and pH homeostasis in coccolithophores.

IN PRESS

Cellular pH measurements in *Emiliana huxleyi* reveal pronounced membrane proton permeability.

Suffrian, K., ¹Schulz, K.G., Gutowska, M., ¹Riebesell, U., Bleich, M.

In review process at “New Phytologist”

ACKNOWLEDGEMENTS

I am especially grateful to my supervisor Prof. M. Bleich for providing the chance to work on this interesting and challenging, interdisciplinary thesis and especially for the constant challenge and support. I want to thank Prof. U. Riebesell for supporting the thesis on the marine biogeochemistry side. A special thank goes to my working group in the physiological department, namely Nina Himmerkus, Magdalena Gutowska, Wiebke Holtmann, Verena Trzeciak, Birte Sievers and Nadja Fischer for fruitful discussions and constant support in many ways: Go, girls, go!

I want to thank Kai Schulz, especially for inspiring discussions on the marine carbonate system. I also highly acknowledge support and fruitful discussions with Alison R. Taylor, C. Brownlee, Paul Steels, Sebastian Krug & Luke Mackinder. A thank you for cheering me up and input into finalising the manuscript also goes to Frank Melzner.

I thank the technical staff of the IFM-GEOMAR, FB2, namely Peter Fritsche for support with culture and nutrient measurements. I simply have to acknowledge the IFM-GEOMAR library, namely M. Lembke, B. Schmidt and C. Siemen, for ongoing support over the last 7 years, in between other things with literature.

I kindly acknowledge the technical assistance at the physiological institute by Regina Lingg, Thomas Stegmann, and Jan Brdon. I am very grateful to the workshop of the physiological institute, especially Holger Voigt and Martin Müller, for the construction of special technical equipment like the OOE mixing unit. Marius N. Müller is kindly acknowledged for providing *E. huxleyi*, and Alison R. Taylor for providing *C. pelagicus*.

Last but not least I want to thank Rouven for always being there and supporting me.

The project has been performed and supported within the cluster of excellence “The Future Ocean”, CP0602 and CP0701, at the Christian-Albrechts-Universität zu Kiel. I thankfully acknowledge the support of Federal Ministry of Education and Research (BMBF; FKZ 03F0608M).

CURRICULUM VITAE

Persönliche Daten

Name: Kerstin Suffrian, geb. Schmidt
Geburtsdatum: 12. April 1975
Geburtsort: Kappeln/Schlei, SH
Nationalität: deutsch
Familienstand: verheiratet
Wohnsitz: Muhliusstraße 49, 24103 Kiel

Schule und Studium

1981-1994 Grundschule (BW, Berlin)
 Gymnasium Klosterschule, Hamburg
 Carl-Duisberg-Gymnasium, Wuppertal
1994 Allgemeine Hochschulreife
1994-1995 Studium Englisch, Spanisch (FH Köln, abgebrochen)
1997-1998 Auslandsaufenthalt (Australien) zur Sprachvertiefung
 Tauchausbildung, Abschluss als Rettungstaucher, PADI
1999-2003 Studium der Biologie (HHU, Düsseldorf)
2003 Vordiplom
2003-2005 Studium der Biologie (CAU, Kiel)
2005 Tauchausbildung, Abschluss als Divemaster, PADI
2005-2006 Diplomarbeit
 "Selective grazing and calcite dissolution by microzooplankton
 during a mesocosm experiment"
2006 Erlangung des akademischen Grades „Diplom-Biologin“

Beruflicher Werdegang

2007-2010 “Ion transport and pH homeostasis in coccolithophores”
 Promotion in „Physiologie“
 Abteilung Med. Physiologie, CAU und Abteilung Biologische
 Ozeanographie, IFM-GEOMAR, Leibniz-Institut für Meeres-
 wissenschaften

Lehre

WS 2006/07 Betreuung Großpraktikum Biologische Meereskunde,
 Biogeochemischer/ Planktologischer Teil
 SS 07 Betreuung Physiologiepraktikum (Membranpotential)
 WS 07/08 Betreuung Physiologiepraktikum (Niere)
 SS 08 Betreuung Physiologiepraktikum (Somatosensorik)
 WS 08/09 Betreuung Physiologiepraktikum (Niere)
 SS 09 Betreuung Physiologiepraktikum (Membranpotential)
 WS 09/10 Betreuung Physiologiepraktikum (Arbeitsphysiologie)
 SS 10 Betreuung Physiologiepraktikum (EEG)

Veröffentlichungen

12.05.07 “Impact of an Increasing CO₂-Level on Coccolithophorids”,
 Ostseephysiolgentreffen, Kiel (Vortrag)
 15.09.07 “Effect of increased CO₂ on cellular ion transport mechanisms”,
 Excellence cluster retreat, Salzau (Vortrag)
 17.-18.03.08 Exzellenzcluster Retreat Salzau, (Poster)
 18.-19.04.08 “New approaches in sea urchin physiology”,
 Ostseephysiolgentreffen, Rostock (Vortrag)
 09.-13.06.08 “New insights in *E. huxleyi* physiology”, EPOCA Kickoff meeting,
 Nizza (Poster)
 07.07.08 “Microzooplankton grazing and phytoplankton growth in marine
 mesocosms with increased CO₂ levels”, Biogeosciences 5,
 1145-1156, Special Issue; PeECE: Pelagic Ecosystem CO₂

- Enrichment Studies. **K. Suffrian**, P. Simonelli, J. Nejstgaard S. Putzeys, Y. Carotenuto, and A. Antia
- 24.-26.02.09 “Experimental approaches to measure the influence of pH and pCO₂ on coccolithophores”, Training workshop on the fundamentals of carbon biogeochemistry (EPOCA, CARBOOCEAN, and IOC), Bergen (Poster)
- 31.03.09 “Experimental approaches to measure the influence of pH and pCO₂ on coccolithophores”. Salzau. Exzellenzcluster retreat proceedings, Salzau (Poster)
- 12.09 “Die Umwege der Wissenschaft” MARE 77, S. 42-43, 12/09-01/10, Essay. C. Fehling, A. Heinemann, K. O’Brien, S. Sudhaus und **K. Suffrian**.
- 2010-08-31 *In Revision:*
„Cellular pH measurements in *Emiliana huxleyi* reveal pronounced membrane proton permeability.” New Phytologist. **K. Suffrian**, K.G. Schulz, M. Gutowska, U. Riebesell, M. Bleich,

Kurse / Konferenzen / Seminare

- 07.-08.02.08 ISOS-Kurs ‘Academic Presentations - Hard and Soft Skills’:
- 02.-03.04.08 BIOACID Workshop, IFM-GEOMAR,
- 18.-19.04.08 Ostseephysioligentreffen (Vortrag)
- 09.05.-04.06.08 ISOS-Kurs ‘Mass Spectrometry and Optical Spectroscopy’:
- 30.-31.05.08 Teilnahme Doktorandenretreat (Rendsburg)
- 09.-13.06.08 EPOCA Kickoff meeting, Nizza (Poster)
- 19.-21.11.08 CO2 Guide to best practice Workshop, IFM-GEOMAR
- 24-26.02.09 Training workshop on the fundamentals of carbon biogeochemistry (EPOCA, CARBOOCEAN, and IOC), Bergen (Poster)
- 02.-23.04.09 ISOS-Kurs: "Von der Idee zur DVD - Erstellung von Dokumentarfilmen"
- 08.-09.05.09 Ostseephysioligentagung, Greifswald
- 06.-09.10.08 Future ocean workshop on “marine organisms used to understand basic mechanisms underlying development and disease” and 2nd biannual symposium of future ocean cluster, Kiel

26.10.09 Seminar AWI, L. Nooijer , AWI Bremerhaven (Vortrag)
27.-29.10.09 BIOACID Kickoff-Meeting, IFM-GEOMAR

Wissenschaftliche Hilfskraft (IFM-GEOMAR)

2003-2006 Marine Biogeochemie (U. Riebesell)
Meereschemie (D. Wallace)
Experimentelle Ökologie (U.Sommer)
Biologische Ozeanographie (K. Lochte, A. Antia)
IFM-GEOMAR Bibliothek Westufer (B.Schmidt)

ERKLÄRUNG

Hiermit erkläre ich an Eides statt, dass die vorliegende Dissertation, abgesehen von der Beratung durch meinen akademischen Lehrer, nach Inhalt und Form meine eigene Arbeit ist und ich keine anderen als die angegebenen Quellen und Hilfsmittel verwendet habe. Des Weiteren versichere ich, dass die vorliegende Dissertation weder im Ganzen noch zum Teil einer anderen Stelle im Rahmen eines Prüfungsverfahrens vorgelegen hat und unter Einhaltung der Regeln guter wissenschaftlicher Praxis entstanden ist.

Kiel, den 24. September 2010

Kerstin Suffrian

References

- Aidley DJ, Stanfield PR. 1996.** *Ion Channels: Molecules in Action*. Cambridge: Cambridge University Press.
- Alper S. 2006.** Molecular Physiology of SLC4 Anion Exchanges (Vol 91, Pg 159, 2006). *Experimental Physiology* **91**: 481.
- Anning T, Nimer NA, Merrett MJ, Brownlee C. 1996.** Costs and Benefits of Calcification in Coccolithophorids. *Journal of Marine Systems* **9**: 45-56.
- Balch WM, Fritz JJ, Fernandez E. 1996.** Decoupling of Calcification and Photosynthesis in the Coccolithophore *Emiliana Huxleyi* Under Steady-State Light-Limited Growth. *Marine Ecology-Progress Series* **142**: 87-97.
- Balch WM, Holligan PM, Ackleson SG, Voss KJ. 2010.** Biological and Optical Properties of Mesoscale Coccolithophore Blooms in the Gulf of Maine. *Limnology and Oceanography* **36**: 629-643.
- Berry L, Taylor AR, Lucken U, Ryan KP, Brownlee C. 2002.** Calcification and Inorganic Carbon Acquisition in Coccolithophores. *Functional Plant Biology* **29**: 289-299.
- Bleich M, Köttgen M, Schlatter E, Greger R. 1995.** Effect of $\text{NH}_4^+/\text{NH}_3$ on Cytosolic PH and the K^+ Channels of Freshly Isolated Cells From the Thick Ascending Limb of Henle's Loop. *Pflügers Archiv - European Journal of Physiology* **429**: 345-354.
- Boron WF. 2004.** Regulation of Intracellular PH. *Advances in Physiology Education* **28**: 160-179.
- Boron WF, Chen L, Parker MD. 2009.** Modular Structure of Sodium-Coupled Bicarbonate Transporters. *Journal of Experimental Biology* **212**: 1697-1706.
- Broecker W & Clark E. 2009.** Ratio of Coccolith CaCO_3 to Foraminifera CaCO_3 in Late Holocene Deep Sea Sediments. *Paleoceanography* **24**: 11pp.
- Brown CW & Yoder JA. 1994.** Coccolithophorid Blooms in the Global Ocean. *Journal of Geophysical Research-Oceans* **99**: 7467-7482.
- Brownlee C, Taylor AR. 2004.** Calcification in Coccolithophores: A Cellular Perspective. In: Thierstein HR, J.R.Young, eds. *Coccolithophores-from molecular processes to global impact*. Germany: Springer, 31-49.
- Buitenhuis ET, De Baar HJW, Veldhuis MJW. 1999.** Photosynthesis and Calcification by *Emiliana Huxleyi* (Prymnesiophyceae) As a Function of Inorganic Carbon Species. *Journal of Phycology* **35**: 949-959.
- Delille B, Harlay J, Zondervan I, Jacquet S, Chou L, Wollast R, Bellerby RGJ, Frankignoulle M, Borges AV, Riebesell U, Gattuso JP. 2005.** Response of Primary Production and Calcification to Changes of PCO_2 During Experimental Blooms of the Coccolithophorid *Emiliana Huxleyi*. *GLOBAL BIOGEOCHEMICAL CYCLES* **19**.

- Dickson AG. 1990.** Standard Potential of the Reaction - AgCl(S)+1/2H₂(G)=Ag(S)+HCl(Aq) and the Standard Acidity Constant of the Ion HSO₄⁻ in Synthetic Sea-Water From 273.15-K to 318.15-K. *Journal of Chemical Thermodynamics* **22**: 113-127.
- Dixon GK, Brownlee C, Merrett MJ. 1989.** Measurement of Internal PH in the Coccolithophore *Emiliana Huxleyi* Using 2',7'-Bis-(2-Carboxyethyl)-5-(And-6)Carboxyfluorescein Acetoxymethylester and Digital Imaging Microscopy. *Planta* **178**: 443-449.
- Dong LF, Nimer NA, Okus E, Merrett MJ. 1993.** Dissolved Inorganic Carbon Utilization in Relation to Calcite Production in *Emiliana Huxleyi* (Lohmann) Kamptner. *New Phytologist* **123**: 679-684.
- Elzenga JTM, Prins HBA, Stefels J. 2000.** The Role of Extracellular Carbonic Anhydrase Activity in Inorganic Carbon Utilization of *Phaeocystis Globosa* (Prymnesiophyceae): A Comparison With Other Marine Algae Using the Isotopic Disequilibrium Technique. *Limnology and Oceanography* **45**: 372-380.
- Endeward V, Musa-Aziz R, Cooper GJ, Chen LM, Pelletier MF, Virkki LV, Supuran CT, King LS, Boron WF, Gros G. 2006.** Evidence That Aquaporin 1 Is a Major Pathway for CO₂ Transport Across the Human Erythrocyte Membrane. *FASEB Journal* **20**: 1974-1981.
- Gallempore RP & Steinberg RH. 1989.** Effects of DIDS on the Chick Retinal-Pigment Epithelium .1. Membrane-Potentials, Apparent Resistances, and Mechanisms. *Journal of Neuroscience* **9**: 1968-1976.
- Guillard RRL. 1975.** Culture of Phytoplankton for Feeding Marine Invertebrates. In: Smith W.L., Chanley MH, eds. *Culture of Marine Invertebrate Animals*. New York, USA: Plenum Press, 26-60.
- Guiry MD & Guiry GM. 2010.** AlgaeBase. World-Wide Electronic Publication. *Www Algaebase Org, Searched on 02 August 2010* . National University of Ireland, Galway.
- Hansen H, Koroleff F. 1999.** Determination of Nutrients. In: Grasshoff K, Ehrhardt M, Kremling K, Anderson L, eds. *Methods of seawater analysis*. Weinheim: Wiley-VCH, 159-228.
- Hasselblatt P, Warth R, Schulz-Baldes A, Greger R, Bleich M. 2000.** PH Regulation in Isolated in Vitro Perfused Rat Colonic Crypts. *Pflügers Archiv - European Journal of Physiology* **441**: 118-124.
- Herfort L, Loste E, Meldrum F, Thake B. 2004.** Structural and Physiological Effects of Calcium and Magnesium in *Emiliana Huxleyi* (Lohmann) Hay and Mohler. *Journal of Structural Biology* **148**: 307-314.
- Herfort L, Thake B, Roberts J. 2002.** Acquisition and Use of Bicarbonate by *Emiliana Huxleyi*. *New Phytologist* **156**: 427-436.

- Ho T-Y, Quigg A, Finkel ZV, Milligan AJ, Wyman K, Falkowski PG, Morel FMM. 2003.** The Elemental Composition of Some Marine Phytoplankton. *Journal of Phycology* **39**.
- Holligan PM, Viollier M, Harbour DS, Camus P, Champagnephilippe M. 1983.** Satellite and Ship Studies of Coccolithophore Production Along A Continental-Shelf Edge. *Nature* **304**: 339-342.
- Johnstone RM, Laris PC, Eddy AA. 1982.** The Use of Fluorescent Dyes to Measure Membrane-Potentials - A Critique. *Journal of Cellular Physiology* **112**: 298-301.
- Kester D, Duedall I, Connors D, Pytkowicz R. 1967.** Preparation of Artificial Seawater. *Limnology and Oceanography* **12**: 176-179.
- Lemtiri-Chlieh F, MacRobbie EAC, Webb AAR, Manison NF, Brownlee C, Skepper JN, Chen J, Prestwich GD, Brearley CA. 2003.** Inositol Hexakisphosphate Mobilizes an Endomembrane Store of Calcium in Guard Cells. *Proceedings of the National Academy of Sciences of the United States of America* **100**: 10091-10095.
- Leonardos N, Read BA, Thake B, Young JR. 2009.** No Mechanistic Dependence of Photosynthesis on Calcification in the Coccolithophorid *Emiliana Huxleyi* (Haptophyta). *Journal of Phycology* **45**: 1046-1051.
- Lewis E & D.W.R.Wallace. 1998.** CO2SYS_Calc_DOS_Original: Program Developed for CO₂ System Calculations. ORNL/CDIAC-105. Oak Ridge, Tennessee, Carbon Dioxide Information Analysis Center, Oak Ridge National Laboratory, U.S. Department of Energy.
- Lu J & Boron WF. 2007.** Reversible and Irreversible Interactions of DIDS With the Human Electrogenic Na/HCO₃ Cotransporter NBCe1-A: Role of Lysines in the KKMVK Motif of TM5. *American Journal of Physiology-Cell Physiology* **292**: C1787-C1798.
- Mackinder L, Wheeler G, Schroeder D, Riebesell U, Brownlee C. 2010.** Molecular Mechanisms Underlying Calcification in Coccolithophores. *Geomicrobiology Journal* **submitted**.
- Miao XL & Wu QY. 2002.** Inorganic Carbon Utilization in Some Marine Phytoplankton Species. *Acta Botanica Sinica* **44**: 395-399.
- Müller MN, Antia AN, LaRoche J. 2008.** Influence of Cell Cycle Phase on Calcification in the Coccolithophore *Emiliana Huxleyi*. *Limnology and Oceanography* **53**: 506-512.
- Musa-Aziz R, Chen LM, Pelletier MF, Boron WF. 2009.** Relative CO₂/NH₃ Selectivities of AQP1, AQP4, AQP5, AmtB, and RhAG. *Proceedings of the National Academy of Sciences* **106**: 5406-5411.
- Nakhoul NL, Davis BA, Romero MF, Boron WF. 1998.** Effect of Expressing the Water Channel Aquaporin-1 on the CO₂ Permeability of *Xenopus* Oocytes. *American Journal of Physiology-Cell Physiology* **43**: C543-C548.

- Neher E & Sakmann B. 1976.** Single-Channel Currents Recorded From Membrane of Denervated Frog Muscle-Fibers. *Nature* **260**: 799-802.
- Nimer NA, Brownlee C, Merrett MJ. 1994a.** Carbon Dioxide Availability, Intracellular PH and Growth Rate of the Coccolithophore *Emiliana Huxleyi*. *Marine Ecology-Progress Series* **109**: 257-262.
- Nimer NA, Dixon GK, Merrett MJ. 1992.** Utilization of Inorganic Carbon by the Coccolithophorid *Emiliana Huxleyi* (Lohmann) Kamptner. *New Phytologist* **120**: 153-158.
- Nimer NA, Guan Q, Merrett MJ. 1994b.** Extracellular and Intracellular Carbonic-Anhydrase in Relation to Culture Age in A High-Calcifying Strain of *Emiliana Huxleyi* Lohmann. *New Phytologist* **126**: 601-607.
- Nimer NA & Merrett MJ. 1992.** Calcification and Utilization of Inorganic Carbon by the Coccolithophorid *Emiliana Huxleyi* Lohmann. *New Phytologist* **121**: 173-177.
- Nimer NA, Merrett MJ, Brownlee C. 1996.** Inorganic Carbon Transport in Relation to Culture Age and Inorganic Carbon Concentration in a High-Calcifying Strain of *Emiliana Huxleyi* (Prymnesiophyceae). *Journal of Phycology* **32**: 813-818.
- Paasche E. 1964.** A Tracer Study of the Inorganic Carbon Uptake During Coccolith Formation and Photosynthesis in the Coccolithophorid *Coccolithus Huxleyi*. *Physiologica Plantarum Suppl* **3**: 1-82.
- Paasche E. 1968a.** Biology and Physiology of Coccolithophorids. *Annual Review of Microbiology* **22**: 71-&.
- Paasche E. 1968b.** Effect of Temperature Light Intensity and Photoperiod on Coccolith Formation. *Limnology and Oceanography* **13**: 178-&.
- Paasche E. 2002.** A Review of the Coccolithophorid *Emiliana Huxleyi* (Prymnesiophyceae), With Particular Reference to Growth, Coccolith Formation, and Calcification-Photosynthesis Interactions. *Phycologia* **40**: 503-529.
- Pressman BC. 1976.** Biological Applications of Ionophores. *Annual Review of Biochemistry* **45**: 501-530.
- Pusch M, Zifarelli G, Murgia AR, Picollo A, Babini E. 2006.** Channel or Transporter? The CLC Saga Continues. *Experimental Physiology* **91**: 149-152.
- Pushkin A & Kurtz I. 2006.** SLC4 Base (HCO₃⁻, CO₃²⁻) Transporters: Classification, Function, Structure, Genetic Diseases, and Knockout Models. *American Journal of Physiology-Renal Physiology* **290**: F580-F599.
- Quinn P, Bowers RM, Zhang YY, Wahlund TM, Fanelli MA, Olszova D, Read BA. 2006.** CDNA Microarrays As a Tool for Identification of Biomineralization Proteins in the Coccolithophorid (Haptophyta). *Applied and Environmental Microbiology* **72**: 5512-5526.
- Quiroga O & Gonzalez EL. 1993.** Carbonic-Anhydrase in the Chloroplast of A Coccolithophorid (Prymnesiophyceae). *Journal of Phycology* **29**: 321-324.

- Riebesell U. 2004.** Effects of CO₂ Enrichment on Marine Phytoplankton. *Journal of Oceanography* **60**: 719-729.
- Riebesell U, Schulz KG, Bellerby RGJ, Botros M, Fritsche P, Meyerhofer M, Neill C, Nondal G, Oschlies A, Wohlers J, Zöllner E. 2007.** Enhanced Biological Carbon Consumption in a High CO₂ Ocean. *Nature* **450**: 545-548.
- Riebesell U, Wolf-Gladrow DA, Smetacek V. 1993.** Carbon-Dioxide Limitation of Marine-Phytoplankton Growth-Rates. *Nature* **361**: 249-251.
- Rink TJ, Tsien RY, Pozzan T. 1982.** Cytoplasmic PH and Free Mg²⁺ in Lymphocytes. *Journal of Cell Biology* **95**: 189-196.
- Ritchie RJ. 1984.** A Critical-Assessment of the Use of Lipophilic Cations As Membrane-Potential Probes. *Progress in Biophysics & Molecular Biology* **43**: 1-32.
- Ritchie RJ. 1999.** Tetraphenylphosphonium Cation (TPP⁺) Is Not a Reliable Membrane Potential Probe in the Cyanobacterium *Synechococcus* R-2 PCC 7942. *New Phytologist* **141**: 387-399.
- Romero MF, Fulton CM, Boron WF. 2004.** The SLC4 Family of HCO₃⁻ Transporters. *Pflügers Archiv - European Journal of Physiology* **447**: 495-509.
- Rost B, Kranz SA, Richter KU, Tortell PD. 2007.** Isotope Disequilibrium and Mass Spectrometric Studies of Inorganic Carbon Acquisition by Phytoplankton. *Limnology and Oceanography-Methods* **5**: 328-337.
- Rost B, Riebesell U. 2004.** Coccolithophores and the Biological Pump: Responses to Environmental Changes. In: Thierstein HR, Young JR, eds. *Coccolithophores: From molecular processes to global impact*. Berlin: Springer, 99-125.
- Rost B, Riebesell U, Burkhardt S, Sultemeyer D. 2003.** Carbon Acquisition of Bloom-Forming Marine Phytoplankton. *Limnology and Oceanography* **48**: 55-67.
- Rost B, Riebesell U, Sultemeyer D. 2006.** Carbon Acquisition of Marine Phytoplankton: Effect of Photoperiod Length. *Limnology and Oceanography* **51**: 12-20.
- Rost B, Zondervan I, Riebesell U. 2002.** Light-Dependent Carbon Isotope Fractionation in the Coccolithophorid *Emiliana Huxleyi*. *Limnology and Oceanography* **47**: 120-128.
- Roy RN, L.N.Roy, Vogel KM, C.Porter-Moore, Pearson T, Good CE, Millero FJ, D.M.Campbell. 1993.** The Dissociation Constants of Carbonic Acid in Seawater at Salinities 5 to 45 and Temperatures 0 to 45°C. *Marine Chemistry* **44**: 249-267.
- Sakmann B & Neher E. 1984.** Patch Clamp Techniques for Studying Ionic Channels in Excitable-Membranes. *Annual Review of Physiology* **46**: 455-472.
- Scheel O, Zdebik AA, Lourdel S, Jentsch TJ. 2005.** Voltage-Dependent Electrogenic Chloride/Proton Exchange by Endosomal CLC Proteins. *Nature* **436**: 424-427.

- Schulz KG, Riebesell U, Rost B, Thoms S, Zeebe RE. 2006.** Determination of the Rate Constants for the Carbon Dioxide to Bicarbonate Inter-Conversion in PH-Buffered Seawater Systems. *Marine Chemistry* **100**: 53-65.
- Shampine LF & Reichelt MW. 1997.** The Matlab Ode Suite. *Siam Journal on Scientific Computing* **18**: 1-22.
- Shiraiwa Y. 2003.** Physiological Regulation of Carbon Fixation in the Photosynthesis and Calcification of Coccolithophorids. *Comparative Biochemistry and Physiology Part B* **136**: 775-783.
- Siegenthaler U & Sarmiento JL. 1993.** Atmospheric Carbon-Dioxide and the Ocean. *Nature* **365**: 119-125.
- Sikes CS, Roer RD, Wilbur KM. 1980.** Photosynthesis and Coccolith Formation - Inorganic Carbon-Sources and Net Inorganic Reaction of Deposition. *Limnology and Oceanography* **25**: 248-261.
- Sikes CS & Wilbur KM. 1982.** Functions of Coccolith Formation. *Limnology and Oceanography* **27**: 18-26.
- Solomon S, Qin D, Manning M, Chen Z, Marquis M, Averyt KB, Tignor M, Miller HL. 2007.** Climate Change 2007: The Physical Science Basis. Contribution of Working Group I to the Fourth Assessment Report of the Intergovernmental Panel on Climate Change. 996 pp. Cambridge, United Kingdom and New York, NY, USA, Cambridge University Press.
- Soto AR, Zheng H, Shoemaker D, Rodriguez J, Read BA, Wahlund TM. 2006.** Identification and Preliminary Characterization of Two cDNAs Encoding Unique Carbonic Anhydrases From the Marine Alga *Emiliana Huxleyi*. *Applied and Environmental Microbiology* **72**: 5500-5511.
- Spivack AJ, You CF, Smith HJ. 1993.** Foraminiferal Boron Isotope Ratios As A Proxy for Surface Ocean Ph Over the Past 21-Myr. *Nature* **363**: 149-151.
- Stewart WDP. 1974.** *Algal Physiology and Biochemistry*. Berkeley and Los Angeles, CA: University of California Press.
- Taylor AR & Brownlee C. 2003.** A Novel Cl⁻ Inward-Rectifying Current in the Plasma Membrane of the Calcifying Marine Phytoplankton *Coccolithus Pelagicus*. *Plant Physiology* **131**: 1391-1400.
- Trimborn S, Langer G, Rost B. 2007.** Effect of Varying Calcium Concentrations and Light Intensities on Calcification and Photosynthesis in *Emiliana Huxleyi*. *Limnology and Oceanography* **52**: 2285-2293.
- Tsuji Y, Suzuki I, Shiraiwa Y. 2009.** Photosynthetic Carbon Assimilation in the Coccolithophorid *Emiliana Huxleyi* (Haptophyta): Evidence for the Predominant Operation of the C-3 Cycle and the Contribution of -Carboxylases to the Active Anaplerotic Reaction. *Plant and Cell Physiology* **50**: 318-329.
- von Dassow P, Ogata H, Probert I, Wincker P, Da Silva C, Audic S, Claverie JM, de Vargas C. 2009.** Transcriptome Analysis of Functional Differentiation Between

Haploid and Diploid Cells of *Emiliana Huxleyi*, a Globally Significant Photosynthetic Calcifying Cell. *Genome Biology* **10**: 33pp.

Wehner F, Rosinsteuer S, Beetz G, Sauer H. 1993. The Anion Transport Inhibitor Dids Increases Rat Hepatocyte K⁺ Conductance Via Uptake Through the Bilirubin Pathway. *Journal of Physiology-London* **471**: 617-635.

Westbroek P, Brown CW, Vanbleijswijk J, Brownlee C, Brummer GJ, Conte M, Egge J, Fernandez E, Jordan R, Knappertsbusch M, Stefels J, Veldhuis M, Vanderwal P, Young J. 1993. A Model System Approach to Biological Climate Forcing - the Example of *Emiliana Huxleyi*. *Global and Planetary Change* **8**: 27-46.

Westbroek P, Young JR, Linschooten K. 1989. Coccolith Production (Biomineralization) in the Marine Alga *Emiliana Huxleyi*. *Journal of Protozoology* **36**: 368-373.

Young J. 1994. Functions of Coccoliths. In: Winter A, Siesser WG, eds. *Coccolithophores*. UK: Cambridge University Press, 63-82.

Zeebe RE & Wolf-Gladrow DA. 2001. CO₂ in Seawater: Equilibrium, Kinetics, Isotopes. [65], 346pp. Amsterdam. *Elsevier Oceanography Series*. Halpern, David.

Zhao JH, Hogan EM, Bevensee MO, Boron WF. 1995. Out-Of-Equilibrium CO₂/HCO₃⁻ Solutions and Their Use in Characterizing A New K/HCO₃ Cotransporter. *Nature* **374**: 636-639.